A concept for a regional coastal zone mission

vorgelegt von

Dipl.-Ing. Jens Nieke

Von der Fakultät V - Verkehrs- und Maschinensysteme
der Technische Universität Berlin
zur Erlangung des akademischen Grades

Doktor der Ingenieurwissenschaften (Dr.-Ing.)

genehmigte Dissertation.

Tag der wissenschaftlichen Aussprache: 19. Dez 2001

Berichter:
Prof. Dr. H.-P. Röser
Prof. Dr. J. Albertz
Prof. Dr. G. Zimmermann

Berlin 2002

D 83

The discharge of the River Thames observed by MOS-IRS:
Colour composite, pigment and sediment distribution in Sep. 1996

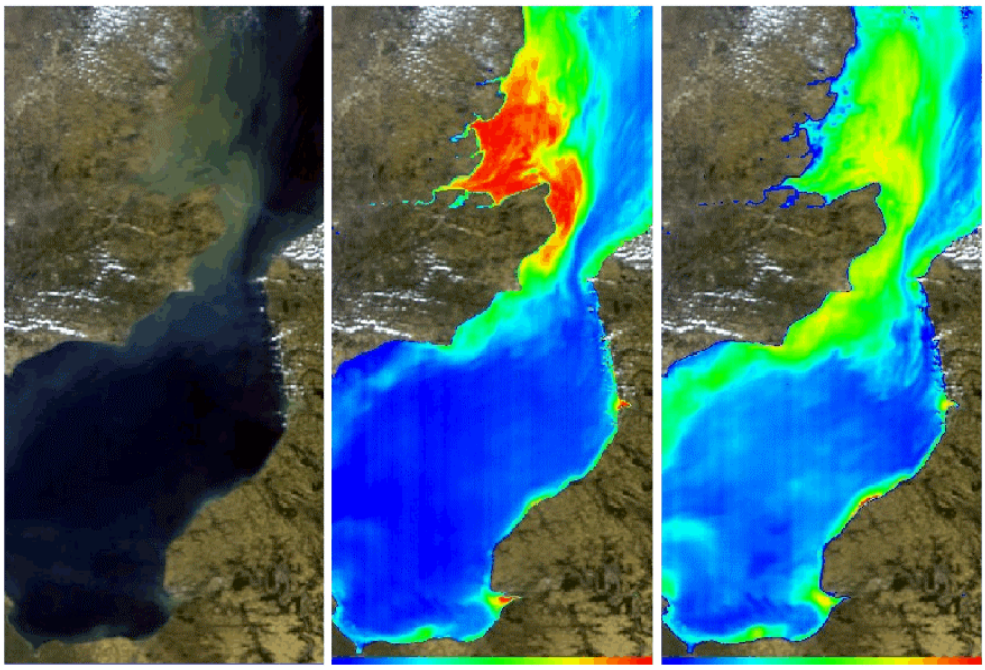

An example for successful coast-zone remote sensing: The DLR imaging spectrometer MOS-IRS detecting the English Channel in Sep. 1996. The colour composite is using channel 2, 3, 5, 6, 7 and 8. The pigment concentration colour index and the backscattering coefficient index vary from low (blue) to high (red) values. MOS-IRS images courtesy of DLR Institute of Space Sensor Technology (http://www.ba.dlr.de/NE-WS/ws5/index_mos.html).

A concept for a regional coastal zone mission

Abstract

Due to increasing population pressure there is a world-wide concern to improve the observation of coastal zones for a better assessment of the growing impact of human being on the coastal ecosystem (e.g. pollution in river estuaries, flooding in contaminated regions). In contrast to globally oriented remote sensing missions, monitoring and management of rapid changes of the coastal ecosystem demand specific regional coastal zone mission features.

Therefore a low-Earth orbit mission study has been carried out at DLR, Berlin together with industry and partner research institutes. In the scope of this study also various technical investigations have been performed, such as ray-tracing and grating simulations, a signal-to-noise model analysis and an experimental prototype set-up. Thus, the ability of a new imaging spectrometer has been demonstrated to fulfil the requirements for coastal zone observation. In a module arrangement analysis the system orbit–satellite–payload has been optimised in arranging VIS-NIR spectrometers, SWIR cameras and a TIR scanner in a way they cover best the science community needs.

The resulting mission concept covers the spectral region from the visible to the thermal infrared in 21 partly programmable spectral channels, with a relatively high spatial (ΔX_{VIS} = 100 m) and spectral ($\Delta\lambda_{VIS}$ = 1.5 nm) resolution. For monitoring of hazardous events a high repetivity (1–3 days) is ensured by the tilt capability (± 30° off nadir) of the mini satellite (< 300 kg).

Kurze Inhaltsangabe

Aufgrund der Bevölkerungsexplosion gibt es einen weltweiten Konsens die Fernerkundung der Küstengebiete zu intensivieren, um so den wachsenden Einfluss der Menschheit auf das Küstenökosystem besser bewerten zu können (z.B. die Verschmutzung von Flussmündungen, Flutungen in kontaminierten Regionen). Doch im Gegensatz zu global ausgerichteten Fernerkundungsmissionen ist für die Beobachtung der Küstengewässer eine Mission mit regional-spezifischen Parametern notwendig.

Aus diesem Grunde wurde im DLR, Berlin zusammen mit der Industrie und anderen Partnerforschungsinstituten eine Studie für eine Mission in einem erdnahen Orbit angefertigt. Im Rahmen dieser Studie wurden auch verschiedene technische Untersuchungen realisiert, wie eine Optik- und Gitter-Simulation, eine Signalrauschverhältnis-Analyse und ein experimenteller Prototypaufbau. In diesen Untersuchungen wurde gezeigt, dass ein neues abbildendes Spektrometer eine sehr gute VIS–NIR Komponente für eine Küstenfernerkundungsmission ist. In einer Modulanordnungsuntersuchung wurde das System Orbit–Satellit–Nutzlast optimiert in dem mehrere VIS–NIR Spektrometer, SWIR Kameras und ein TIR Scanner so angeordnet wurden, dass sie den wissenschaftlichen Anforderungen der internationalen Küstengewässer-Nutzergemeinschaft gerecht werden.

Das vorgeschlagene Missionskonzept überdeckt das Spektralgebiet vom Sichtbaren zum Thermischen Infrarot in 21 teilweise programmierbaren Kanälen, mit einer relativ hohen räumlichen (ΔX_{VIS} = 100 m) und spektralen ($\Delta\lambda_{VIS}$ = 1.5 nm) Auflösung. Für die Beobachtung von besonderen ökologischen Ereignissen ist eine hohe Wiederholungsrate (1–3 Tage) durch die Kippmöglichkeiten (±30° von Nadir) des Minisatelliten (< 300 kg) sichergestellt.

Table of Contents

Abstract / Kurze Inhaltsangabe iii

Abbreviations viii

Zusammenfassung (deutsch) 3

1 Introduction to regional remote sensing of coastal zones 7

1.1 Remote sensing of the Earth in the VIS-TIR 9
1.1.1 Physical conditions of remote sensing 9
1.1.2 Overview of remote sensing observation requirements 12

1.2 Remote sensing of the coastal zone 21
1.2.1 The atmosphere-ocean system 21
1.2.2 Scientific background and research needs 25

1.3 Experience from recent ocean-colour missions 28

1.4 Requirements for a regional coastal zone mission 31

2 Remote sensing instrument overview and optimisation for a regional coastal zone mission 33

2.1 The evolution of coastal zone remote sensing instruments 33

2.2 State-of-the-art of remote sensing instruments (VIS–TIR) 37
2.2.1 Optical remote sensing instrumentation in general 37
2.2.2 Hyperspectral imager technology 39

2.3 Sensor and orbit optimisation for a regional coastal zone mission 56
2.3.1 Orbit-satellite optimisation 56
2.3.2 Sensor and payload optimisation 58
2.3.3 Observation Requirements 62

3 Specific investigations for the mission's sensor and calibration concept 63

3.1 Sensitivity analysis for imaging spectrometers 64
3.1.1 Top-of-atmosphere radiance 65
3.1.2 Classical signal-to-noise ratio analysis 65
3.1.3 Refined signal-to-noise ratio analysis for 2-d detectors 67
3.1.4 Comparison of refined and classical SNR analysis 70
3.1.5 Conclusion 73

3.2 The Offner-type imaging spectrometer 74
3.2.1 Ray-tracing and grating simulations 74
3.2.2 Sensitivity model analysis 77
3.2.3 Experimental prototype study 80
3.2.4 Concluding remarks and outlook 82

3.3 Capabilities of LEDs for in-flight calibration 84
3.3.1 Calibration requirements and LED-set selection 84
3.3.2 LED characterisation 87
3.3.3 Conclusion 94

4 Summary of the regional coastal zone mission 97

4.1 Orbit 97

4.2 Payload 99
4.2.1 Offner-type imaging spectrometer 103
4.2.2 SWIR camera 103
4.2.3 TIR scanner 104
4.2.4 The Sensor Control Unit (SCU) 104
4.2.5 In-flight Calibration 107

4.3 Spacecraft Platform 109

5 General Conclusion 111

6 References 115

Appendix A: Systematisation of sensors 121

A.1 Spaceborne sensors 121

A.2 Airborne sensor 124

A.3 Sensors and mission acronyms 126

Appendix B: ECOMON S/C details 128

Danksagung 131

Abbreviations

2-d	Two Dimensional
A/D	Analogue/Digital
AISA	Airborne Imaging Spectrometer for different Applications
AOF	Acousto-Optical Filter
APEX	Airborne Prism Experiment
APS	Active Pixel Sensor
CATIA	Computer Aided Three-Dimensional Interactive Application
CCD	Charge-Coupled Device
CID	Charge-Injection Device
CMOS	Complementary-Metal-Oxide-Semiconductor
CODE-V	Computer Tool for Optical Designers and Engineers
COIS	Coastal Zone Imager
CZCS	Coastal Zone Colour Scanner
ECOMON	Regional Ecological Research and Monitoring
EEV Ltd.	a GEC Group Company, Essex, UK
FOR	Field of Regard
FOV	Field of View
FPGA	Field-programming gate array
FTHSI	Fourier Transform Hyperspectral Imager
FTS	Fourier Transform Spectrometers
GEO	Geo-Stationary Orbit
GLI	Global Imager
HAB	Harmful Algal Bloom
HRIS	High Resolution Imaging Spectrometer
HSI	Hyperspectral Spaceborne Imager
IFOV	Instantaneously Field of View
IRS-P3	Indian Remote Sensing Satellite P3
LCF	Liquid Crystal Filter
LED	Light Emitting Diode
LEO	Low-Earth Orbit
LIDAR	Light Detection and Ranging
LISA	Linear Etalon Imaging Spectrometer Array
MIL STD	Military Standard
MIPAS	Michelson Interferometer for Passive Atmospheric Sounding
MIR	Mid-Wave Infrared
MODIS	Moderate-Resolution Imaging Spectroradiometer
MOS	Modular Optoelectronic Scanner
NDVI	Normalised Difference of the Vegetation Index
NIST	National Institute of Standards and Technology
PCB	Printed Circuit Board
P/L	Payload
PTB	Physikalisch-Technische Bundesanstalt, Germany
SAGE	Stratospheric Aerosol and Gas Experiment
S/C	Spacecraft
SAR	Synthetic Aperture Radar
SCU	Sensor Control Unit
SeaWiFS	Sea-viewing Wide Field of view Sensor
SMIFTS	Spatially Modulated Imaging Fourier Transform Spectrometer
SNR	Signal to Noise Ratio
SunCal	Sun Calibration Unit
SWIR	Short Wave Infrared
TFOV	Total Field of View
TIR	Thermal Infrared
TOA	Top of Atmosphere
UNEP	United Nations Environment Programme
UNFCCC	UN Framework Convention on Climate Change
VIS–NIR	Visible – Near Infrared
WMO	World Meteorological Organisation

Zusammenfassung (deutsch)

Motivation

In den letzten Jahren ist man in der internationalen Nutzergemeinschaft (z. B. der International Ocean-Colour Coordinating Group) zu der Überzeugung gekommen, die Küstengebiete genauer beobachten zu müssen, um so bessere Aussagen über räumlich-zeitliche Vorkommen und Verteilungen von Umweltparametern (wie Wasserinhaltstoffen und Wasserqualität) zu erhalten[1]. Aus diesen Aussagen sollen dann wichtige Schlussfolgerungen über die Stabilität und Belastbarkeit des Umweltsystems Küstengebiet im regionalen Sinn abgeleitet werden. Hieraus resultiert die Forderung nach einer regional ausgerichteten Küstengewässermission, die im Gegensatz zu lokal oder global ausgerichteten Sensoren (wie COIS oder MODIS, MERIS, SeaWiFS) die Möglichkeit bietet, Informationen über das sich schnell ändernde Umweltsystem der Küstengebiete (z.B. über die Verschmutzungen in Flussmündungen, die Überflutung verunreinigter Regionen, kritische Algenblüten) zu sammeln.

Hintergrund

Die erste und bisher erfolgreichste Fernerkundungsmission zur Ozeansondierung war der Coastal Zone Color Scanner auf Nimbus 7 (1978–1986). Mit diesem noch stark experimentellen Sensor wurden wesentliche Beiträge zur Entwicklung der globalen Ozean-Fernerkundungsmethodik und der Algorithmenfindung erbracht. Seit März 1996 liefert ein neuer experimenteller Sensor, das abbildende Spektrometer MOS-IRS, einen wichtigen Beitrag zur methodischen Weiterentwicklung der Fernerkundung der Erde. Als Nutzlast des indischen Satelliten IRS-P3 sammelt es Daten über Ozeane und insbesondere deren Küstengebiete mit Hilfe von 18 spektralen Kanälen (17 VIS–NIR und 1 SWIR). Der MOS Sensor stellt einerseits eine Technologiedemonstration dar, andererseits konnten neue Algorithmen zum besseren Verständnis des Umweltsystems Land-Ozean entwickelt werden. Aufgrund der weitreichenden Erfahrungen am Berliner DLR Standort auf dem Gebiet der Sensor- und Algorithmenentwicklungen begannen die ersten Untersuchungen zur MOS-Nachfolgerentwicklung. Die Arbeiten mündeten in einem technisch-realistischen Missionskonzept[2], welches als Missionsvorschlag bei der ESA (ESA Call for Earth Explorer Opportunity Missions) eingereicht wurde; jedoch erhielten andere Missionsziele bei der Auswahl höhere Präferenzen.

Ziel der Dissertation

Das Ziel der Dissertation war es, in einer Reihe von Untersuchungen im Rahmen der Missionsstudie Beiträge für ein technisch-realistisches Konzept zu erarbeiten, welches der Forderung der internationalen Nutzergemeinschaft nach einer regional ausgerichteten Küstengewässermission gerecht wird.

[1] IOCCG–2000
[2] Neumann et al.–1998

Ergebnisse der Dissertation

Für die Entwicklung eines Missionskonzeptes wurden unterschiedliche theoretische und experimentelle Untersuchungen durchgeführt, die sind hier kurz zusammengefasst sind:

0. Systematisierung und Bewertung von Erderkundungssensoren

In einem ersten Schritt wurde eine Systematisierung existierender und in Entwicklung befindlicher Erdbeobachtungssensoren erarbeitet, um über das Zusammenstellen von Sensor-Basisinformationen Schwerpunkte für eigene Entwicklungen ableiten zu können. Somit bietet diese Systematisierung einen Überblick über verschiedene Konzeptansätze und legt den Grundstein für die anschließende Missionskonzeptentwicklung.

1. Entwicklung eines detaillierten Sensor und Kalibrationskonzepts

Eine CODE-V und Gitter-Simulation zeigt[3], dass ein abbildendes Offner Spektrometer mit konvexem Trapezprofil-Gitter die geforderte geometrische und spektrale Bildqualität liefern kann. Dieses Spektrometer zeichnet sich insbesondere durch eine geringe Polarisationsempfindlichkeit (< 1%), die geringe Beugungseffektivität der zweiten Ordnung (≤ 0.5%) und einer kompakten Bauweise aus. Im Rahmen der Dissertation wurden die Signal-Rausch-Verhältnisse für die aus der Simulation und der CCD-Auswahl abgeleiteten Spektrometerparameter (spektrale und geometrische Auflösung, Effektivitäten von Optik und Detektor u.a.). berechnet. Ergebnis sind die radiometrischen Eigenschaften des Systems Optik-Gitter-Detektor für Top-of-Atmosphere Radianzen. Weiterhin verdeutlicht diese Analyse den Effekt der Bildverschmierung, und beweist, dass das Photonenrauschen dieser Bildverschmierung für einen frame-transfer Detektor in Verbindung von niedrigem Eingangssignalpegel, geringer Integrationszeit und vielen Spektralkanälen nicht vernachlässigt werden darf. Möglichkeiten der Korrektur bieten beispielsweise mechanische und elektronische Shutter.

In einem experimentellen Prototypaufbau [4] wurde gezeigt, dass die spektralen und geometrischen Ergebnisse der Modellierung verifiziert werden konnten: In einem 800 km Orbit würde eine Bodenauflösung des untersuchten Spektrometers von 100 m und eine Schwadbreite von 100 km erreicht werden. Der Spektralbereich reicht von 400 bis 1050 nm mit einer Auflösung von $\Delta\lambda$ < 1,5 nm. Im Rahmen der Dissertation wurde der Aufbau des Prototypen verbessert, indem die Fokalebene über 5 Freiheitsgrade durch einen schrittmotorgesteuerten Goniometerkopfes mit einer hohen Einstellgenauigkeit (0,4 µm/Schritt; 0,0004 °/Schritt) für Labormessungen und Parameteroptimierung justiert werden kann.

[3] List–1997
[4] Roth–1998

In einer weiteren experimentellen Untersuchung wurde die Möglichkeit analysiert, Lumineszenzdioden (LEDs) künftig für Kalibrationszwecke im Orbit zu verwenden. Im Rahmen dieser Untersuchung wurden die charakteristischen Eigenschaften (z.B. Abhängigkeiten von Lage und Höhe der LED-Emissionsmaxima im Temperaturbereich von 5°–50°C, elektromagnetische Verträglichkeit der LEDs für typische Weltraumbedingungen u.a.m) ermittelt. Als Ergebnis wurde gezeigt, dass LEDs sich gut für Kalibrationszwecke im Orbit verwenden lassen, wenn eine LED-Umgebungstemperaturstabilisierung vorgenommen wird. Es ist ein Verfahrenskonzept entwickelt worden, das unabhängig von der Umgebungstemperatur eine LED Langzeittemperaturstabilisierung garantiert.

2. Definition einer Mission für die regionale Fernerkundung von Küstengebieten

Das am Berliner DLR Standort entwickelte abbildende Pushbroom-Spektrometer bietet eine ausgezeichnete Möglichkeit zur Fernerkundung von Küstengebieten im VIS-NIR. In einer Mission für regionale Fernerkundung von Küstengebieten könnte somit dieses Spektrometer als VIS-NIR Komponente integriert werden. Die Kompaktheit dieses Spektrometers erlaubt eine fächerartigen Modulanordnung mehrerer baugleicher Geräte, um so den typischen Pushbroom-Spektrometer Nachteil der geringen Schwadbreite (aufgrund der Abbildungsgeometrie) zu umgehen. Über die Integration zusätzlicher Sensoren kann eine Abdeckung des SWIR/TIR Bereichs für die Fernerkundungsmission realisiert werden.

In einer Modulaufstellungsanalyse wurde eine Sensoraufstellung entwickelt, die es ermöglicht, verschiedene Sensoren (z.T. fächerartig) auf einem Minisatelliten (~ 300 kg) so anzubringen, dass sowohl Nutzeranforderungen, Satelliteneinbaubedingungen und Kalibrationsanforderungen erfüllt werden. Dank dieser Modulaufstellung kann die vorgeschlagene Mission die Abdeckung des VIS–SWIR–TIR Spektralbereichs über 21 z.T. programmierbare Kanäle realisieren. Die geometrischen Eigenschaften umfassen eine Schwadbreite von 400 km und eine Bodenauflösung von 100 m. Ein Blickfeld (Field of regard) von 87° wird über die Kippeigenschaften (± 30° von Nadir) des kompletten Satelliten sichergestellt. In Verbindung mit geeigneten Bahnparametern (sonnensynchroner Orbit, 775 km Bahnhöhe) kann so beispielsweise jeder Ort über dem Breitengrad 30° innerhalb von 2 Tagen erfasst werden; eine globale Wiederholungsrate ist am 3. Tag garantiert.

Folglich wurde mithilfe am DLR entwickelter Technologien und vorliegender Dissertationsergebnisse gezeigt, dass die vorgeschlagene Mission ein exzellentes technisch realistisches Konzept ist, um das Ökosystem Küstengebiet kosteneffektiv untersuchen zu können.

Ausblick

Die Polarisationsempfindlichkeit wurden in der Gitter-Simulation mit <1% angegeben. Diese Angaben sind noch experimentell zu bestätigen. Weiterhin sind die exakten spektralen geometrischen und radiometrischen Auflösungen unter Verwendung des Trapezprofilgitters (aus der Simulation) und der noch in Entwicklung befindlichen rauscharmen Videoelektronik zu bestimmen.

Die Verringerung der Bildverschmierung kann über die Verwendung von APS-Detektoren (Active Pixel Sensor) bzw. elektronischen Shuttern in Frametransfer-CCDs erfolgen. Jedoch sind beide Detektorarten z.Zt. auf dem freien Markt noch nicht mit den gewünschten Leistungsparametern erhältlich (militär- und kundenspezifisches Design). Dies könnte sich absehbarer Zeit ändern, so dass mit einer Eliminierung der Bildverschmierung gerechnet werden kann. Die Verwendung von APS-Detektoren muss jedoch sorgfältig bedacht werden — insbesondere bezüglich der individuellen Kalibrationscharakteristik jedes einzelnen Detektorpixels.

Die Fokalebeneneinstellung des experimentellen Prototypen erfolgt über die Schrittmotoransteuerung eines Goniometerkopfes. Um konstruktiven Aufwand und Gewicht zu reduzieren, bietet sich folgende Flugmuster-Variante an: die Fokalebene kann in der Endeinstellung an eine Spektrometerwand angeklebt werden. Dem stehen Nachteile nicht-lösbarer Klebeverbindung gegenüber, die noch untersucht werden müssen (z.B. die Verschiebung des idealen Einstellpunktes während des Klebeprozesses).

1 Introduction to regional remote sensing of coastal zones

Background of the study

Since the launch of MOS-IRS on board the Indian Remote Sensing Satellite in March 1996, the ocean-colour science community received after a long pause of almost 10 years the essential information on open oceans and coastal zones. Moreover, the MOS sensor itself is a proof-of-concept instrument representing the first pushbroom imaging spectrometer for spaceborne Earth observation. With the background of these experiences a team headed by Prof. Dr. G. Zimmermann and Dr. A. Neumann of the DLR, Berlin, Germany started with an approach for a successor development. The performed investigations cover initial simulations, an experimental prototype study in the DLR laboratory and a detailed mission concept for regional coastal zone observation.

Structure of the introduction

The introduction gives an physical survey on passive nadir viewing remote sensing from low-Earth orbit (LEO) in the visible (VIS) and thermal infrared (TIR) parts of the electromagnetic spectrum. Therefore the scientific background of remote sensing — both generally and regarding coastal zone problems — is introduced. With this background and with experiences gained during other coastal zone missions the requirements for a new regional coastal zone mission could be concluded.

Goal of environmental remote sensing

Owing to increasing population pressure there is a world-wide scientific and public concern that natural disaster and climate changes will have growing impacts on the environment, e.g. the rate of climate change and depletion of stratospheric ozone caused by human activities.
In response to the problem of potential global climate change, international organisations (WMO[5], UNEP[6]) promoted the establishment of the Intergovernmental Panel on Climate Change (IPCC) in 1988, the development of a Global Climate Observing System and the adoption of the Kyoto Protocol to the UN Framework Convention on Climate Change (UNFCCC) in 1997. As results these activities made clear[7], the prediction of climate change — with respect to time, quantity and regional distribution — contains many uncertainties, particularly the incomplete understanding of

- the sources and sinks of *greenhouse gases* (distribution of CO_2, CH_4, O_3),
- the influence of *clouds* (quantification of radiative transfer),
- the influence of *oceans* (distribution and timing of water constituents),
- *polar ice* sheets (prediction of future sea-levels) and
- the influence of *land surface* (energy and water exchanges with atmosphere).

[5] World Meteorological Organisation
[6] United Nations Environment Programme
[7] UNEP–1998

Obtaining additional information on regional and local bio-productivity, occasional monitoring of catastrophic events are further goals of environmental remote sensing.
The geophysical information for improving our understanding of environmental processes can be retrieved by aircrafts, ships, balloons or buoys. However such data are usually severely limited temporally and spatially, while observations from spaceborne sensors in the recent decades have proved the ability of satellite data to provide the desired information on adequate scales in space and time[8].

Spaceborne remote sensing techniques

In its most general meaning remote sensing encompasses measurements made without physical contact between the sensor and the object. The more specific aspect of spaceborne remote sensing techniques is to focus on the measurement of the earth's surface and atmosphere from space.
Recently, remote sensing has become a major tool for both global weather forecasting, including climate predictions, and regional or local quantification of climate change distributions. For achieving this information a wide spectral range of the electromagnetic radiation reflected, emitted or scattered by atmospheric constituents in conjunction with land or sea surfaces has to be analysed. Depending on the radiation sources remote sensing is separated into active and passive methods. For active remote sensing the major sources are reflected laser beams (LIDAR[9]) or microwaves (e.g. SAR[10]). In contrast, passive methods detect the reflected/scattered solar light or Earth radiative emission. These passive sensors for remote sensing of the Earth are further divided into passive space sounding techniques like limb sounding (MIPAS[11]), solar or stellar occultation (SAGE III[12]) or nadir sounding devices. Whereas limb and occultation sounding are only able to measure vertical concentration profiling of atmospheric components (O_3, N_2O, NO_x, FCKW, H_2O, temperature), nadir viewing space sensors detect radiance from land or sea surfaces with additional atmospheric signal components.
These nadir viewing Earth observation sensors can be placed in various Earth orbits each offering different advantages. Either a geo-stationary (GEO), an elliptic or a low-Earth orbit (LEO) can be chosen for the collection of desired data. While elliptical orbital sensors cannot detect the Earth with constant spatial resolution, GEO sensors provide data with continental-only coverage combined with (so far) relatively low spatial resolution. Therefore both observation modes require numerous satellites for covering most of the Earth's surface.
In contrast, LEO sensors are able to provide both, high spatial ground resolution for local observations and daily or weekly information retrieval for global or regional monitoring.

[8] CEOS–1997
[9] Abreau–1980
[10] Harger–1970
[11] Endemann and Fischer–1994
[12] Chu et al.–1997

Why regional coastal zone remote sensing?

The coastal zone consists of both, land and water, and it includes areas such as open coastline, estuaries, and bays. This coastal zone has always been in the centre of human activities including all possible influences of industries, tourism, agriculture and fisheries on the ecosystem of the coastal zone. In finding solutions for certain regionally oriented environmental problems the coastal zone has to be imaged at adequate space-time resolution. Examples of regional environmental problems are critical (e.g. toxic) algal blooms, coastal eutrophication, (toxic) pollution in river estuaries and flooding in contamination regions. For detecting the location and tracing these environmental events or hazards high ground resolution (~100 m) as well as high repetivity (1–3 days) is required.

The resulting regional-scale and high-spatial resolution data requirements for providing the needed coastal zone information can be met by passive nadir viewing remote sensing instruments in LEO. The spectral regions for an adequate observation are the VIS, the SWIR and the TIR, i.e. the visible (e.g. for water constituents retrieval[13]), the short-wave infrared (e.g. for snow, ice, cloud discrimination) and the thermal infrared (for temperature measurements).

1.1 Remote sensing of the Earth in the VIS-TIR

For receiving scientific overview on remote sensing of the Earth the physical conditions of remote-sensing have to be described. Thereinafter remote-sensing applications and the specific observation requirements for retrieving the needed information are summarised.

The term remote sensing of Earth will be used in the following for remote sensing in the electromagnetic range of 0.4 – 14 µm (particularly the region 0.4 – 2.5 and 8 – 14 µm) retrieved from passive, nadir sounding instruments which are placed in LEO.

1.1.1 Physical conditions of remote sensing

A space sensor observing the Earth in the electromagnetic spectrum from 0.4 – 14 µm measures radiance originating from reflected/scattered sunlight and from Earth radiant emission. Figure 1 shows this part of the electromagnetic spectrum and the spectral regions used for remote sensing observation. While the human eye is capable to 'see' in the visible only, multispectral remote sensing instruments (e.g. spectro-radiometer, scanner) are able to detect electromagnetic radiation over a wider spectral region. Main constrain for using the complete spectrum is related to limited atmospheric transmission. This limitation is shown in the transmission plot in form of hatched areas. The figure also shows the energy level of the exo-atmospheric Sun radiation and compares it with the blackbodies (5300 K, 600 K and 300 K) emission spectra. Both, the Sun (~5300 K) and the Earth (~300 K) are Planckian emitters, however the radiance peak for the solar emission spectrum is located at ~0.5 µm and for the Earth's at ~10 µm. This leads to difficulties during daytime measurements in separating Earth emission and solar reflectance spectra in the region from 3 to 5 µm because both emission and reflectance spectra account for a similar signal level at the sensor[14].

[13] Gordon and Morel–1983
[14] Twomey–1963

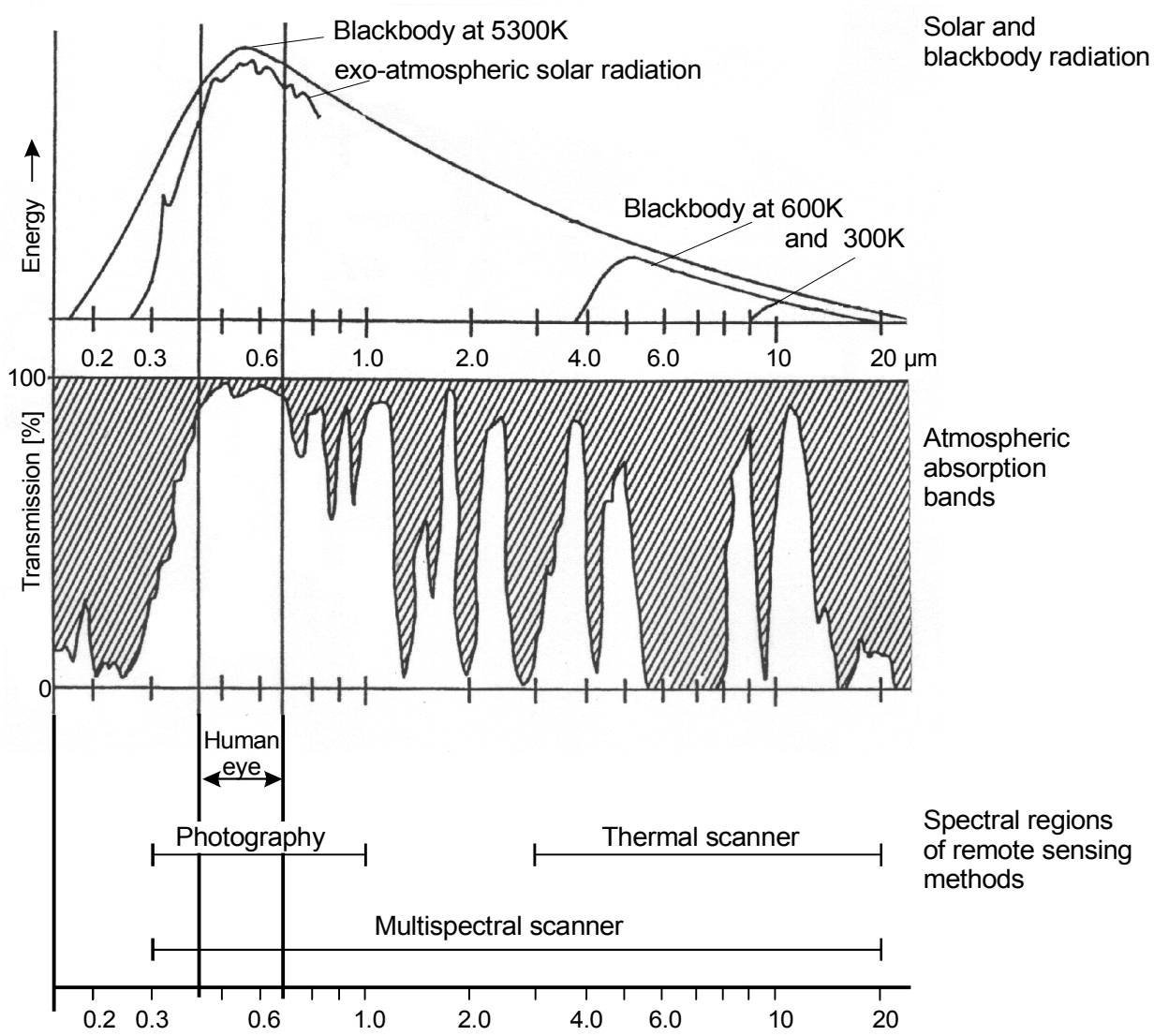

Figure 1: Electromagnetic energy spectrum, the transmission of the atmosphere and spectral regions for remote sensing instruments[15]

The Earth's atmosphere absorbs, scatters or backscatters (reflects) the incoming sunlight and the Earth emission. Insufficient atmospheric transmission limits the possibility of retrieving desired information over the whole spectral region. Consequently, the parts of the regions from 0.4 – 2.5 and 8 – 14 µm are chiefly used for daytime remote sensing. In contrast to the Earth emission, the sunlight has to pass the atmosphere twice (down-welling and up-welling radiance path) before being detected at the orbiting space sensor. To demonstrate the multidimensionality of the problem

[15] adapted from Scherz et al.–1970

Figure 2 shows first order (direct) and second-order (single-scattered) radiance components in the sensor's field of view (FOV).

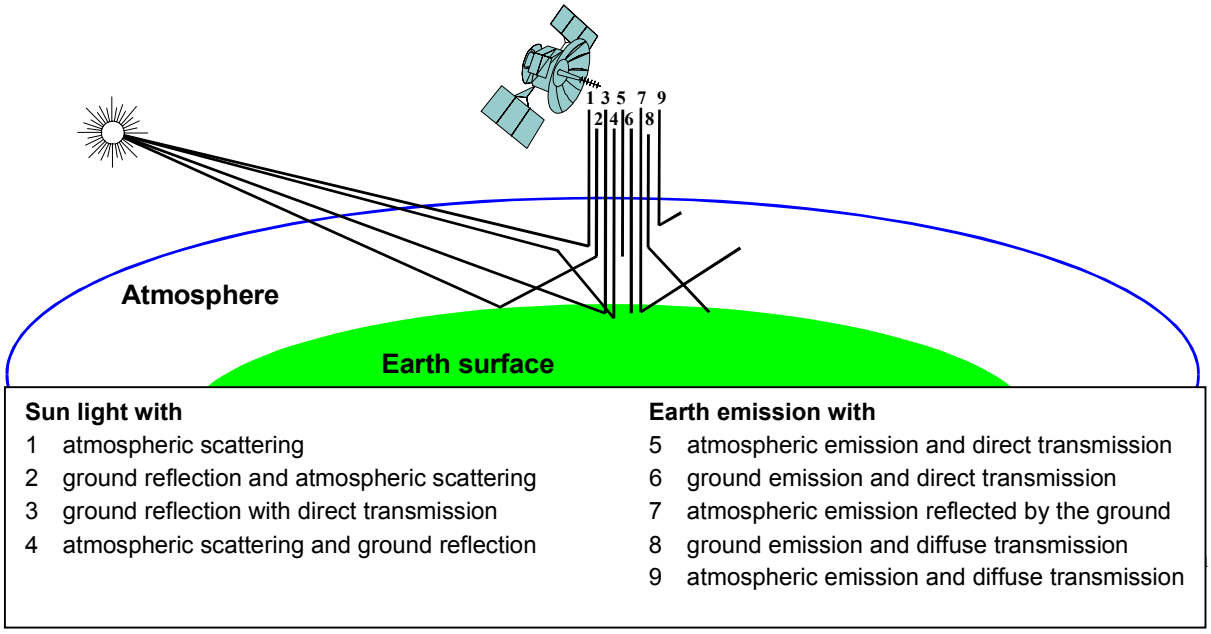

Figure 2: First and second order radiance components in the sensor's FOV[16]

A spaceborne multi-spectral remote sensing instrument produces in general a three-dimensional (3-d) data cube representing two spatial and one spectral dimension of information from the Earth surface. One spatial dimension is created by the forward motion of the satellite, the other results from the FOV of the sensor perpendicular to the ground track. By imaging each ground pixel simultaneously in specified spectral bands the third dimension of the data cube is produced (see Figure 3). The more spectral channels and the narrower the bandwidth the better the representation of the real top-of-atmosphere (TOA) radiance spectral distribution. The term "hyperspectral imaging spectrometry" has been coined to describe remote sensing in many (30 – 200) narrow contiguous spectral bands[17].

[16] adapted from Palmer–1992
[17] Goetz–1990

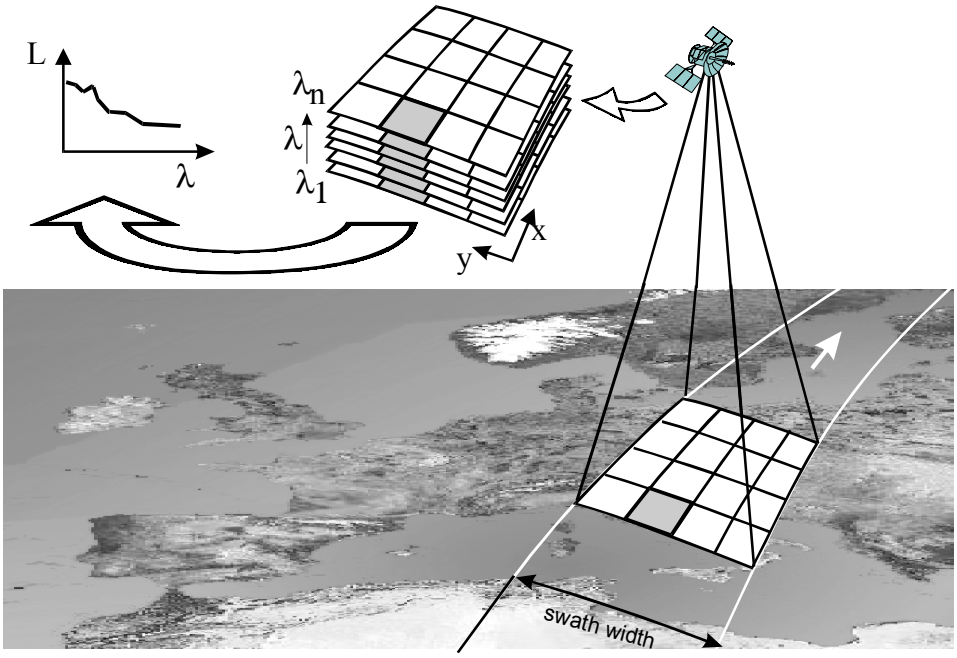

Figure 3: The image cube principle

1.1.2 Overview of remote sensing observation requirements

With hyperspectral spaceborne remote sensing instruments it is possible to acquire dense sampled, nearly continuous reflectance/emission spectra for each pixel of the Earth's surface and/or the atmosphere. This section outlines in a very compressed form possible applications and the resulting observation requirements for several Earth science disciplines. It is shown that each application has their specific spectral and spatial requirements. More details can be found in the literature[18,19,20,21].

1.1.2.1 Remote sensing applications

In general remote sensing application can be divided in object-related and non-object-related applications. The object-related applications are subdivided into ocean and coastal waters, atmosphere, vegetation, minerals–soil, and snow–ice–clouds. Examples for non-object-related applications are land use (e.g. agriculture, forestry, vegetation, urban, industrial), surface covering (vegetation, snow, ice, soils), event monitoring (e.g. hazards, floods, bio-burning) and texture determination (e.g. geological lineaments, roads, railroads, airports). In the following the object-related application are discussed in more detail.

Oceans, coastal and inland waters:

[18] Zimmermann–1991
[19] Goetz et al.–1987
[20] Readings et al.–1991

With the collection of remote-sensing ocean-colour data it is possible to study mesoscale processes in the open ocean, e.g. maps of phytoplankton. Moreover, spaceborne remote sensing enables the retrieval of regional-scale information to study phenomena of temporal and spatial variability (e.g. spring bloom, coastal up-welling events, fish distributions, detection of algae blooms). It is also possible to retrieve information on coastal environmental problems such as coastal eutrophication, pollution in river estuaries, flooding in contaminated regions, heavy rainfall in catchment areas and many more.
However, for the retrieval of water constituents (e.g. chlorophyll) it is necessary to treat atmospheric effects (molecular and aerosol scattering) and direct surface reflectance accurately[22]. The correction is realised in assuming that the radiance in the near infrared will be absorbed by the water. This means that a near infrared top-of-atmosphere signal measured by the satellite sensor results from atmospheric backscattering (such as aerosol scattering) and direct surface reflectance. By applying a wavelength dependency of these terms the visible channels can be corrected. This assumption for atmospheric and water surface correction is valid only for the open ocean (black water in the near infrared) where the retrieval of water constituents can be realised successfully. Note, that in literature the term atmospheric correction often includes both, atmospheric and water surface corrections.
In contrast to open ocean waters, only modest advances have been made in the examination of inland and coastal water. These waters require special attention because of limited geographical extent, complex interfaces between land and water and vigorous dynamics. Moreover, a special problem arises for the atmospheric correction over waters with higher sediment or pigment concentration: The classical atmospheric correction fails because the near infrared can not be assumed to be black for aerosol scattering corrections[23] (see also Chapter 1.2).
Further remote sensing applications over water surfaces are the mapping of various continental and maritime aerosols over clear water, the possible correction of atmospheric effects in land scenes close to oceans and the ocean current investigations by means of temperature measurements.

Atmosphere:

The main purpose of nadir remote sensing data is the detection of Earth surface targets, however atmospheric influences cannot be neglected: up to 90 % of the signal measured by the sensor over Ocean can account for the atmosphere (Rayleigh and aerosol scattering in the shorter wavelengths). This demonstrates the importance of adequate detection of atmospheric contributions (e.g. total aerosol load) for achieving a good atmospheric correction.
Other remote sensing applications are the retrieval of atmospheric constituents (e.g. CO_2 mapping, methane measurements). But this task is mainly performed by special limb sounding remote sensing instruments (e.g. SCIAMACHY, MIPAS) and will not be discussed here.

[21] Rast–1991
[22] Gordon et al.–1983
[23] Krawczyk et al.–1995

Vegetation:

In the spectral range from 0.4 – 2.5 μm the biomass and the water content of leaves can be detected. Other vegetational applications of remote sensing data are physiological processes including photosynthetic activities and transpiration. This information can serve meso- and local-scale scientific needs. An example of a mesoscale parameter is the net primary productivity by plant communities which is related to the total leaf area. In the local scale space remote sensing helps to map vegetation stress by detecting excesses or deficiencies in the soil.

Minerals and soil:

With spaceborne remote sensing instruments it is possible to identify many minerals directly when the Earth surface is not covered (e.g. in deserts) by vegetation or water. In the spectral region from 0.4 – 2.5 μm the spectral characteristics of more than 1000 minerals (Fe^{2+}, Fe^{3+}, OH, CO_3, SO_4 – bearing minerals)[24] can be retrieved because of the mineral's diagnostic electronic and vibrational transition. For global studies it is necessary to characterise and map the surface materials, providing a better understanding of the nature and the distribution of crustal units (e.g. search for nonrenewable resources, detection of the deformation history of the Earth).

Snow, ice, clouds:

Ice and snow target parameters (snow/ice extent, concentration, motion, albedo, absorbing impurities) can be retrieved using the spectral range from VIS to SWIR[25]. An important example is the snow–ice–cloud discrimination by using additional SWIR measurements because it is hardly possible to perform this discrimination in the visible only (compare spectral characteristics of fresh snow and clouds in Figure 4).

[24] Goetz et al.–1982
[25] Warren–1982

1.1.2.2 General observation requirements

For multispectral remote sensing applictation it is necessary to choose adequate observation requirements. These requirements cover spectral, spatial, radiometric and orbital parameters. Not considered in this section are calibration requirements which are discussed separately in Chapter 1.3.

Spectral requirements of various applications

The spectral requirements for a remote sensing instrument are subdivided into the specific location of the channels' centre wavelength and the bandwidth $\Delta\lambda$. Both parameters have to be selected adequately corresponding the specific research task.

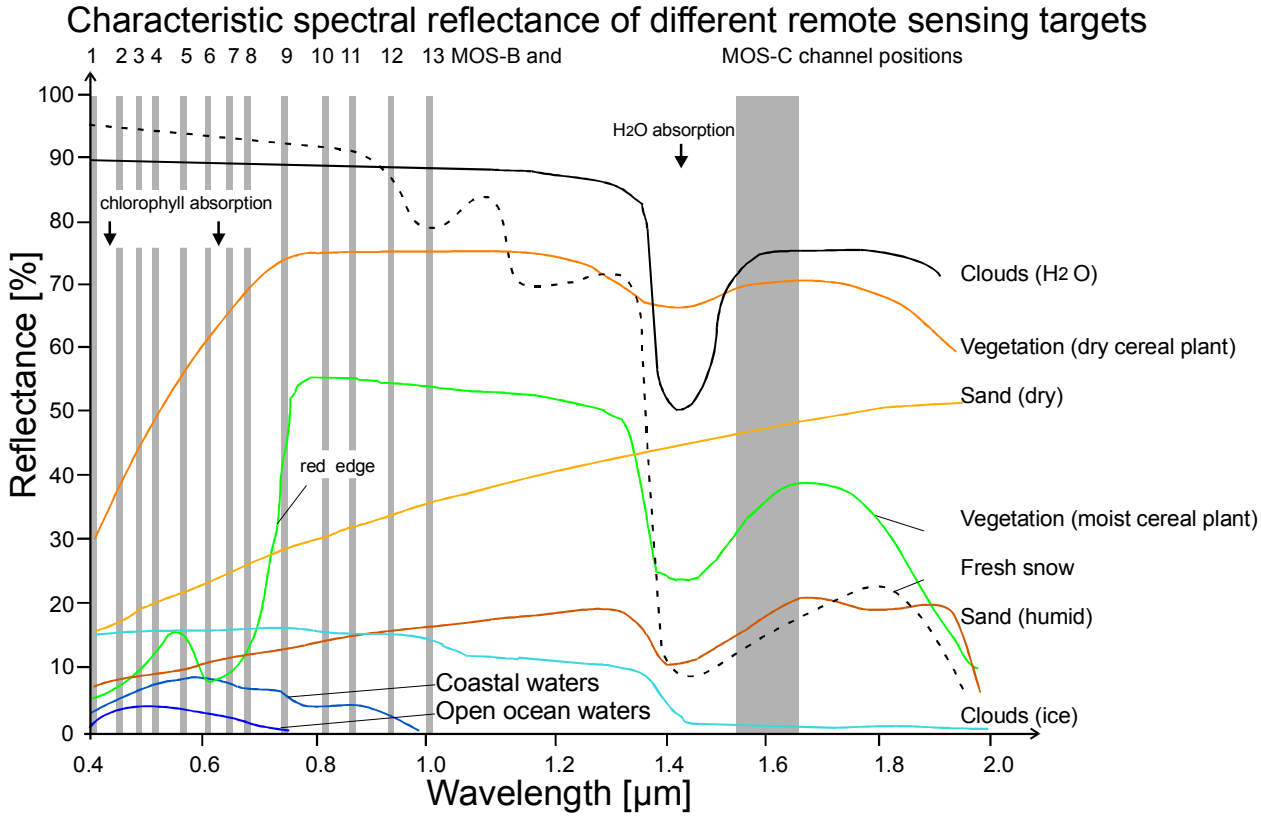

Figure 4: Spectral characteristics for different remote sensing targets and the position of MOS-B and -C channels[26]

In Figure 4 the typical spectral characteristics (spectral signatures) of various targets are shown as reflectance curves plotted over the wavelength. For example the reflectance of moist cereal crops has few significant absorption bands, i.e. spectral regions where only a small amount of radiance is reflected: the chlorophyll absorption (at ~450 and ~650 nm) and the H_2O absorption located in the SWIR (1.4 µm, 1.9 µm, 2.7 µm). When the state of the vegetation changes from moist to dry cereal crops, the number of chlorophyll pigments and the water content in the plant decrease. Hence, the irradiating photons will be reflected instead

[26] after Zimmermann–1999

of absorbed. As a result the reflectance curve increases and it is possible to sense remotely the state of the vegetation (e.g. by using the Normalised Difference of the Vegetation Index NDVI[26]).
For different applications the specific spectral characteristics can be defined in applicational target parameters. In general the sampling of a certain number of spectral channels is necessary to retrieve these spectral signatures. Since some target parameters can be retrieved by only one single channel (e.g. surface temperature), most applications require the detection of a representative spectral signature (a group of specific spectral bands) for retrieving the desired information (e.g. red edge for analysing vegetation stress).
Figure 5 gives an overview of main applications and corresponding target parameters, plotted over the spectral range from 0.4 – 14 μm (excluding the MIR). The black lines represent the spectral regions where the target parameter's representative spectral signature can be detected. It can be seen that the number of spectral channels of specific spectral and radiometric resolution increases with the number of parameters which a sensor is required to detect.

For detecting a variation of the signature in these spectral regions an adequate spectral bandwidth $\Delta\lambda$ has to be selected. The classical spectral resolution requirement for VIS-NIR remote sensing applications has been $\Delta\lambda_{land} < 90$ nm for typical land and vegetation measurements (e.g. NDVI, land classification) and $\Delta\lambda_{water} < 20$ nm for (open-ocean) water measurements. These requirement has been chiefly made up by technical sensor constrains than by applicational needs. As it will be shown in the following section, future sensors should have an improved spectral resolution of $\Delta\lambda < 5$ nm for enabling better vegetation (e.g. red edge) and (coastal) water measurements. The requirements for spectral resolutions at longer wavelengths are $\Delta\lambda_{SWIR} < 20$ nm in the SWIR. For temperature measurements in the TIR the complete bandwidth of atmospheric window can be used ($\Delta\lambda_{TIR} < 2$ μm) for most environmental applications[27]. More accuracy can be provided by split window methods which also require at least two thermal channels and a higher spectral resolution[28].

[27] Readings et al.–1991
[28] Prabhakara etal.–1974

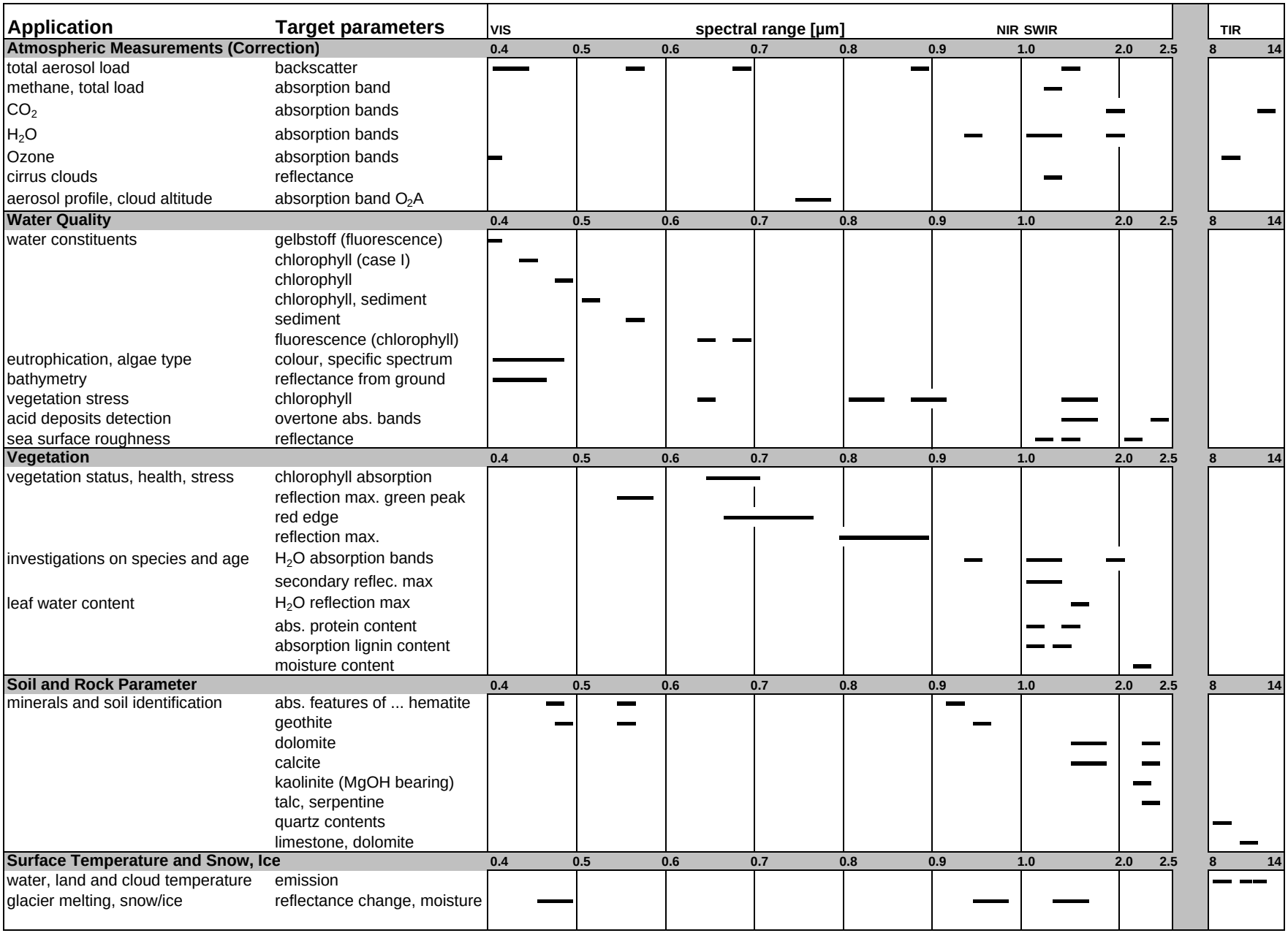

Figure 5: Spectrally orientated survey of main applications for environmental remote sensing

Radiometric requirements

One of the most crucial requirements for adequate remote sensing is the radiometric performance of the remote sampled data, i.e. signal level, noise equivalent radiance (*NeΔL*), signal-to-noise ratio (*SNR*).

These parameters shall be explained for an example which is very important for the oceanography: the detection of the change of 10% in chlorophyll concentration in the open ocean waters. For the atmospheric contribution a marine type aerosol, 23 km visibility is assumed. The atmospheric contribution has a strong wavelength dependency and can reach values over 95%. The calculation of the needed radiometric requirements is performed for the chlorophyll detection channels only.

For chlorophyll measurements over open ocean a channel at ~443 nm can be used for absorption measurements of the chlorophyll[29]. The difference of chlorophyll concentration from 0.1 to 0.01 mg m^{-3} would cause a change from 3 to 5% of the water reflectance. Adding about 95% atmospheric contribution the expected sensor signal at a solar zenith angle of 40° from sub-satellite point is in the range of 5 $\mu Wcm^{-2}sr^{-1}nm^{-1}$. In the case the chlorophyll concentration has to be detected with an accuracy of 10% and assuming a relatively linear increase of radiance levels between 0.1 to 0.01 mg m^{-3} chlorophyll, a required minimum resolvable radiance, i.e. the noise equivalent radiance *NeΔL*, of 0.01 $\mu Wcm^{-2}sr^{-1}nm^{-1}$ is necessary. For this example the *SNR*, i.e. the ration of the maximum observed radiance to the minimum detected change in radiance coming from the chlorophyll, would be 500. Note that these radiometric requirements do not consider the requirements for an adequate atmospheric correction in the NIR.

Spatial requirements

In general, the spatial (also geometric) parameters can be subdivided into the sensor's spatial resolution on ground and the swath width of the sensor. The spatial resolution Δx is expressed by the size of the resolved ground pixel. It depends on the sensor's instantaneous field of view (*IFOV*). The *IFOV* is defined on one side by the solid angle $IFOV = d/f$ [rad], where d is the detector size and f the optic's focal length. On the other side, it is defined in linear dimensions by $IFOV = Hd/f$ [m], where H is the sensor's altitude. The *IFOV* describes the area, which is captured by the solid angle at the distance H. This area is called picture element (pixel).

A number of ground pixels perpendicular to the flight path (see also Figure 3) make up one swath. The swath width SW is $2H * \tan(FOV/2)$ [m], where *FOV* is the sensor's field of view across the flight direction.

With current sensor development towards high ground and spectral resolution with many contiguous spectral bands, high data rates are expected. These hyperspectral imagers have some technology related restriction (e.g. limited FOV, data rate and image read-out frequency). That is why a minimum scene size has been defined. It is the smallest size of the

[29] Gordon et al.–1984

investigation field in which scientists are able to retrieve desired information for the specific applications. These restriction are listed in Table 1 regarding various applications.

Table 1: Spatial sensor requirements for different applications[30]

Application	IFOV Δx	Scene size (min)	Desired coverage
Non-renewable resources exploration	2 – 30 m	40 km x 40 km	seasonally
Land use planning	2 – 10 m	10 km x 10 km	weekly-monthly
Cartography (Mapping)	1 – 5 m	30 km x 30 km	monthly
Resource Management	5 – 30 m	40 km x 40 km	weekly-monthly
Environmental Assessment	2 – 10 m	40 km x 40 km	weekly
Agricultural/Forestry	5 – 30 m	40 km x 40 km	2 days – 2 weeks
Marine	20 – 1000 m	80 km x 80 km	2 – 7 days

For remote sensing applications the terms local, regional, and global observation are commonly used. These are related to the sensor's IFOV and the size of the observable scene. Whereas local observation is defined by a ground resolution of < 20 m and a scene size of 10 km x 10 km, regional observation requirements are about 100 m (IFOV) and 400 km x 400 km (scene size) and global observation 1000 m and 1600 km x 1600 km, respectively.

Low Earth orbit (LEO) requirements

A sensor placed in a LEO will mostly have an orbital height in the range of 250 – 1000 km combined with an inclination angle from 28° to 104° (angle between orbital track and equator). The orbital height and inclination in conjunction with the sensor's imaging parameters define operational parameters such as ground resolution, area coverage and repetivity of the measurements. For example, the satellite altitude affects the ground resolution and the swath width: The higher the sensor (with given IFOV and FOV), the larger the area which can be observed, but the smaller the ground resolution. The ground resolution can be increased by using a larger aperture with additional costs for size and weight. Alternatively the ground resolution can also be increased by reducing the orbit altitude, with the disadvantage of orbit perturbation owing to atmospheric drags and reduced repetivity. An other important orbit parameter is the overflight time: when a constant local overflight time (i.e. constant Sun illumination conditions) is required the sensor has to be placed in a Sun-synchronous orbit. This orbit is defined with an inclination angle between 96.16° (250 km) and 99.49° (1000 km).

Since no single satellite can cover the entire surface of the Earth by a single scan, the parameters coverage rate and repetition rate have also to be defined. The coverage rate is the percentage of the Earth's surface which is covered by the sensor in a defined time period and depends on both, the satellite's orbit (e.g. height, inclination) and the sensor's FOV. The repetivity rate is the time the sensor will be able to repeat the measurement of the same spot

[30] adapted from Claybaugh–1997

on Earth surface and depends like the coverage rate on the satellite's orbit (e.g. height, inclination). But in contrast, the repetivity depends also on the sensor's *FOR*. Whereas the Earth's swath width is defined by the sensors *FOV*, the *FOR* defines the possible swath width, which can be increased by a tilt capability ($FOR = FOV + 2 * \left|\delta_{tilting}\right|$).

Consequently, the optimal orbit for the specific research task is a compromise of various parameters and depends on the specific application requirements. Depending on these specific application requirements the orbital parameters have to be analysed separately in a mission study.

1.2 Remote sensing of the coastal zone

The term coastal zone includes both, water (such as open coastline, estuaries, and bays) and land (such as vegetation at coastal shores) and it has become the standard term in use by government and scientists.

The motivation for remote sensing research in the coastal zone originate from the need to understand the role of the world coastal regions for global circulation and climate and from the necessity to find solutions for certain regional environmental problems (environmental management). Further on the coastal zones waters have the highest bio-activity of all waters with the result that these waters are also very important from the economic point of view (e.g fishery) [31,32].

These goals can be met by sampling Earth surface data (with mainly high spectral and medium spatial resolution) and developing new algorithms for a better quantitative retrieval of geo-/bio- physical properties of the coastal zone.

1.2.1 The atmosphere-ocean system

For remote sensing of the coastal zone the most important target parameter, i.e. the reflectance of the water, has to be detected. This is a very complex task because the total radiance measured by the space sensor is influenced by many components. Only a very small part of the measured signal is related to the needed information.

For passive optical remote sensing the Sun is the illumination source. The space sensor will detect this radiance after it has passed the atmosphere twice. During these atmospheric passes the radiance will vary in terms of intensity (e.g. variation of the spectral signature) and spatial distribution because of the influence of the atmosphere. The only solution to retrieve the desired information is to handle this influence accurately.

1.2.1.1 Influence of the atmosphere

The influence of the atmosphere on the remote sensing signal can be described by three major effects: absorption, scattering and blurring

Absorption

In the electromagnetic spectrum there are different absorption bands in which the transmitted radiance is attenuated. In the VIS–NIR the main absorber are H_2O, O_3, and NO_2 (see Figure 6). When selecting adequate spectral channels for remote sensing special attention has to be taken for these absorber bands.

Scattering

The scattering from air molecules (Rayleigh scattering) and aerosols cause a crucial effect for remote sensing: Down-welling Sun irradiation is scattered by molecules and aerosols.

[31] IOCCG–1998
[32] IOCCG–1999

Therefore the coastal zone ground pixel will be brightened by diffuse irradiation additionally to the direct solar irradiance. After interaction with water constituents the up-welling radiance will be scattered again. In the case of ocean remote sensing the top-of atmosphere radiance consists of ≤ 10% reflected radiation from the water body. More than 90% of the signal results from diffuse radiation effects. In addition these effects have a spectral dependency which increase the blue radiance level.

Blurring

While the diffuse radiation effect of the atmosphere changes the spectral distribution of the down- and up-welling radiation, the same effect changes the spatial distribution of the ground signal: A part of the radiation which is outside the observed ground pixel attain in the observing cone of the sensor. As a result the sensor measures additional photons which originate from neighbouring pixels. Blurring becomes crucial when observing inhomogeneous ground (e.g. estuaries, inland water) where the vegetation can cause additional radiance components for the water pixel.

Because of this effect the effective ground resolution is coarser and can reach factor 3–4 depending on the optical depth of the atmosphere.

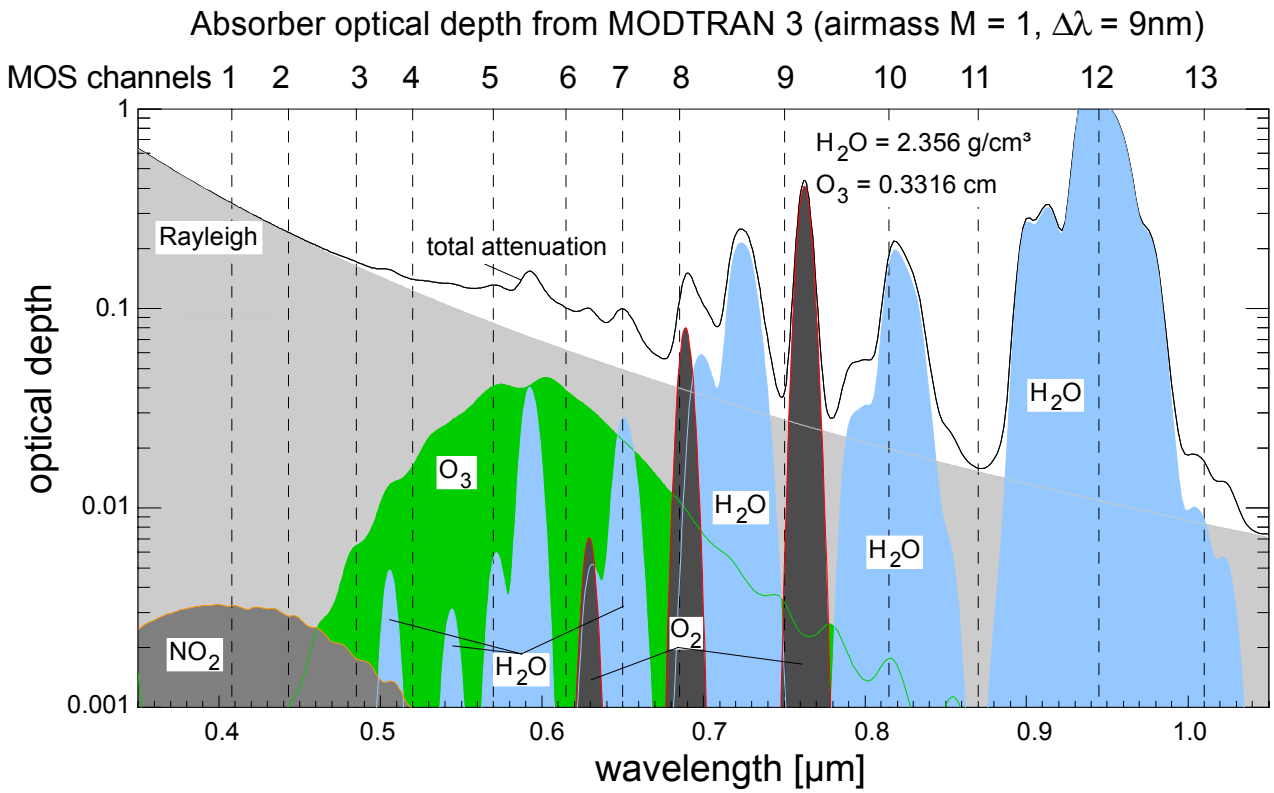

Figure 6: Influence of the main absorber on the optical depth in the VIS–NIR[33]

[33] after Pflug–1999

1.2.1.2 The general remote sensing equation

Because of the scattering in the atmosphere the measured space sensor signal consists of a number of radiance terms which are composed by the observed ground pixel, the atmosphere and the surrounding of the observed pixel. These signal components expressed in dimensionless reflectance R can be described in the following equation[34].

$$R_S = R_a + R_{pg} + R_{pw} + R_{ap} + R_{apw} + R_{ua} + R_{aua} + R_{ms}$$

where R_S is the (top-of-atmosphere) reflectance at the sensor. Out of these eight terms only the term R_{pW} and R_{apW} contain information on the target, however for quantitatively determination of these terms it is important to assess all terms of the remote sensing equitation. Otherwise it is not possible to retrieve the desired information out of the detected R_S. The different terms are:

1) R_a (atmosphere): The radiance of this term originates from single or multiple scattering in the atmosphere (Rayleigh and aerosol scattering). The kind of scattering delivers the largest contribution to the TOA ocean signal R_S. Moreover this term has a high variability and it consists of no information about the ground pixel. It is very essential to correct the sensor signal for this term because of its high contribution (factor 3–5 compared to water reflectance) to R_S.

2) R_{pg} (Sun glitter): This term is the result of the direct reflection (Fresnel reflection) of the Sun's photons at the water surface in the observed pixel. Sun glitter causes problems mainly for remote sensing of water surfaces because the glitter does not carry any information on the water constituents. A possibility of avoiding this term is the adequate selection of the illumination (Sun angle) and sensor observation geometry.

3) R_{pW} (water, direct): The photons for this component are transmitted from the Sun directly to the water pixel. They pass the boundary air–water and and after interaction with water constituents they are remitted to the atmosphere again. After another direct transmission these photons will be detected by the space sensor. This term carries the main information on water body and constituents.

4) R_{ap} (sky glitter): The photons for this term come from the scattering process in the atmosphere. The diffuse radiation is reflected directly at the water surface to the space sensor. In contrast to the Sun glitter, this term is not avoidable by changing the sensor observation geometry.

[34] Zimmermann–1991

5) R_{apw} (water, diffuse): The photons of the diffuse sky radiance penetrates the water, interacts with the water and are directly transmitted to the space sensor. This is the other information carrying term of the equation.

6 + 7) R_{ua} (blurring, direct), R_{aua} (blurring, diffuse): These components are related to photons which are transmitted directly/diffuse to a pixel neighbouring the observed pixel. After (Fresnel) reflection on the surface these photons are scattered and they will find the way in the observing cone of the sensor.

8) R_{ms} (multiple scattering): This term carries all these reflectance components which originate from multiple interaction process in the atmosphere, the neighbour pixels and the observer pixel.

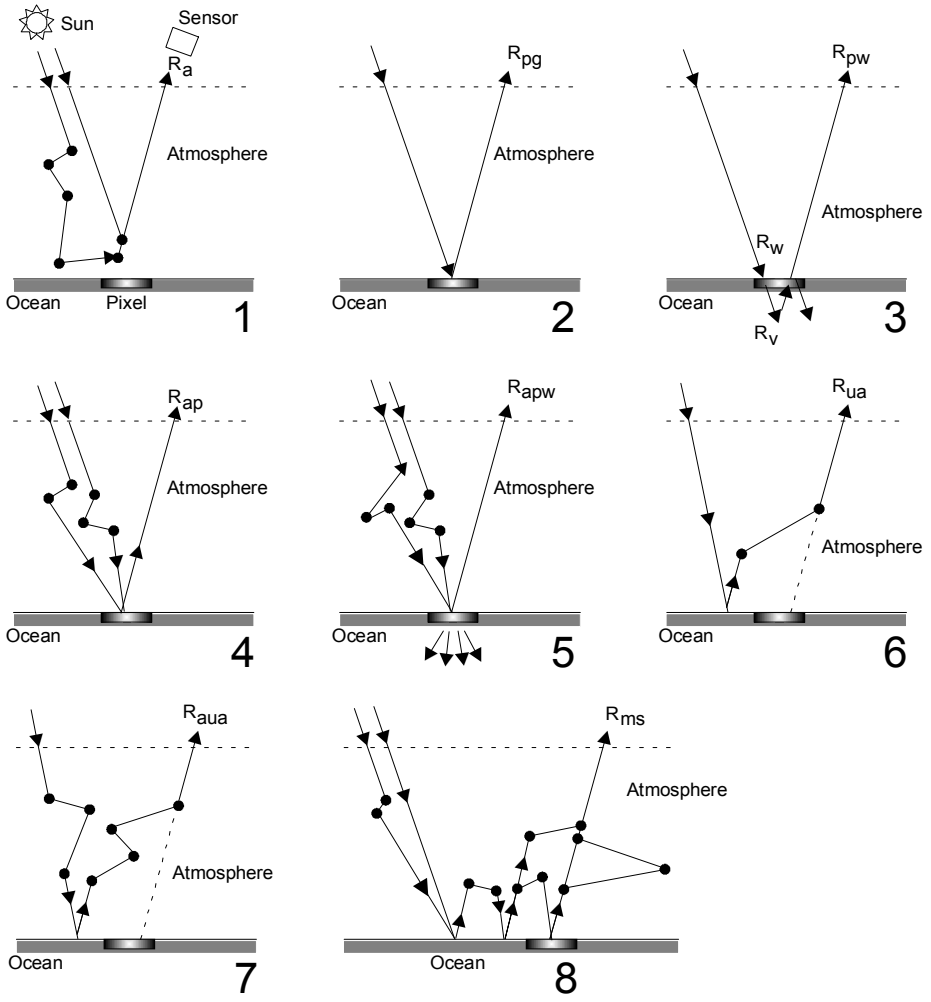

Figure 7: Interaction processes of the incoming solar radiance for the ocean: terms 1–8 [35]

[35] after Zimmermann–1991

1.2.2 Scientific background and research needs

Ocean colour remote sensing performed the first footsteps in the operational time of the Coastal Zone Color Scanner CZCS (1978–1986)[36]. Since that time algorithms and ocean models found the way from theory to general applications. Also new remote sensing instruments were developed on the basis of this first experience. Up to the year 2003 many new ocean colour missions are planned following the track marked by CZCS. However these missions are orientated on global ocean research, i.e. dedicated to understand better and to quantify the role of the ocean in global circulation and climate. But in contrast the awareness is increasing among scientists and in government that coastal waters and ecosystems are of critical importance for a suitable environment management[37]. An overview of this scientific background is given in this section by summarising the research needs for regional coastal zone applications published recently[38].

In general, the coastal zone can be divided in land and water regions. Whereas water appears as case-1 and case-2 waters[39], coastal land follows the common land classification (see Chapter 1.1.2.2). The matter exchange between land and ocean is called land-ocean interaction.

1.2.2.1 Case-1 waters

Case-1 or open ocean waters are waters for which phytoplankton and their natural decay materials control the optical properties. For retrieving an accurate determination of the amount of phytoplankton an atmospheric correction has to be performed. This correction algorithm uses a simple fact: case-1 waters can be assumed to be ‘black’ in the NIR. After an extrapolation of the atmospheric properties to shorter wavelengths, an atmospheric correction of the VIS channels can be performed. Subsequently single-variable water constituents, e.g. chlorophyll plus covarying constituents can be determined quantitatively. For these case-1 waters various physical and bio-optical algorithms and models have been developed, and consequently open ocean remote sensing is quite well understood[34].

1.2.2.2 Case-2 waters

In contrast to the open ocean, case-2 waters (or coastal waters) consist of a mixture of organic and/or inorganic water constituents. This coastal zone water mixture contains also suspended or dissolved matter in the surface layers. These can be constituents originating from land and/or atmosphere, or components transported to coastal waters by river run-off, wind and sewage discharge. Constituent and property distribution may also be depend on season and region. Therefore the tracking of coastal processes (coastal dynamics) and algae type discrimination and distribution are important research tasks for adequate environmental remote sensing of the coastal waters.

In the following the scientific background is described on the basis of different optical effects: retrieval of optical active components in the case-2 waters, algae type determination,

[36] Evans and Gordon–1994
[37] IOCCG–2000
[38] Neumann et al.–1998
[39] Morel and Prieur–1977

atmosphere over coastal waters, and coastal dynamics. The scientific background of inland water remote sensing has also been introduced because of comparable problematic to the case-2 waters.

Optically active components in coastal waters

As mentioned above, the problem of water constituent retrieval (phytoplancton) in case-1 waters is more or less solved. Case-2 waters have more constituents and an high complexity of interactions, so that the two classical open-ocean approaches of bio-optics and data interpretation fail:

In coastal waters there are at least three possibly constituents (phytoplankton, suspended inorganic matter, dissolved organic matter) jointly influencing the spectral signature. No part of the spectrum can be related to the influence of one component only. Therefore new bio-optical interpretation algorithms have to be developed. For the specifics of case-2 water and the motivation of needed environmental monitoring these algorithms should be capable to retrieve several water constituents in case-2 waters.

For a decomposition of the components it is necessary to use the full information contained in the spectral characteristics. Therefore the space sensor should have sufficient number of spectral channels (number of bands >> number of parameters), a sufficient spectral coverage and resolution (VIS, NIR) to assess water constituents, and an extended spectral coverage (SWIR) to account for the surface term and atmospheric influence over highly turbid waters.

Atmosphere over coastal waters

The atmospheric correction of the remote sensing signal is essential for having a chance for water constituent determination. This has been successfully demonstrated for case-1 waters (see Chapter 1.2.2.1). However, the case-1 waters approach for the atmospheric correction procedure is not applicable because case-2 waters can not assumed being black in the NIR due to high turbidity and bottom effects at shallow waters contributing to the radiances in the NIR. Therefore new approaches in form of algorithms (atmospheric correction algorithms) have to be developed to account for atmospheric influence over case-2 waters.

The observational requirements for a space sensor are additional programmable spectral channels which allow the development of the targeted algorithms. An extended spectral coverage (SWIR) is needed to assess the atmospheric influence (see above).

Different types of algae

There are critical events (e.g. enhanced blooms of Phytoplankton, blooms of toxical algae) which may occur along the coast line. To enable detection and monitoring of these events the specific spectral characteristics of the blooms can be used.

The scientific task is to provide specific algorithms which are able to discriminate the algae type, to assess HAB's/red tides and to assess spatial characteristics of coastal waters phenomena.

A space sensor should have adequate and maybe programmable spectral channels to allow the adaptation to specific phenomena, the development of new algorithms and a better retrieval accuracy.

Coastal dynamics

The coastal zone phenomena have a high dynamics in terms of space and time. These processes are in much shorter scales than for the open ocean. The scientific tasks are to detect and trace these phenomena accurately for regional and seasonal specifics of case-2 waters.
Therefore the space sensor should provide high spatial resolution and a short ground repetition time (1–2 days revisit time).

Inland waters

Inland waters (e.g. lakes, water reservoirs) have a comparable characteristic as coastal waters. Although there are differences in the amount of suspended minerals and organic materials most of the above mentioned coastal-water scientific tasks are also valid for inland waters.

1.2.2.3 Land-ocean interaction and coastal land

Since a huge part of the human activity is concentrated in coastal zones, the direct (e.g. toxical pollution) and indirect (e.g. surface matter exchange) impact of human being can play a crucial role on the coastal ecosystem. For tracing all possible sources of environmental disturbers it is necessary to investigate the land-ocean interactions in conjunction with coastal land classification.
Land-ocean interactions cover significant impact in form of material exchange and pollution and from urban/industrial expansion, tourism, fishery, agriculture. Therefore high spectral and spatial resolved VIS–NIR data has to be provided. Synchronous measurements in the SWIR and TIR can provide an unique synergetic data for detecting and tracing the spread of pollution (e.g. flooding in contaminated regions, heavy rainfall in catchment areas).
On the other hand investigations on the coastal land are necessary to evaluate the erosion and desertification, soil type, vegetation type,snow/ice cover and land-use classification. Up to now, these classical land research tasks have been performed with data from sensors (Landsat, Spot) which detect the Earth surface with high spatial resolution (Δx = 20-30 m). However, these sensors have channels with a spectral resolution of $\Delta\lambda$ = 70-90 nm in the VIS-NIR. This relative low spectral resolution follows land use and planning requirements with applications (such as NDVI and land classification) where such a spectral resolution is sufficient. In contrast, higher spectral resolution is needed for analysing the impact (e.g. vegetation stress, coastal eutrophication) on the coastal ecosystem.
Concluding, these phenomena of land-ocean interaction together with coastal land classifications can be analysed with the assessment of waters, vegetation, catchment areas and snow/ice cover. Consequently, the channels in the VIS should be adaptable to vegetation features (e.g. red edge), too. Additional bands in the SWIR and TIR should allow the retrieval of more land-related target parameters (see Figure 5). Moreover, sufficient spatial and

temporal accuracy is necessary to locate the impacts on the coastal ecosystem (e.g. for monitoring the pollution's source (type) and trace (velocity)). Therefore a revisit time within 1–3 days should be provided by the space sensor.

1.3 Experience from recent ocean-colour missions

Although there were many spaceborne instruments that had sensed the ocean recently, most of these instrument's spectral bands, spatial resolution and dynamic range were optimised for land or meteorological use. That is why instruments devoted to the measurements of ocean colour and flown on a spacecraft are very rare. In the past decades experiences in spaceborne open ocean and coastal zone remote sensing have been provided by mainly three missions: The Coastal Zone Color Scanner (CZCS) [40], the Mehrkanal Spektrometer (MKS)[41,42] and the Modular Optoelectronic Scanner (MOS-IRS)[43].

The very successful multi-channel scanning radiometer CZCS viewed the ocean on global scale in the years from 1978 to 1986. It provided the user community a new tool: phytoplankton concentration maps. Additional, the sensor's infrared channel was used for the surface temperature measurements, e.g. for the determination ocean currents.

In contrast, the MKS experiments were non-imaging 18–channel spectrometers on board various satellites and space stations (Intercosmos–20, –21, Salyut and MIR station) providing data from 1979 till 1988[44]. The main goal of these experiments was the collection of the VIS–NIR spectrum data on the ocean-atmosphere system for the development of algorithms for the determination of the state of the ocean (in particular its bio-productivity).

The follow-on instruments of the MKS series were the MOS pushbroom imaging spectrometers MOS-PRIRODA[45] and MOS-IRS, which have been launched in 1996. Since then especially MOS–IRS provides data from 17 narrow spectral VIS–NIR and one SWIR channels at medium spatial resolution on the atmosphere-ocean system. The acquired spectral high resolution data give new and improved potential to transfer measured data into the spectral characteristics of the ocean and allow better quantitative retrieval of the geo-/bio-physical properties of water, especially for the more turbid case-2 waters.

Recently, further global ocean colour remote sensing instruments have been launched (SeaWiFS, MODIS)[46]. Many useful information and experiences are expected from these sensors in near future.

[40] Evans and Gordon–1994
[41] Bischoff et al.–1983
[42] Zimmermann et al.–1985
[43] Zimmermann and Neumann–2000
[44] Intercosmos–1984
[45] Zimmermann et al.–1993
[46] see Appendix A

In the following only the gained experiences during the CZCS, MKS-M and MOS-IRS missions are summarised:

With CZCS sensor layout it is possible to achieve case-1 water constituent determination in a global scale. However, future ocean colour missions should provide improved capabilities which are the result of experiences of the CZCS experiments[38, 47]:

- Pre-flight calibration with an absolute uncertainty of 3–5%.
  This calibration accuracy is practicable with today's calibration technology. It provides a proper setting of the saturation radiances and a starting point for effective vicarious calibration after launch, however, this calibration uncertainty will not yield a system which can retrieve realistic pigment concentrations.
- Overall sensor performance with a radiometric stability of ± 0.5%.
  This sensor stability inferred from the accuracy of the pigment retrieval, will be in the order of 0.5 to 1%. For ensuring that a single (vicarious) calibration effort will suffice for the live of the instrument the stability of the instrument has to have at least this accuracy. As a result future sensors should provide the capability of quantitatively characterising variations in their radiometric state with an error of no more then ± 0.5%. The goal is to perform this characterisation at the noise level of the instrument.
- Improved in-flight calibration capabilities.
  The capability of quantitatively characterising variations in the radiometric state can only be provided by improved on-board systems for monitoring the radiometric stability of the sensor which utilise the entire optical train. Monitoring and calibration methods like frequent solar and lunar calibration can ascertain the observation of long-term variations of the sensor.
- Improvement of the accuracy of the system sensor–algorithm.
  For an improvement of the accuracy of the system sensor–algorithm it is necessary to use an initialisation process which provides atmospheric as well water-leaving radiance measurements. Hence an accurate setting and tuning of the system (sensor plus algorithms) can be performed.
- Ocean observation from ground station in relatively clear waters.
  To obtain daily in-situ measurements simultaneously with satellite overflight on open ocean, at least one clear water station should be established to provide data where a strong horizontal variation of Chlorophyll can be avoided (no subpixel structure).
- others: maximum values of polarisation sensitivity, recommended saturation radiance and the noise equivalent radiance ($NE\Delta L$) for case-1 waters for future sensors.

Whereas CZCS was dedicated to case-1 waters remote sensing, MOS-IRS (and the preceding sensor MKS-M) provided more specific experiences on case-2 waters.

[47] Gordon–1988

The experience MKS experiment and lessons which have been learnt are concluded in the following[48]:

- Higher spectral resolution
  To have a chance for case-2 waters remote sensing, one must be able to measure the spectral characteristic or signature with better spectral resolution ($\Delta\lambda < 20$ nm) than with operational sensors.
- More spectral channels over a broad spectral range
  To get a promising chance to retrieve quantitative values about coexisting and covarying water constituents (chlorophyll, sediments and Gelbstoff) one should obtain spectral data in a larger number of channels with small bandwidth and by using a broad spectral range.
- Appropriate channel position
  The instrument channels must be carefully selected with respect to the target signature and the unavoidable absorption bands of atmospheric gases like ozone (Chappuis-band), oxygen (A- and B-bands) and the number of water vapour bands. The latter influence the multispectral image because of high regional and time variability of atmospheric humidity, which can barley be corrected.
- Higher spectral and radiometric calibration accuracy
  The data of the spectral high dimensional (hyperspectral) must be of high quality with respect to spectral purity, radiometric resolution, and calibration and also long term stability of these parameters.

And some recently received results from the MOS experiment[46]:

- Demanded sensor parameters can be realised with inexpensive hardware.
  It has been demonstrated that the needed sensor parameters (high spectral resolution, small non-overlapping channels, high radiometric resolution, long term stability of performance and calibration) can be realised with relative simple and inexpensive hardware.
- Additional SWIR channels provide useful data interpretation capabilities.
  The spectral extension into the SWIR region at 1.6 µm with MOS-C is very helpful for the atmospheric part in the TOA signal and for ice, snow and water discrimination.
- Development of new case-2 waters algorithms.
  New algorithms (PCI) have demonstrated the separation of atmospheric and water part in the TOA signal. The water constituents Chlorophyll, Sediment, Gelbstoff) can be separated and quantified in case-2 water. The application of the PCI algorithm gives useful level-2 parameter images for monitoring coastal state and management decisions.

Particularly the outlined experiences obtained during the MKS and MOS missions show that the methodical background for coastal zone research is encouraging for further applications. A follow-on mission should result in a more operational scenario for regional coastal zone monitoring.

[48] after Zimmermann and Neumann–2000

1.4 Requirements for a regional coastal zone mission

In the above sections the scientific background and the research needs for a regional coastal zone mission have been discussed. Thereafter the experiences from precedent and ongoing missions were summarised in the Chapter 1.3. In consequence, the precise requirements for a regional coastal zone mission can be concluded: high spectral resolution data from VIS to SWIR and additional TIR channels at adequate spatial-temporal resolution are needed for coastal water remote sensing. Land-water specific spectral bands and higher resolution are required for the synchronous assessment of coastal waters and near-shore land features. With respect to coastal waters and ecosystems the scientific goals are summarised in Table 2. In the same table the corresponding consequences in terms of technical requirements are listed.

Table 2: Research needs and technical requirements for regional coastal zone imager[49]

Research task	=>	regional coastal zone mission requirements
• algorithm development for retrieval of water constituents in case-2 waters		➢ high spectral resolution ($\Delta\lambda$ ~ 5 nm, 400-800 nm) ➢ sufficiently large number of spectral channels (~ 10-12) ➢ absolute calibration, Sun calibration, high radiometric resolution
• algorithm development for regional and seasonal specifics of case-2 waters		➢ programmability of spectral position and halfwidth
• discrimination of alga types		➢ programmability of spectral position and halfwidth
• development of specific algorithms to assess HAB's/red tides		➢ programmability of spectral position and halfwidth
• account for atmospheric influence over case-2 waters, atmospheric correction algorithms		➢ extended spectral range (800 – 1000 nm, SWIR), water vapour channels
• assess water characteristics of lakes and water reservoirs		➢ spatial resolution ≤ 100 m
• assess spatial characteristics of coastal waters phenomena		➢ spatial resolution ~ 200 m ➢ swath width > 200 km
• assess time dynamics of coastal wasters and lakes phenomena, e.g. algal blooms		➢ ground repetivity ≤ 2 days ➢ swath width ~ 400 km
• asses near-shore land features (vegetation, catchment areas, snow/ice cover)		➢ spatial resolution ≤ 100 m ➢ extended spectral range VIS/NIR + SWIR ➢ spectral adaptation in VIS/NIR to land features
• primary production in coastal waters		➢ thermal infrared
• coastal dynamics		➢ spatial resolution ≤ 100 m
• coastal currents, water masses discrimination		➢ thermal infrared
• Investigation of special events and hazards		➢ repetivity for special events 1 day ➢ cross-track tilt capability
• up-down-scaling of physical variables, data merging		➢ compatibility of selected spectral channels with other missions

[49] Neumann et al.–1998

2 Remote sensing instrument overview and optimisation for a regional coastal zone mission

For developing a concrete mission and sensor concept which is optimised for the scientific observation requirements (of a regional coastal zone mission), it is necessary to systemise and evaluate the state-of-the-art of sensor instrumentation. As result of the systematisation and evaluation new strategies for sensor design and mission concept can be concluded.

2.1 The evolution of coastal zone remote sensing instruments

The challenge of coastal zone remote sensing

In contrast to classical land observation, the accurate detection of spectral radiance signatures of water bodies demands higher radiometric and spectral resolution:

It has been outlined in Chapter 1.2 that the water-leaving radiances are comparably small due to high light absorption, i.e. about ~90% of the TOA radiances detected by the satellite's sensor can result from light scattered in the atmosphere by molecules (Rayleigh scattering) and aerosols (aerosol scattering). This means that for the detection of 1% variation of the residual water-leaving radiances the total signal has to be known with a radiometric resolution of almost 0.1%.

For detecting the atmospheric contribution accurately (atmospheric correction) and for analysing the spectral signatures of the water (e.g. detection of water constituent) the spectral resolution has to be much higher than for remote sensing of general land applications. Only a adequate classification of the water signature using the data of many narrow spectral bands over the entire VIS–NIR spectrum enables quantitative determination of the water characteristics.

Furthermore, a mission dedicated to coastal areas has to detect with as high as possible spatial resolution for helping to analyse the typical behaviour of the coastal region phenomena. These coastal phenomena have also be assessed depending on the time dynamics. This means that the repetivity of measurements have to be as high as possible. These requirements are of opposing character and a sensor design conflict is inevitable: The reduction of both the bandwidth ($\Delta\lambda$) and the ground pixel size (Δx) results in a lower input signal for each pixel and spectral channel because the available radiance is proportional to $\Delta\lambda$ and Δx^2 (area). This leads to a decrease in the sensor's signal-to-noise ratio and the residual water-leaving radiance will be difficult to obtain with the demanded radiometric resolution. Moreover, by enlarging the sensor's swath width and the number of spectral channels a high data rate is inevitable. Due to data transmission limitations (satellite–ground station) and processing capabilities (at the ground station) a data handling problem can occur. In the following sensors are listed which were able to cover these observation requirements to a certain extent. Moreover, it is obvious that no (existing or planned) sensor is dedicated to the specific problem of regional coastal zone observation.

The forerunner

The launch of the Coastal Zone Color Scanner[50] (CZCS) in 1978 aboard NIMBUS-7 was the first spaceborne instrument devoted to the measurement of ocean colour. Almost one decade of successful data sampling followed. After years of spontaneous shut downs or seasonal turnoffs the mission was officially declared non-operational in 1986. Grace to this sensor major advances in the development and assessment of new algorithms for case-1 waters (i.e. phytoplankton detection) could be achieved. The CZCS design followed the whiskbroom principle: the top-of-atmosphere radiance was collected via scanning mirror and spectrally separated by a grating (five VIS channels) or a filter (TIR channel) and detected by a single detector (silicon or mercury cadmium telluride) in the focal plane of each spectral channel.

The follow-ons

A decade later — in 1996 — the Modular Optoelectronic Scanner (MOS-IRS)[51] was launched as experimental payload on the Indian satellite IRS following the CZCS mission with a more sophisticated instrument. MOS-IRS is the first spaceborne pushbroom imaging spectrometer which is the result of the experience gained during numerous imaging (MOS-PRIRODA) and non-imaging (e.g. MKS-M) experiments which go back to the year 1979. MOS-IRS provides data in the VIS-NIR spectrum for remote sensing of the ocean-atmosphere system. The swath width is 200 km and the ground pixel has a size of 500 x 500 m². MOS-IRS consists of two separate spectrometer blocks: the atmospheric spectrometer MOS-A provides four narrow ($\Delta\lambda$ = 1.4 nm) channels in the O_2A-absorption band at ~ 760 nm to allow estimation of aerosol-optical thickness and stratospheric aerosols. MOS-A measures simultaneously with MOS-B which has 13 channels of 10 nm width in the 408 to 1010 nm range. The 18th channel of MOS-IRS is provided by the SWIR MOS-C camera (λ = 1.6 µm) for improved ocean surface roughness and aerosol estimation. The two imaging spectrometers MOS-A and MOS-B follow a similar opto-electronic design: Entrance optics, slit, collimator, planar grating and CCD line-array detectors are responsible for detecting the radiances from the Earth's surface pixels at appropriate wavelengths. The MOS-IRS sensor is a proof-of-concept experiment and not a fully operational mission (the IRS satellite is in stellar mode 30 % of the year).

Since 1997 NASA's Sea-viewing Wide Field of view Sensor[52] (SeaWiFS) is collecting data for ocean-colour in global scale as operational mission. SeaWiFS follows a conventional design of a whiskbroom imager and includes sun and moon calibrations. Eight visible channels, a swath width of more than 2000 km and a ground resolution of 1100 m provide scientists with a powerful tool for global ocean-colour observation.

The next sensor in the line is the Moderate-Resolution Imaging Spectroradiometer[53] (MODIS) which has been launched successfully in December 1999. MODIS is a combined Land/Ocean

[50] Evans and Gordon–1994
[51] Zimmermann and Neumann–1996
[52] McClain et al.–1994
[53] Pagano and Durham–1993

instrument and has spectral channels which are comparable to SeaWiFS channels. Additional VIS, SWIR, MIR and TIR channels and an augmented spatial resolution in a few vegetation-orientated visible channels provide data for many more applications. The MODIS design follows an advanced whiskbroom principle: a line of detectors provide simultaneous detection of several along-track pixels during the sweep over the swath. A swath width of 2300 km, 36 spectral bands and a ground resolution between 250 and 1000 m makes MODIS one of the most comprehensive sensors ever launched for civil Earth observation in terms of size, spectral range and spatial resolution.

Future sensor perspectives

For the year 2000 and beyond three further missions are planned for operation. Whereas MERIS[54] and GLI[55] are globally oriented missions with a swath width of more than 1000 km, the COIS[56] mission will concentrate on local coastal scenarios and algorithm development. GLI follows in the design philosophy the MODIS whiskbroom technique principle. In contrast MERIS and COIS will demonstrate a new sensor design philosophy for Earth observation sensors: These sensors are pushbroom imaging spectrometers but in contrast to the MOS spectrometers the spectrum of a single pixel will be dispersed and focused on different locations of a two-dimensional detector array. This design philosophy has the unique advantage of programmable spatial and spectral resolution.

A summary of the above mentioned coastal-zone and ocean-colour imagers is given in Table 3. Besides the pathfinder CZCS this overview includes sensors which are planned to produce data in the upcoming years. Further sensor information can be retrieved from Appendix A.

Table 3: Extract of coastal and ocean colour imagers

Sensor	**CZCS**	**MOS**	**SeaWiFS**	**MODIS**	**GLI**	**COIS**	**MERIS**
Operation period	1978–86	1996–	1997–	1999–	from 2002	from 2002	from 2002
Spatial resolution	825 m	520 m	1100 m	1000 (250) m	1000 (250) m	30 m	300 - 1000 m
Swath width	1556 km	200 km	2800 km	2330 km	1600 km	30 km	1450 km
Recurrent period of S/C	6 days	24 days	16 days	16 days	4 days	7 days	35 days
Coverage	no global coverage	no global coverage	2 days global coverage	1 - 2 days global coverage	3 days global coverage	no global coverage	3 days global coverage

[54] Rast–1998
[55] Nakajima et al.–1998
[56] Myers et al.–1998

Conclusion

The sensor design improvements have been chiefly in increasing the radiometric performance (in terms of dynamical range and signal-to-noise ratio), the number of spectral channels (from 5 for CZCS up to 36 for MODIS/GLI) and the calibration accuracy (improvement of in-flight calibration tools). Such increased sophistication in the sensor design was essentially based on new research objectives, i.e. in response to scientific community demands.

Demands from the scientific community for the next evolution steps are (1) similarity of future sensor's spectral bands and (2) a regional oriented tool for improved monitoring and management of coastal zones:

- A first, general demand for future sensor design is the similarity of at least some the spectral bands (inter-calibration bands) to other sensors. To fulfil this demand would facilitate inter-comparison between sensors, to obtain an easier comparability of operational algorithms and to simplify data merging. Future sensors can meet this demanded similarity by an agreement to apply defined channels or by designing sensors with programmable spectral channels.
- The second demand results from governmental and scientific needs for an adequate observation of coastal zones. A regionally oriented tool for the observation of coastal zones would fill an information gap by providing high spectral and relatively high spatial resolution (< 100 m) data with a repetition rate of at least two days. These data would allow monitoring and management of coastal zones (e.g. monitoring of catastrophic environmental hazards). However, no present or future sensor is able to fill this gap, because these instruments are either locally (low repetivity) or globally oriented (lower spatial resolution).

2.2 State-of-the-art of remote sensing instruments (VIS–TIR)

2.2.1 Optical remote sensing instrumentation in general

Remote sensing instruments, i.e. sensors which operate in the VIS and IR region of the electromagnetic spectrum can be subdivided in different sensor approaches for realising the Earth observation from satellite: photographic cameras, television cameras, opto-mechanical scanners, solid-state cameras and imaging spectrometers.

Whereas photographic and television cameras have been applied very successfully in the beginning of remote sensing activities, today's technology focuses on opto-mechanical and electronic scanners which use solid-state detectors (instead of photographic films or vidicon cameras) for the detection of the incoming light. Especially the increasing requirements to enlarge the dynamic range and improve the radiometric accuracy are the main reasons for the utilisation of these sophisticated systems.

Opto-mechanical scanners

The operation principle of an opto-mechanical scanner (also: whiskbroom scanner) is shown in Figure 8. The radiation from the ground pixel is intercepted by the scan mirror which diverts the radiation to the collecting optics. The optics (e.g. a telescope) focuses the incoming radiation on to a detector. By rotating the scan mirror the detector views adjacent ground pixels and collects the information pixel by pixel. The scanning frequency is adjusted in a way that by the time the sensor platform moves through one pixel the scan mirror is set to the start of the next scan line. Hence, successive and contiguous scan lines can be produced. Finally, a contiguous image is ensured by the correct adjustment of the scan frequency depending on the velocity of the platform. A trade-off is the whiskbroom spectrometer which combines the opt-mechanical scanner with the features of a spectrometer (sensor example is the CZCS[50]). This trade-off is subject of the discussion in Chapter 2.2.2.1.

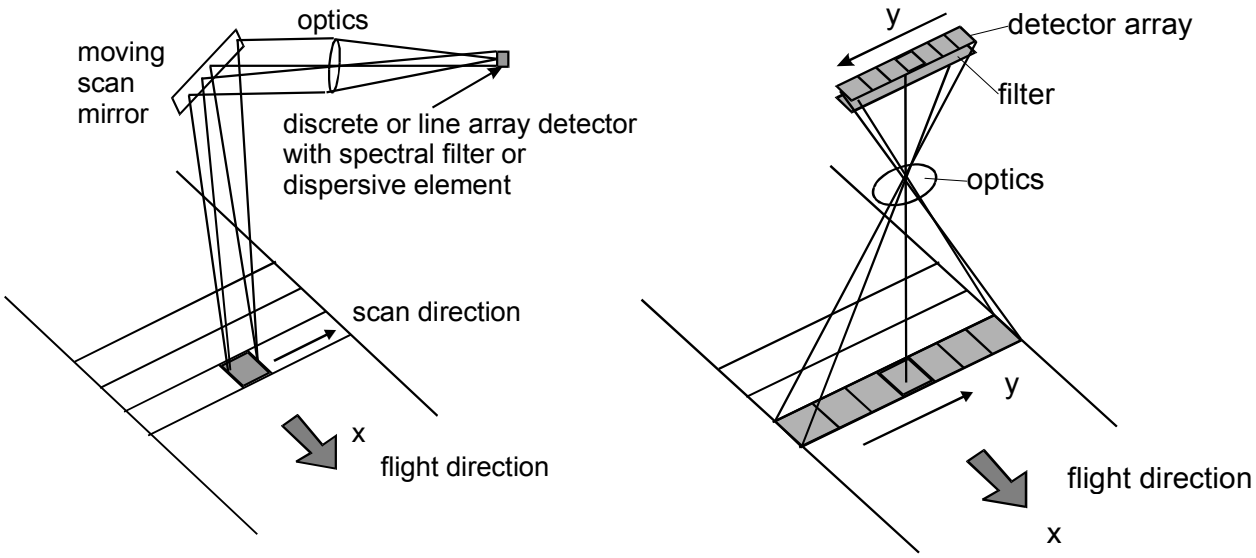

Figure 8: Operation principle of opto-mechanical scanner and solid-state camera

Solid-state cameras

The pushbroom camera is in common use to increase the spatial and spectral resolution when compared to those provided by opto-mechanical scanners. Instead of mechanical scanning, the operation principle is electronic scanning (see Figure 8). The full swath of the Earth surface is focused by a lens on a linear detector. The number of resolved and detected Earth pixel depend on the number of detector elements. By moving the camera's platform (in flight direction) successive scan lines can be produced. Hence, the detector array is used to produce one scan line of information. This imaging mode is referred as pushbroom scanning (see also Chapter 2.2.2.1). For very high ground resolution and low sensitivity applications the integration time for each swath can be extended by using Time Delay Integrating (TDI) imagers where rectangular 2-d detectors (e.g. 80 x 1025 pixels) enable the signal of one line (swath) to be read out from multiple lines caused by the forward movement of the sensor. Therefore the sensitivity of a TDI with *n* lines is *n* times that of an imager using a single line array detector. Examples[57] for a pushbroom camera is the VGT on SPOT 4, the TDI principle is used by OrbView–3.

Imaging spectrometer

The opto-mechanical scanners and the solid-state cameras acquire images in a few spectral bands of various width. More spectral channels in conjunction with higher radiometric efficiency is provided by an imaging spectrometer. As pushbroom imager it scans a row of pixels over the two dimensional scene. The image is generated electronically in along track direction by the motion of the host platform (aircraft or LEO satellite). The incoming radiation of the swath is dispersed into different spectral angles and focused at different locations on the focal plane (see Figure 10). ROSIS is an example for an airborne imaging spectrometer using a 2–dimensional detector. A spaceborne counterpart using a hybrid focal plane of numerous line array detectors is MOS-IRS[57].

The operation principle and a technology overview on imaging spectrometers is subject of the following section.

[57] see table in Appendix A (pp. 121)

2.2.2 Hyperspectral imager technology

Recently the scientific demand came up to detect the Earth surface in many contiguous very narrow spectral bands (instead of the few broad spectral camera bands) for retrieving the desired reflectance/emittance information of minerals, vegetation, and water constituents. Only hyperspectral imagers (see Chapter 1.1.1.) are able to provide this kind of data. These imagers consist of three elementary parts: an imaging unit, a spectral selection unit and a detector unit. The imaging unit defines the way the image is produced in the sensor. The spectral selection unit is responsible for the spectral separation of the incoming radiance into discrete narrow bands. Finally the detector has to count the incoming spectrally separated photons. The analogue output of the detector is converted in digital units and is sent through electronic processing circuits. Finally, the data from the scene are combined with other data (e.g. housekeeping data such as temperature, calibration data) and recorded in a storage medium and/or transmitted through telemetry to the ground station. The relation between transmitted data from the scene (i.e. sensor output in counts) and the to be measured radiance (i.e. sensor input radiance in photons) is provided by the sensor's calibration. With the demand of quantitatively remote sensing (e.g. increasing radiometric requirements) the in-flight calibration method became more and more important in the last years.
Hence, in the following a technology overview is given for the three elementary parts (imaging, spectral selection and detector unit), and for in-flight calibration approaches used during various missions.

2.2.2.1 Imaging unit

An hyperspectral imager creates a three-dimensional data cube (2-d spatial and 1-d spectral). The spatial dimension in along-flight direction is provided by the forward movement of the host platform. The across-track image generation is realised either by a scan mechanism (whiskbroom principle) or by the simultaneous detection of the all pixels in a swath (staring or pushbroom principle). This is why imaging units of hyperspectral imager are classified in three classes: whiskbroom, pushbroom and staring scanners (see Figure 9).

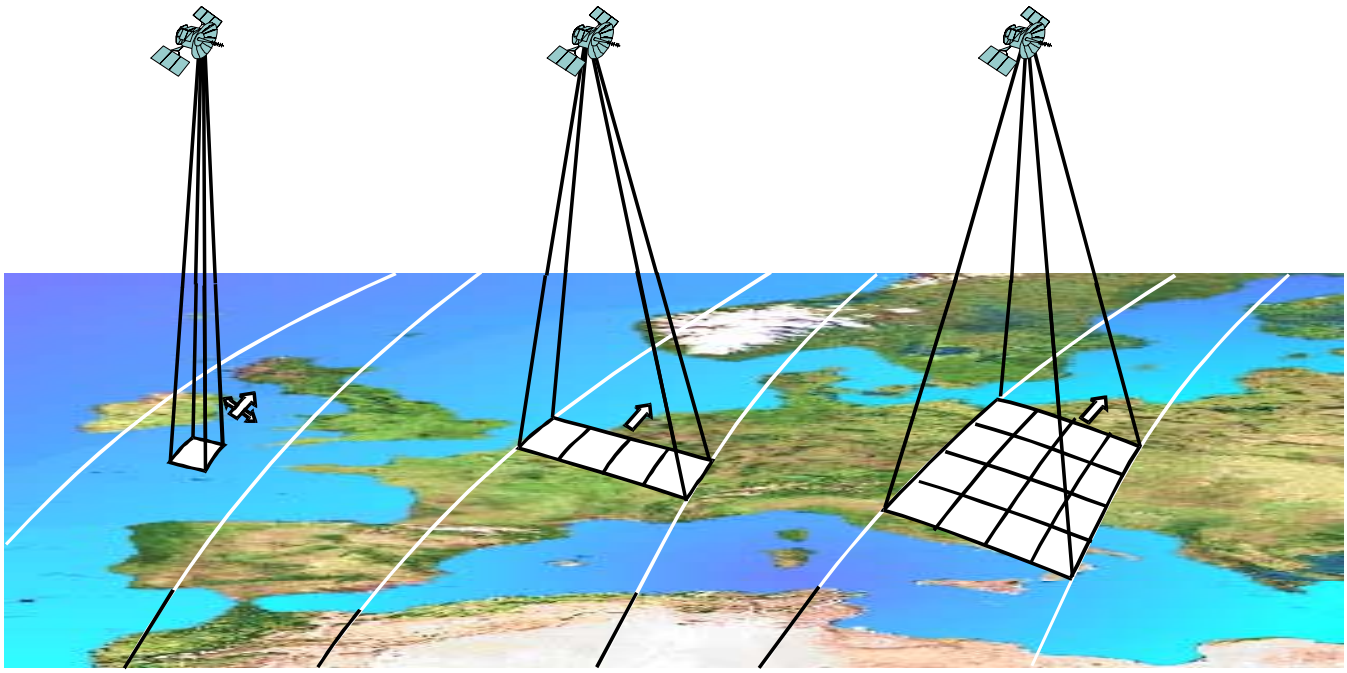

Figure 9: Image generation principles

The whiskbroom imager is an electromechanical scanner, having on-axis optics or telescopes and a scan mirror. One data-cube axis — in flight direction — is created by the single-pixel FOV moving on the Earth surface with satellite platform velocity. The next axis of the whiskbroom image is produced by the mechanical scanner (mirror), which sweeps the FOV perpendicular to the satellite flight direction from one side of the swath to the other. The third axis (the spectral information) is produced by a spectral dispersing element (e.g. grating, prism) which disperses the single-pixel FOV into many defined spectral bands. Advantages of the whiskbroom imager are a simple over-all design, wide FOV and easy calibration. The main disadvantage is the short integration time available for each ground pixel due to the whiskbroom scanning principle along and across track direction.

In contrast to the whiskbroom scanner, the pushbroom scanner has no moving parts because it uses a line of detectors to generate the first spatial dimension of a 2-d scene. The second spatial dimension is created by the movement of the host platform. Pushbroom imagers have no mechanical scanner and the potential integration time for each ground pixel is longer than for the whiskbroom imager. In contrast, the disadvantages are a high complexity of the focal plane, calibration and optics.

The staring scanner is an electronic scanner which detects a 2-d FOV instantaneously on a 2-d detector. A third axis is created by time-sequential spectral selection (e.g. filter wheels) during the forward movement of the satellite platform. The staring principle has the advantage of being simple and compact. But the main disadvantages are the spatial and spectral

incongruence because of the successive image sample procedure. Hence, design constraints may appear with increasing numbers of spectral bands and spatial resolution (long switching time of the filters).

The advantages and disadvantages of each imaging unit are summarised in Table 4.

Table 4: Comparison of imaging units

Scanning approach	Advantages	Disadvantages
Whiskbroom	• simple over-all design • wide FOV • (easy calibration)	• mechanical scanner (moving parts in vacuum) • post-processing required (spatial incongruence) • constraints of high spectral and spatial resolution requirements (low integration time)
Pushbroom	• no moving parts • congruence of spectral images • longer integration time for each ground pixel	• complex focal plane • narrow FOV • complex calibration • complex optics • spectral curvature
Staring	• simple and compact	• post-processing required (spatial and spectral incongruence) • constraints when many spectral bands and high spatial resolution requirements

Conclusion

Depending on the hyperspectral imager application, each of the imaging units can represent an optimal design. However, with the mission constraints of a LEO sensor platform (platform velocity ~7.5 km/s) the optimal imaging unit mode is the pushbroom imager owing to the required spectral and spatial resolution and the envisioned simultaneous detection of many spectral bands. The staring scanner is impractical because the wavelength switching time has to be very short for simultaneous detection of many bands and the whiskbroom principle will reach physical limitations when high spectral and spatial resolution is required. The new imager concept has to overcome the disadvantages high complexity of focal plane, optics and calibration, and a narrow FOV.

2.2.2.2 Spectral selection unit

It has been shown in the preceding section, that the pushbroom imager is the most promising scanning principle for providing a high number of spectral channels in conjunction with high radiometric efficiency. In the following the spectral selection units are compared with special focus on this pushbroom approach.

The spectral selection unit is responsible for the spectral separation of the incoming radiance into discrete narrow bands. This can be realised by dispersive elements, spectral filters or Fourier transform interferometric principle.

Dispersive elements

In general, dispersive elements systems have either a diffractive (grating) or a refractive (prism) element for the spectral discrimination of the incoming radiation (see also Figure 10). There are also various multi-element dispersive systems which combine prisms and gratings (e.g. the grism) in interesting trade-offs[58,59]. For all these dispersive elements the incoming radiation will be dispersed into distinct angles and focused at different locations on a detector array. These systems have also a disadvantage in common: The slit length (i.e. the cross track FOV) is limited by the variation in dispersive power across the cross-track FOV. This variation in dispersive power leads to a phenomenon which is known as spectral smile (curvature), i.e. the change of the dispersion angle with field position. To overcome this problem, similar sensors can be arranged to cover a TFOV congruently. The MERIS spectrometers are following this arrangement technique[57].

With a grating as spectral selector the incoming light is diffracted linearly with wavelength. Therefore over of a broad spectral range a linear dispersion is guarantied. However, several (partly overlapping) diffraction orders are created simultaneously. This phenomenon is usually overcome by applying broadband order-sorting filters which eliminate possible overlying orders before detecting the desired spectral orders. But this reduces the optical throughput and leads to a low efficiency[60]. A method to increase the grating efficiency is the utilisation of blazed gratings [61] . This approach has been realised by the MOS-IRS spectrometers[57].

In contrast, the prisms gives a non-linear dispersion because the refraction angle is a function of the wavelength. Therefore multi-element prisms have been designed to obtain a linearity of the dispersion. Advantages of single-element prisms are high throughput (transmission) and no false light problems because of order overlap, but with the costs of relative high mass and non-linear dispersion. An airborne spectrometer using a prism as spectral selector is APEX[57].

A grism uses both a prism and a transmissive grating for dispersing the incoming light. This reduces the instrument's size and the polarisation sensitivity (no reflective optical

[58] ESA Report–1994
[59] Blechinger et al.–1995
[60] Cerutti and Durpaire–1982
[61] Flügge–1967

components). However, there are still manufacturing problems in joining the grism (prism-grating-prism) without producing much straylight[62]. AISA is a spectrometer example using a grism as spectral selector.

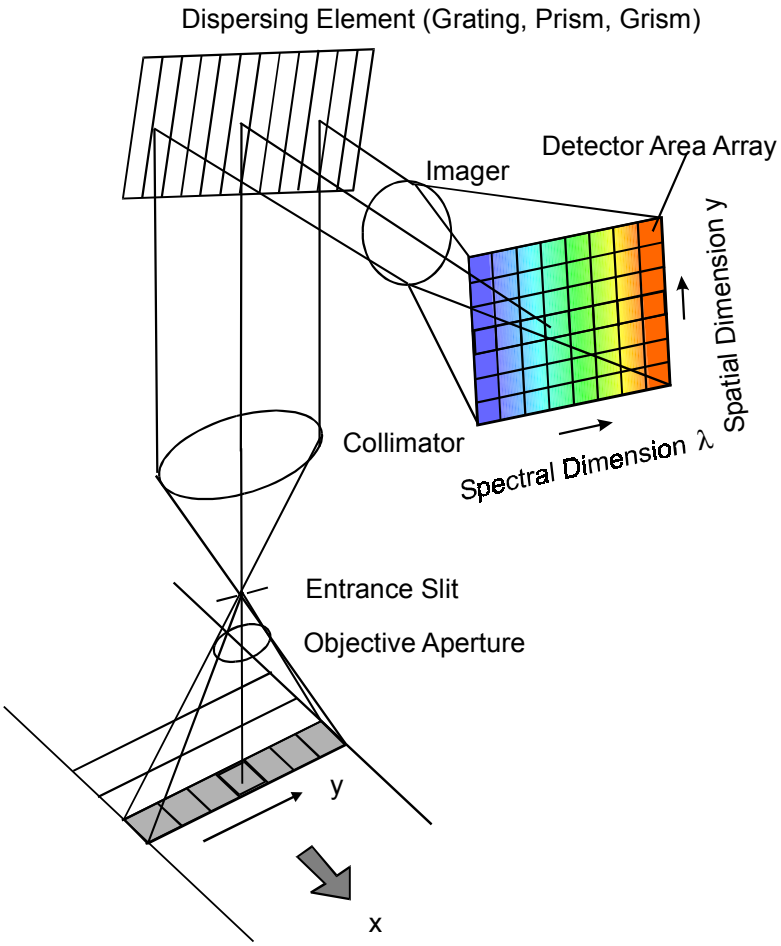

Figure 10: Imaging spectrometer principle using a dispersive element as spectral selector

Spectral filters

Spectral filters select the desired spectral bands via filter wheel, wedge filter or tuneable filter (e.g. acousto-optical-AOF or liquid crystal-LCF filter). These filters only transmit a narrow waveband of the ground pixel to the detector. The tuning time of filter wheels or discrete filters is too long for remote sensing applications. However, AOF and LCF represent interesting tuneable filter solutions in various development phases. With typical switching times of 100 µs for AOF and 50 ms for LCF for a wavelength switch[63], the tuning time is still too long to be considered for a LEO satellite platform. In consequence, only the wedge filter is considered here.

[62] Braam et al.–1997
[63] Puschell and Tompkins–1997

In general, a wedge filter system combines a multi-layer wedge (spatially varying) interference filter with a 2d detector array. The incoming light is transmitted at a centred wavelength which depends on the spatial position of illumination (see also Figure 11). Advantages are high efficiency, broad spectral range (VIS-TIR) and a compact layout. But the wedge filter has the disadvantage of a non-simultaneous acquisition of all spectral bands from one ground pixel. Sensor examples are the airborne WIS and the spaceborne counterpart AC on EO–1[57].

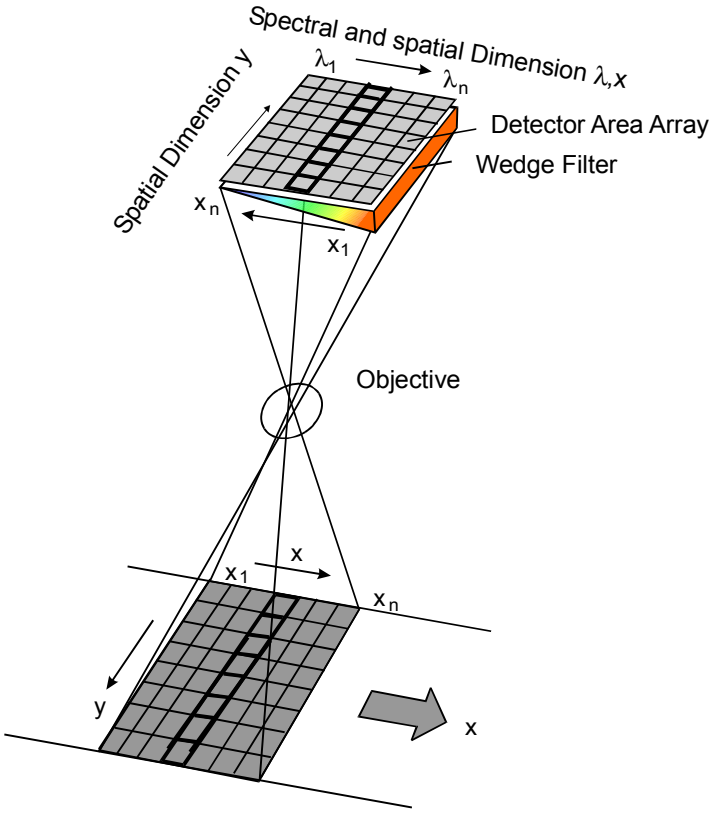

Figure 11: Linear wedge filter system

Fourier transform spectrometers (FTS)

Fourier transform spectrometers split the incoming light into two parts using a beamsplitter and recombine it afterwards into a single beam with a varying optical path difference. The resulting interferogram of the scene spectrum can be sampled temporally (time domain) or spatially (spatial domain) in the focal plane.

A well known example of the time domain FTS is the Michelson interferometer[64]. Following the staring mode principle the information of a 2-d FOV will be imaged on a 2-d detector. But instead of time-sequential spectral selection (like filter wheels), the time-domain FTS separates the incoming light by using a beamsplitter and two mirrors. One mirror is stationary the other moves at a constant velocity. The beamsplitter divides the incident light and recombines it after an optical path difference has been introduced (by the moving mirror). The

[64] Persky–1995

resulting modulated Earth radiation is imaged as an interference fringe signal on a detector. This means, that for each ground pixel a temporal interference fringe pattern can be recorded (over time) at one detector pixel. Assuming a constant Earth signal, the shape of the signal depends on the wavelength and on the velocity of the moving mirror. By means of post-processing the interferogram must be transformed for remote sensing applications into the spectrum of the corresponding pixel. However, the tuning time of the moving mirror and for recording the temporal interference fringe pattern is too long for being practical for nadir remote sensing from LEO with high spatial and spectral resolution.

In contrast, the spatial domain FTS follows as monolithic Sagnac interferometer the pushbroom imaging principle[65]. Moreover, it consists of two mirrors and a beamsplitter (see Figure 12). In contrast to the time domain FTS, the spatial domain FTS's mirrors are not moveable because it samples the incident light spatially: Two coherent points interfere during the movement of the sensor. The resulting variation of the optical path difference is therefore created in the flight direction and imaged as an interferogram in one dimension of the 2-d detector. The other dimension is the second image dimension and it belongs to the cross track direction of the pushbroom scan. This approach has been realised by FTHSI and SMIFTS [57].

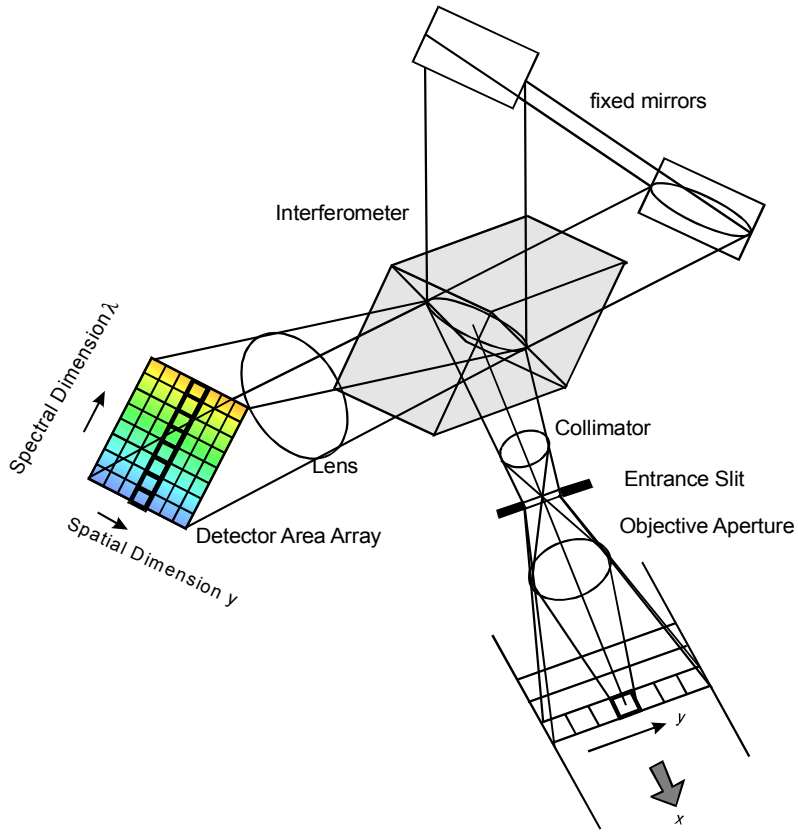

Figure 12: Spatial domain Fourier transform spectrometer principle

[65] Lucey et al.–1993

Comparison of spectral selection modes

The properties of the various spectral selection modes are listed in Table 5. The selection modes are evaluated with special focus on LEO remote sensing. There is no spectral selection mode which represents the optimal design for all applications of remote sensing. However, the requirements for coastal zone remote sensing give a certain frame in which the optimal hyperspectral imager can be found:

The common prism design has the disadvantages of non-linear dispersion, relatively high mass and a medium spectral resolution. This does not meet the requirement of high spectral resolution measurements (e.g. in the oxygen band O_2A with $\Delta\lambda < 2$ nm). The grism and the spatial domain FTS are both interesting solutions for future sensors, however these technologies are still in various development phases. This means that for grisms the straylight and polarisation problem (interface prism-grating) can hardly be handled over the broad VIS–NIR spectrum and is only solved in small spectral regions with high manufacturing costs. Degrading factor for reasonable high spectral and spatial resolution with the spatial domain FTS plays the incapability of current sensor designs to meet these requirements and the sensitivity of the interferometer to the satellite platform motion accuracy, what might be overcome in the upcoming years[66].

Since the wedge filter imager's spectral selection mode is not capable of simultaneous detection of all spectral bands from one ground pixel, this solution is not very useful for spatial high resolution measurements.

The grating has the advantage of providing the desired spectral resolution, not causing a critical amount of straylight and not being sensitive to satellite motion. Disadvantages are slit curvature and polarisation sensitivity. The problem of slit curvature can be solved by using several similar modules with short slit lengths.

In any case, an imaging spectrometer should have a low sensitivity to polarisation, i.e. a variation in the sensitivities of the spectral channels with polarisation direction. Since the polarisation mainly depends on the way the incoming light is reflected at the sensors surfaces, the polarisation property can only be considered in the overall sensor design. This means that an overall check of telescope, optics, grating, mirrors and detector for polarisation and straylight sensitivity has to qualify the envisioned concept design.

[66] Kunkel et al.–1997

Table 5: Comparison of spectral selection systems

Properties	Dispersive Systems						Fourier Transform Spectrometers				Spectral Filters	
	grating	**+/–**	**prism**	**+/–**	**grism**	**+/–**	**spatial domain FTS**	**+/–**	**time domain FTS**	**+/–**	**wedge**	**+/–**
Spectral resolution	high	+	medium	**0**	high	+	high	+	high	+	medium	**0**
Optical efficiency (throughput)	medium (several diffraction orders)	**0**	high (good dispersion efficiency)	+	see grating	**0**	high	+	high	+	high	+
Spectral range	broad (UV–IR)	+	narrow (UV-NIR)	–	narrow	–	broad (VIS-TIR)	+	broad (VIS-TIR)	+	broad (VIS-TIR)	+
Sensitivity to S/C motion	no	+	no	+	no	+	yes	**-**	no	+	no	+
Moving parts	no	+	no	+	no	+	no	+	yes	–	no	+
Simultaneous acquisition of all spectral bands	yes	+	yes	+	yes	+	yes	+	no	–	no	–
straylight	medium	**0**	low	+	high	–	high	–	high	–	high	–
Complexity	low	+	low	+	medium	**0**	high	–	high	–	low	+
Compactness	low	**0**	low	**0**	high	+	low	–	low	–	high	+
Miscellaneous	spectral order overlap slit curvature	– –	dispersion in function of λ slit curvature	– –	slit curvature	–						
Examples (see Appendix A)	HSI, HRIS, MERIS, MODIS, MOS		APEX		AISA		FTHSI, SMIFTS				WIS, AC	

+ advantage 0 baseline – disadvantage

2.2.2.3 Detector technology

2.2.2.3.1 Solid state detectors in general

The sensor's detector is responsible for capturing the incident photons and converting them into electrical charges. In the past decades fast development steps were performed in terms of detector types and dimension, e.g the development from single silicon photodiodes in the late 1960's to nowadays two-dimensional complementary-metal-oxide-semiconductor (CMOS) arrays with more than $5x10^6$ pixels. To select the optimal detector for a certain application the specific detector performance data have to be taken into account. These are (among other things) the spectral response, the specific detectivity, the responsitivity and the response time[67].

Spaceborne Earth remote sensing instruments tend to detect the Earth surface with a high spectral and spatial resolution. The resulting low input signal (photons) demands special detector requirements, e.g. high radiometric performance, a low noise concept and a narrow pixel pitch. Additional, the detector should work at ambient temperature and be available for reasonable costs.

The detectors in the spectral region from the VIS to the TIR are of two basic types namely thermal detectors and the quantum detectors.

The thermal detectors absorb radiant energy what leads to an increasing detector temperature. As a result a parameter of the device which changes with temperature can be detected, that is the resistance for the bolometer, the voltage for the thermocouple or the dielectric constant for the pyroelectric crystal. The advantage of the thermal detectors is the more or less constant spectral sensitivity over a wide spectral range — mostly extending also in the far IR. However, the response time is very large and the specific detectivity tend to be low, so that these devices are generally not used for high resolution imaging. Nevertheless, interesting uncooled mirco-bolometers on vanadium-oxide basis found the way to the market recently[68]. These bolometers are now available in a larger area arrays format (such as 320 x 240 pixels). Unfortunately, the significant reduction of the spectral response to wavelengths smaller than 10 μm is still unsolved; so that these devices can only be used in the TIR where quantum detectors have a long remote sensing tradition.

[67] Wolfe–1978
[68] Jerominek et al.–1996

In the quantum detectors the photons are absorbed and electrons will be excited into the conduction band, the electrical characteristics of the responsive element will be changed or electrons will be emitted. These principles are called photo-voltaic, photo-conductive and photo-emissive effect. A famous detector example using the photo-emissive and the photvoltaic effect is the MMS[69] of Landsat–1, where the photo-multiplier tube is used for channel 1–3 and the photvoltaic photodiode for channel 4. Nowadays the photo-multiplier tubes are replaced by using silicon-based detectors for visible applications. An overview is given in Chapter 2.1.1.3.2, where different types of silicon-based detectors for imaging applications are summarised. Unfortunately, the spectral sensitivity of these devices is currently limited for detection in the spectral region from the ultraviolet to 1µm. This is why IR systems use arrays of photovoltaic or photoconductive detectors with different component: Indium Gallium Arsenide[70] (InGaAs), Indium Antimonide[71] (InSb) and Mercury Cadmium Telluride[72] (HgCdTe, also: MCT) are some commonly used detector compounds in the SWIR. In the thermal infrared mainly HgCdTe[73] detectors are used for Earth observation sensors.

An overview of typical spectral region and operating temperature for various detectors are shown in Figure 13.

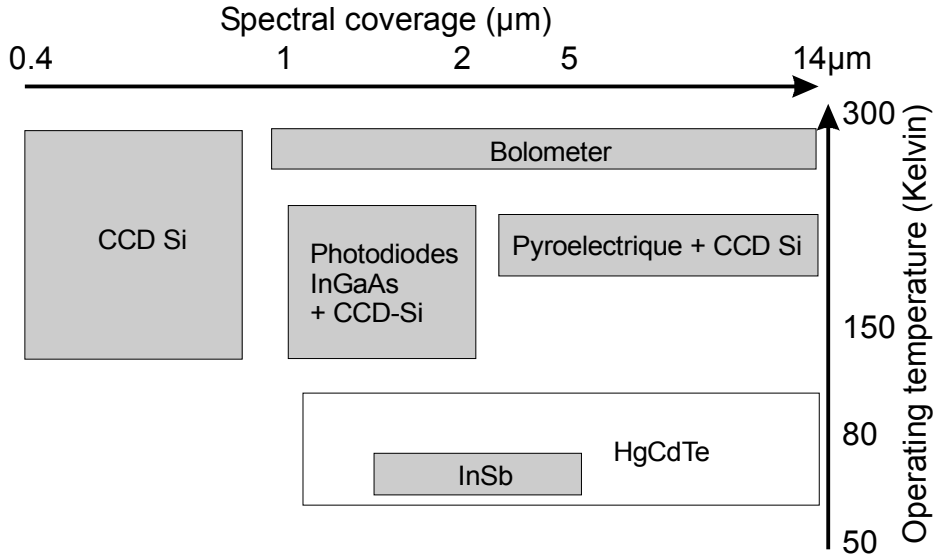

Figure 13: Useful spectral ranges for typical remote sensing detectors

Many state-of-the-art detector systems use what is known as focal plane arrays. The advantage of focal plane detectors is the ability to integrate processing electronics elements right on the same chip as the detector elements. A device in which the roles of radiation detector and signal multiplexer are separated is called hybrid. The device is a sandwich of two

[69] Lansing and Cline–1975
[70] the MOS-C camera of MOS–IRS
[71] Roberts et al.–1995
[72] Willoughby et al.–1996
[73] Pagano and Durham–1993

slabs combining different working principles or components in the same focal plane array. Common example is the multiplexed InGaAs photodiode sensor array[74,75] which incorporates an InGaAs photodiode array, a shift register with CMOS transistors, integration amplifier array etc.
Whereas detectors for solid-state cameras use linear or TDI detector arrays, the imaging spectrometer requires larger 2-d area array detectors. [In general also multi-array line detectors can be used, but to increase the number of spectral channels and/or to enable programmability of the band width 2-d detectors are inevitable.] In contrast to commercial (camcorder) 2-d detectors, the imaging spectrometer device must fulfil very specific requirements. An overview is given in the following section.

2.2.2.3.2 Detectors for imaging spectrometers

Since spectrometers disperse optical illumination from a single spatial point across many pixels, 2-d image sensors with high readout rates are required. Moreover, the incoming light's wavelength is filtered out narrowly by a spectral selector (e.g. grating), so that the photon signal tends to be weak. Hence, the signal can easily be overwhelmed by readout noise — especially at high readout rates. Further on, for most remote sensing applications an extended wavelength performance (high sensitivity over a large spectral region) is required. These scientific detectors — specialised for spectrometer design — can be subdivided in either active pixel sensor (APS), charge-coupled-device (CCD) or charge-injection device (CID) technologies[76,77,78,79]. The basics of these types will be described and compared in the following. An overview of the advantages and disadvantages is given in Table 6.

APS (CMOS)

The active pixel sensor is an addressable imager, designed as a matrix of photodiodes. Each photodiode is connected with a MOS (metal-oxide-semiconductor) transistor located within each pixel for amplifying the signal. To convert the 2-d spatial information into a serial stream of signals, electronic scanning circuits are added to the device to address all pixels sequentially, and reading out the information they contain. Consequently, the charge does not need to be transported across great distances to an output amplifier.
The APS operates under low voltages avoiding degradation of the detector performance with increasing array size. Moreover, the readout rate can be increased and random access architectures are possible. Other advantages are resistance to high energy radiation, non-blooming and random binning features. Additional one-chip lens design and buttable array possibilities make APS to an useful detector type. The disadvantages are high calibration complexity, a low quantum efficiency and low fill factor (aperture ratio indicating the active area on the detector). Whereas quantum efficiency and fill factor problems seem to be

[74] EG&G–1998
[75] Hamamatsu–1997
[76] Lockyer–1997
[77] Barbe–1987
[78] Fossum–1994
[79] Theuwissen–1996

solvable within the next few years[80], a solution for reducing the calibration complexity is not possible because each pixel uses its own amplifier.

CCD

The CCD device is built with MOS capacitors as sensing elements. From the MOS capacitors the photon signals generated by the incoming radiance have to be transported as charges to a common output amplifier. The charge is transferred from one pixel to the next, in shift register fashion, by varying the voltages on the pixel electrodes. CCDs can be subdivided into frame-transfer, interline-transfer and frame-interline-transfer detectors.
The CCD has the disadvantage of not allowing random access or simple window-of-interest readout operations since all data have to pass through the output amplifier or into a dump drain. On the other side this makes data calibration much easier because all channels follow only one single amplifier curve. The high fill factor and the high signal-to-noise ratio make CCDs an attractive candidate for spaceborne spectrometer applications.

CID

Like the APS the CID pixels can be addressed individually, but in contrast to APS's photodiodes, CIDs use MOS capacitors for detecting the signal. These MOS capacitors typically have two overlapping gates for each pixel. Each two gates can be biased differently. The incident light falling on a pixel is converted into an electrical charge signal but CIDs do not transfer the charge. The charges stay at the pixel until they are read out by directly addressing the pixel's x-y co-ordinates, i.e. using row and column addresses.
The CID allows random access or simple window-of-interest readout and it is even more resistant to space radiation than an APS, i.e. the CID can withstand more than 100 times the lethal dose of a CCD. Another advantage is that a CID does not bloom: When a pixel saturates, the charge is spilled into the silicon substrate and not into adjacent pixels. Disadvantages are the relatively high read-out noise, the small fill factor and the limited dynamic range[81].

[80] Kempainen–1997
[81] Zarnowski et al.–1993

The following Table 6 outlines the advantages and disadvantages regarding desired characteristics of a spaceborne imaging spectrometer for Earth observation. The sign (+) indicates a better performance than the baseline (0) and the sign (++) represents more suitable performance parameters.

Table 6: Comparison of detector technologies for imaging spectrometry

Characteristics	CID	CCD	APS
Small pixel size	+	++	+
Low read out noise	0	++	++
High fill factor	+	++	+
Dynamic range	0	+	++
High quantum efficiency (VIS-NIR)	+	+	+
High radiation hardness	++	0	+
Low system power	+	0	++
Low system mass	+	+	++
System volume	+	+	++
Electronic shutter	0	+	++
Electronic windowing	++	0	++
On-chip A/D converter	0	0	++
On-chip timing/control	0	0	++
Calibration complexity	0	++	0

Conclusion

Unfortunately, only several manufacturers have developed detectors for the niche of scientific imaging. Whereas the Japanese manufactures are mostly concentrating on commercial products, the US companies mainly produces custom or defence design sensors only. This gives certain (fiscal) restrictions for the selection of the best detector technology.

From the technology side of view the APS is a very interesting detector once the disadvantages of low quantum efficiency and low fill factor have been solved and these technologies become commercially available.

At present the frame-transfer CCD is still the best solution for spaceborne Earth observation missions but the CCD performance has to be analysed in the context of the overall imaging spectrometer performance (e.g. SNR, frame rate, readout design).

2.2.2.4 In-flight calibration methods

2.2.2.4.1 In-flight calibration methods in general

In-flight calibration methods (also known as: onboard calibration) provide data about the variation of the sensor performance over time. Because of the degradation of electronics, optics and material in the space environment a re-calibration of radiometric, spectral and spatial parameters in orbit is necessary. The in-flight calibration methods can also be subdivided into absolute and relative calibrations:

Absolute calibration methods

The absolute calibration gives coefficients either to standardised radiation sources (e.g. PTB[82] or NIST[83]-calibrated lamps) or the Sun (e.g. applying Neckel & Labs values[84]). Therefore the ratio is composed of the digital counts transmitted from the sensor to the ground station and a value of an accurately known radiance field in the TFOV. The ideal onboard calibration unit offers a well-known amount of photons, filling the whole aperture and TFOV, passing all optics before being detected and generating a signal level which is comparable to the expected TOA signals.

Relative calibration methods

The objective of the relative calibration is to determine the difference and variation of the absolute calibration coefficient. This is done by normalising the output of all detectors in a band to one detector output. In contrast to the absolute calibration, the absolute value of the radiance source need not to be known because the normalisation of the signal can be realised requiring an uniform-radiance field in the focal plane. In general relative calibration is performed for monitoring temporal changes of the absolute calibration coefficients.

For radiometric in-flight calibration in the VIS–TIR spectral range a calibration source has to deliver standardised values which cause sensor signals comparable to those measured during detection of the remote sensing target. It has been shown in Figure 1 that for the VIS–TIR radiation spectrum an adequate calibration source has to provide a blackbody temperature between 300 K (TIR) and 5600 K (VIS). For in-orbit calibration the Sun and special calibration lamps are used for the VIS–SWIR, and internal blackbodies for the TIR spectral range.

[82] Physikalisch-Technische Bundesanstalt (PTB), Germany
[83] National Institute of Standards and Technology (NIST), USA
[84] Neckel and Labs–1984

2.2.2.4.2 Comparison of different radiometric in-flight calibration methods

In the following an overview of different calibration procedures is given by explaining briefly the advantages and disadvantages of each method. Further details can be retrieved from literature in either generalised[85] or individually discussed form (see references in Table 7)
As calibration source in the VIS–SWIR either natural (Sun) or artificial (lamps) sources can be used. For both radiance sources various calibration methods exist:

Sun calibration with diffuser:
For this method a nearly lambertian panel (white) is placed in front of the sensor's optics during the calibration procedure. The Sun's irradiance is reflected via the diffuser into the sensor aperture. In contrast to lamps, the Sun has a strong blue part of the spectrum. The disadvantage is the possible diffuser degradation form exposure to the Sun and space environment.

Sun calibration with pinhole:
The pinhole (diameter ~ 0.5 mm) allows a narrow beam of solar light to pass all optical elements of the sensor by directly viewing the Sun, but without any additional optical elements besides the small aperture of the pinhole which is necessary to avoid saturation. A disadvantage is the possible pinhole degradation (e.g. by particulate and molecular contamination). Other disadvantages are the sensitivity to position uncertainties of the pinhole in relation to the sun and that the light beam does not fill the TFOV.

Sun/lamps calibration with fibre optics:
Using fibre optics for transferring the Sun's or lamp's radiance in the sensor's FOV introduces the problem of fibre-optics degradation caused by the space environment. Another disadvantage occurs because the light beam does not fill the TFOV.

External lamp calibration:
The external lamp ensures the light to pass all optics, hence it enables absolute and relative calibration. Applying lamps introduces in general the disadvantage of a low blue part of the spectrum because the lamp (in contrast to the Sun) emits photons at a relatively low temperature of ~2700 K. However, this calibration approach is practical because of the availability on command. A disadvantage can occur because the radiance field does not fill the TFOV.

Internal lamp calibration:
In contrast to the external lamp calibration, the internal lamp can only be used for relative calibration (e.g. detector stability, linearity) because the light does not pass the full optical path. Disadvantages is also the low blue part of the lamp's spectrum. However this method can easily be integrated in the sensor's design.

[85] Dinguirard and Slater–1999

The following Table 7 summarises the calibration possibilities, gives sensor examples and outlines the specific advantages and disadvantages of each method.

Table 7: Overview of onboard calibration methods

Method	Example	Advantage	Disadvantage
Diffuser + Sun	SeaWiFS[86], MERIS[87], MODIS[88], MOS[89], MOMS-2P[90], HSI[91], AVNIR[92], OCTS[93], ALI[94]	• high blue signal • full aperture • complete TFOV • same optics for pre-flight and in-flight calibration	• possible degradation of diffuser • effort to determine exact diffuser Sun position
Fibre optics + Sun	SPOT 1-4[95]	• passing all optics • high blue signal	• not TFOV • degradation of fibre cable
Pinhole + Sun	ETM+[96]	• high blue signal	• not TFOV • possible degradation of the pinhole
Fibre optics + internal lamps		• high stability of the lamps • available on command	• not TFOV • degradation of fibre cable • low blue signal
External lamps	VEGETATION[97], ASTER[98]	• passing all optics • available on command	• not TFOV • low blue signal
Internal lamps	MOS, ETM+, SPOT 1-4, AVNIR	• available on command • easy design integration	• not TFOV • low blue signal • not passing all optics

The main disadvantage of the solar diffuser (i.e. the possible degradation when exposed to the Sun and space environment) can be overcome by using the concept of the rationing radiometer which has been introduced recently[99]. It provides a reliable method of monitoring the change in radiance of a solar-diffuser panel by using a monitoring spectrometer. The disadvantage of this method is the additional payload mass.

[86] McClain et al.–1994
[87] Olij et al.–1997
[88] Guenther et al.–1996
[89] Sümnich and Schwarzer–1998
[90] Schroeder et al.–1998
[91] Willoughby et al.–1996
[92] Shimada et al.–1997
[93] Oaku et al.–1997
[94] Digenis et al.–1998
[95] Dinguirard et al.–1998
[96] Markham et al.–1997
[97] Saint –1994
[98] Fujisada–1994
[99] Palmer and Slater–1991

Conclusion

The main differences between the calibration approaches is the application of either the Sun or lamps as a radiance source. For remote sensing tasks it is evident to use a calibration source distribution similar to that of the Sun. The apparent disadvantage of lamps — being a Planck continuum emitters at ~2700 K — is the low blue emission what causes problems particularly for the calibration of ocean-colour sensors. In contrast to lamps, the Sun offers a high blue signal but possible degradation of either diffuser or pinhole must be taken into account.

These problems might be solved by introducing a new calibration approach for space sensor calibration: in-flight calibration with LEDs. In the past decade the performance development of LEDs has lead to lower degradation of light output over time, higher luminous efficiencies and broader spectral coverage. This makes the LED a candidate for radiometric calibration. Further investigations should verify whether this light source can be used in space environment.

2.3 Sensor and orbit optimisation for a regional coastal zone mission

The task of the sensor and orbit optimisation is to meet the (scientific) observation requirements by finding a compromise between mission constrains on one side and available sensor and satellite technologies on the other side. Out of this compromise the basic sensor and satellite parameters can be concluded.

2.3.1 Orbit-satellite optimisation

An important mission parameter is the repetition rate in which the sensor will be able to repeat the measurement of the same Earth surface spot. High repetivity is one of the main scientific observation requirements for regional applications. However, global coverage is not needed, therefore large slant viewing angles like a swath ≥ 1000 km can be avoided. These would produce problems in data processing and ground resolution. The goal of achieving a short repetition rate on ground can be realised by choosing an adequate spacecraft and suitable orbit parameters.

The repetition rate depends on the satellite's orbit in terms of height and inclination. The Sun-synchron orbit has the great advantage of ensuring the required constant overflight time. This means that the satellite has to be placed in an orbit with an inclination angle (orbit height) between 96.16° (250 km) and 99.49° (1000 km). But since lower altitude orbits cannot be regarded as drag-free, an altitude of >600 km has to be selected for ensuring a long mission duration (presupposing the S/C has no additional propulsion system). Hence, the first assumption of the satellite's altitude, velocity and orbit inclination with respect to the desired revisit time can be determined and the spatial related sensor parameters can be retrieved, e.g. the definition of the IFOV, the FOV and the integration time.

For the optimisation the following modus operandi is applied: The “basic” repetition rate is determined by a proper orbit parameter selection. Thereinafter for achieving a shorter repetition rate in the case of the necessary detection of special events or dedicated regions of interest, the satellite's cross-track tilt capability can be used. As a result an adequate LEO orbit is determined and the repetition rate is ensured by the cross-track angle.

Orbit selection for the “basic” repetition rate

Preliminary observation calculations show that a 775 km Sun-synchronous orbit with 98.5° inclination would allow a repetition of the same ground track after 3 days. Figure 14 shows all tracks which can be received from the DLR ground station Neustrelitz. The sensor's operation mode is nadir viewing with a swath of 400 km. The equator crossing time is before noon caused by the illumination conditions in the northern hemisphere and the minimisation of Sun glint. The first overflight in the figure is represented by orbit 1 on day 1. The next day's first orbit track lays ~930 km (at the equator) eastwards of the original track. The day 3 orbit will be located another ~930 km further eastwards. The same orbital repetition rate is repeated for orbit 2, 3 and 4 which are placed ~2790, ~5560 and ~8370 km further to the west. The complete ground track pattern for the above described orbits can be retrieved from Figure 24 for the 3 days and 4 orbits. The figure also shows the orbital track of the 4th day which is identical to that of the 1st day.

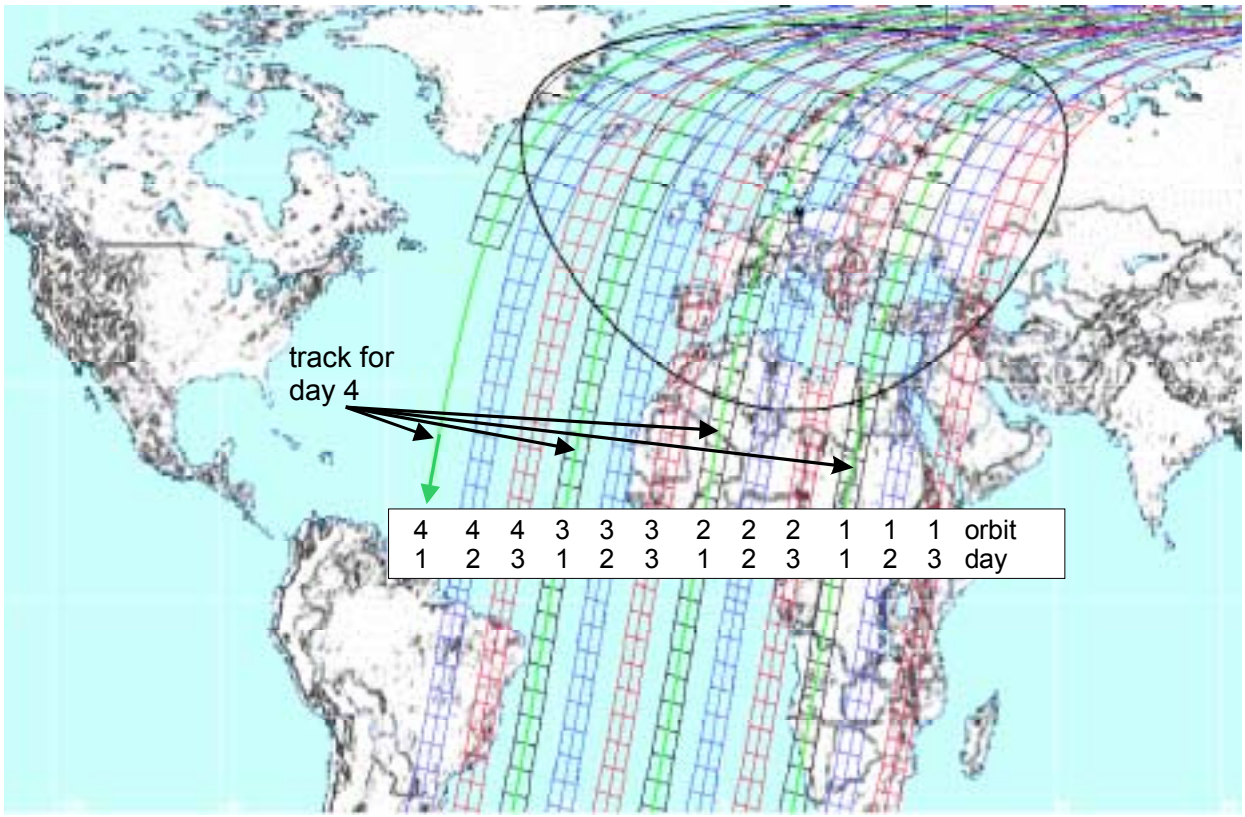

Figure 14: Orbit track for 4 days, height = 775 km, inclination = 98.5°, sun-synchronous, descending passes only

Selection of the tilting capability

A tilting capability, which helps to detect off-nadir ground tracks, can be realised in turning single sensors at the satellite by mechanical system or in pointing the whole satellite in the new off-nadir direction which has a cross-track offset.

The mechanical turning system operates independently to the S/C performance, but at the costs of additional mass. In contrast advanced 3-axis stabilised satellites are able to tilt the whole S/C but at costs of a reduced pointing accuracy at the extreme off-Nadir positions. Hence, a S/C with tilting capabilities is a good solution when the problem of reduced pointing accuracy can be solved. An advanced control systems in conjunction with an improved 3-axis stabilised satellite should be able to solve this problem.

Conclusion

Concluding, the basic repetition rate for the mission concept can be ensured in a 775 km Sun-synchron orbit. The corresponding ground track has a swath width of ~400 km. Using a satellite with a tilting possibility the cross-track tilt angle shortens possible repetitive observations by increasing the basic FOV of the sensors to a large *FOR* of the whole satellite-sensor system.

2.3.2 Sensor and payload optimisation

Using the first orbit-satellite parameters and taking the scientific spectral and radiometric requirements into account the sensor optimisation can be started.

For the successive sensor optimisation a separation of the spectral part in the electromagnetic spectrum (VIS–NIR, SWIR, TIR) has been made because of differences in both, scientific requirements (e.g. spectral, spatial and radiometric resolution, encoding level, calibration accuracy) and available technologies.

VIS-NIR

In the VIS-NIR region a relative high number of spectral channels (~16 mostly programmable), a high signal to noise ratio and a high spectral resolution is required. These requirements make the imaging spectrometer to a suitable solution because it delivers many continuous spectral bands. A comparison of different imaging spectrometers is given in Table 4. It has been shown that with LEO mission constrains (high platform velocity) and observation requirements (basic spectral resolution ~ 1.5nm, ground resolution ~ 100 m) the optimal imaging approach is the pushbroom imaging spectrometer. However, the pushbroom imaging spectrometer's slit length (cross track FOV) is limited by the variation in dispersive power across the cross-track FOV, i.e. a swath width of about 110 km for a 775 km orbit. To guarantee the needed synchronous generation of images for the whole swath width of 400 km four similar spectrometers (FOV ~ 30°) have to be aligned for ensuring congruent swaths.

The spectrometer's spectral selection has to meet diverse requirements, such as high spectral resolution, low straylight and simultaneous detection of all spectral channels. Regarding these requirements, the grating and the prism are the most interesting solutions (see also Table 5). The grating has the advantage of linear dispersion and broad spectral range but often at the

costs of a low throughput and order overlap problems. The prism has the advantage of a high transmission and no order overlap, but with the cost of non-linear dispersion and relatively high mass. While space missions have always mass restrictions and the basic spectral resolution should be ~1.5 nm over the whole VIS–NIR region, a solution for the spectrometer's spectral selector should be searched using a grating. However, grating imaging spectrometer for a future mission must have a reduced polarisation sensitivity and solve the problem of spectral order overlap. Moreover, the grating has to provide enough energy (adequate efficiency) for the detector to meet the high radiometric requirements.

The incident and spectrally separated photons will be captured by a detector. Out of those detector which are commercially available in the small niche market of scientific detectors only the CID, the CCD and the APS technology can be used. A comparison of these detector technologies is provided in Table 6. The high noise is the main constraint for the use of CIDs. Whereas the APS (active pixel sensor) still has the problem of low quantum efficiency, high calibration complexity and low fill factor, the frame-transfer CCD is a reliable solution for Earth observation systems. The determination of the VIS–NIR imaging spectrometer radiometric requirements base on experiences with MOS–IRS: 16 bit as radiometric resolution, 100 as SNR for minimum radiance, and 0.01 – 40 $\mu Wcm^{-2}nm^{-1}sr^{-1}$ as dynamic range.

Beside the above mentioned basic spectrometer elements, also the calibration accuracy has a significant importance for the sensor's figure of merit. While basic calibration accuracy can be provided by extensive pre-flight calibration activities, long-term stability and re-calibration during the mission life has to be ensured by advanced in-flight calibration capabilities. This means that the layout of a detailed calibration concept has to be taken under consideration. Besides developing an enhanced calibration procedure concept which omits Sun and lamp calibration and internal checks, also a performance investigation of LEDs should verify whether LEDs can be used for space sensor calibration provide sufficient information for coastal zone research.

SWIR

For coastal zone remote sensing it is not necessary to cover the complete SWIR from 1.1 to 2.5 µm with many spectral channels because the atmospheric transmission provides only a few windows (see transmission plot in Figure 1) which allow a space sensor to image the Earth surface. These windows are situated at 1.25, 1.6 and 2.1 µm. Additional, water content determination can be provided at 1.38 µm.

Hence, a sufficient coverage in the SWIR is realised with 4 single channels. In this case, it would not be necessary to use an imaging spectrometer (as in the VIS–NIR). A pushbroom camera can also provide the requested spectral information. The classic camera design consists of one entrance optics, one spectral filter and one detector for each channel. However, this camera solution has the disadvantage of relatively high mass and large sensor envelop, when extended from a single to a 4–channel camera. Spot's HRV sensors demonstrated how to reduce mass and sensor envelop size when applying a dichroic

beamsplitter[100]. Here only one entrance optics for all spectral channels is responsible for collecting the ground pixel's radiation. The incoming radiation is separated spectrally and focussed on four different detectors. The spectral separation is carried out by a beamsplitter assembly. It consists of a set of prisms with dichroic coatings. The associated detectors are butted upon the prisms at each output port.

In contrast to the VIS–NIR spectral range sufficient information is provided with coarser spectral resolution of about 20 to 100 nm. However, the radiometric requirements (e.g. radiometric resolution, SNR) are similar to those in the VIS–NIR. Only the maximum expected radiance is lower (L_{MAX}: 10 $\mu Wcm^{-2}nm^{-1}sr^{-1}$) because the Sun provides less energy in this spectral region.

In the VIS–NIR and the SWIR the required swath widths (FOV) are comparable, too: 400 km or 30° provide adequate data for regional observation. But in contrast a coarser spatial resolution of < 400 m is required because the SWIR data will be mainly used for atmospheric investigation (e.g. aerosol optical thickness, cirrus cloud detection).

The experiences with the MOS–C channel show that the InGaAs detector material provide good results. Unfortunately, the maximum pixel number of commercially available detectors is limited to 512 pixels[101,102]. However, a swath width of 400 km with a spatial resolution of <400 m needs at least 1000 pixels. In that case it is possible (similar to the VIS–NIR) to ensure a congruent swath width of 400 km when aligning two similar SWIR cameras in a way they provide the required data.

TIR

The surface temperature can be retrieved by measurements in one TIR channel. The observation requirements need a high temperature resolution of less than 0.5 K. This thermal information can be retrieved at 10.5 µm where the complete bandwidth of the atmospheric window can be used (up to $\Delta\lambda \sim 2$ µm) for emission measurements.

The spatial requirements are similar to those in the SWIR: 400 km swath width and 400 m spatial resolution provides adequate information on coastal current and primary production. In contrast to the SWIR no long line arrays are commercially available. However, a good solution is provided in the TIR: For reasonable costs the well-tried (long military tradition) whiskbroom scanner with a discrete HgCdTe detector[103] provides a good temperature resolution over the whole swath of 400 km.

[100] Jouran et al.–1989
[101] EG&G–1998
[102] Hamamatsu–1997
[103] Schwalb–1979

Conclusion

The result of the sensor optimisation is the selection of very different sensor types which are optimised for the observation requirements. To overcome the physical-technology related constrains several similar sensors have to be aligned to make up a longer swath:
A single pushbroom imaging spectrometer (narrow FOV) or a single SWIR camera (FOV~14.5°) do not span the total desired swath width of 400 km (TFOV~27.3°). Consequently, four spectrometers and two cameras have to be aligned in a way for ensuring congruent swaths. Thus a synchronous generation of images in different spectral ranges has to be guaranteed. In contrast to the pushbroom solutions in the VIS and SWIR, a whiskbroom scanner is the preferable sensor type for covering the TIR region. A single scan is able to span the whole swath width of 400 km with a ground resolution of 400 m.

2.3.3 Observation Requirements

On the basis of the outlined scientific tasks for regional coastal zone observation (see Table 2 in Chapter 1.2.3) and in conjunction with the orbit and sensor optimisation the satellite and payload requirements can be concluded.

The satellite for this mission should be launched in a 775 km Sun-synchron orbit. The satellite should have a tilting capability. The tilting angle should be selectable in the range of ± 30° before each data sampling orbit. However, a high pointing accuracy is required with the result, that the satellite needs an advanced control systems.

The payload should consist of very different sensors, i.e. four similar VIS–NIR pushbroom imaging spectrometers, two similar SWIR pushbroom cameras and a TIR whiskbroom scanner. These sensors provide spectrally resolved data with the following characteristics[104]:

- *VIS/NIR (400 – 1050 nm) data provided by pushbroom grating imaging spectrometers with 2-d frame-transfer CCD*
  - number of spectral channels: roughly 16 spectral channels
  - basic spectral resolution: ~ 1.5 nm
  - spectral position of transmitted channels programmable out of 512 available
  - spectral halfwidth programmable by superposition of single CCD-elements
  - spatial resolution: 100 m
  - radiometric resolution: 16 bit
  - dynamic range: 0.01 – 40 µW $cm^{-2}nm^{-1}$ sr^{-1}
  - signal to noise-ratio at minimum radiance level: 100

- *SWIR data provided by pushbroom four-channel cameras with beamsplitter assembly (prisms with dichroic coating) and InGaAs line arrays*
  - 4 fixed channels at 1.25 µm, 1.38 µm, 1.6 µm, 2.1 µm
  - spectral bandwidth (filter characteristics): 20 – 50 nm
  - spatial resolution: ≤ 400 m
  - radiometric resolution: 16 bit
  - dynamic range: 0.02 – 10 µW $cm^{-2}nm^{-1}$ sr^{-1}
  - signal to noise ratio at minimum radiance level: 100

- *TIR data provided by a whiskbroom scanner with one discrete HgCdTe detector:*
  - one fixed channel at 10.5 µm
  - spatial resolution: ≤ 400 m
  - radiometric resolution: 10 bit
  - temperature range: 240 – 340 K
  - temperature resolution: ≤ 0.5 K

[104] Neumann et al.–1998

3 Specific investigations for the mission's sensor and calibration concept

In the preceding chapter it has been concluded that regional orientated coastal zone mission observation requirements in the spectral range from the VIS-NIR to the TIR are best covered by very specific sensors types: four pushbroom imaging spectrometers with 2-d VIS-NIR detectors, two 4-channel pushbroom cameras with line array SWIR detectors and a whiskbroom scanner with a single TIR detector.

The whiskbroom scanner and the pushbroom cameras with 4-channel beamsplitter assembly are well-tried technologies. Whereas the TIR scanner found many applications in numerous military or space orientated missions[105], an application of a pushbroom camera with 4-channel dichroic beamsplitter assembly was first realised with SPOT HRV[106]. The application of a special InGaAs detector for a spaceborne camera have been demonstrated with MOS–IRS recently. Hence, the needed research effort for these sensors is relatively predictable. In contrast, imaging spectrometer development with 2-d VIS-NIR detectors provides many more unsolved problems, i.e. a higher research effort. These problems for a coastal zone mission can be summarised in three main topics:

- The required spectrally and spatially high resolution cause low input signals for the detector's pixels (see Chapter 2.2.2.1). Thus, the sensor specific noise budget can overwhelm the signal, and as crucial consequence, the sensitivity decreases significantly. Therefore the radiometric performance of the imaging spectrometer has to be simulated to predict the signal-to-noise ratio of the future imaging spectrometer. Such a prediction can be realised by means of a 2-d detectors specific sensitivity analysis.
- The grating as spectral selector in conjunction with the optics in an imaging spectrometer may provide the following problems: low efficiency, second order overlap, high polarisation sensitivity, high straylight, large sensor dimensions (see Chapter 2.2.2.2). The main task is to find appropriated grating parameters (in conjunction with an imaging spectrometer configuration) which is able to overcome these problems.
- To ensure long-term sensor stability is one of the key design problems since the beginning of quantitatively coastal zone remote sensing (see Chapter 1.3). Only an advanced in-flight calibration procedure can provide sufficient long-term stability for the imager. As outlined in Chapter 2.2.2.4, LEDs are a good candidate to improve the sensor calibration concept, however investigations have to verify whether these light sources can be utilised in space environment.

Between 1996 and 1999 various investigation have been performed at DLR, Berlin with the objective to develop an advanced imaging spectrometer and calibration concept which will be capable to overcome the above mentioned problems. The results of the investigations are outlined in the following.

[105] Schwalb–1979
[106] Jouan et al.–1989

3.1 Sensitivity analysis for imaging spectrometers

By means of the sensitivity analysis it is possible to predict the radiometric performance (with given spectral and spatial resolution) of a remote sensing instrument. For this sensitivity analysis numerous environmental and instrumental parameters have to be determined. The environmental parameters are defined by the expected TOA input radiance which depend on factors like: the specific geometry between Sun and observer, the atmosphere and others more. The instrumental parameters are subdivided in optical (e.g. FOV, IFOV, MTF, aperture, focal length, optical transmission), detector (e.g. response constant, spectral response, noise and dynamic) and the electronic (dynamic, amplifier, noise) parameters.

As a result the radiometric performance of a sensor is described by the expected minimum TOA radiance (L_{MIN}), maximum TOA radiance (L_{MAX}), noise equivalent radiance ($Ne\Delta L$) and signal-to-noise ratio (SNR) which have also been outlined in Chapter 1.1.2.2. Whereas L_{MIN}, L_{MAX} and $Ne\Delta L$ are defined by the observation requirements (application), SNR is in response to these observation requirements a sensor specific figure of merit. Consequently, the precise determination of the SNR is one of the latter's most important parameter which defines the quality of new sensor concept.

The SNR represents a ratio where the signal S is defined as the number of photons corresponding to the TOA radiance (input radiance) and the noise N is the total amount of noise generated by the instrument or the signal itself. Calculations of signal-to-noise ratio are summarised in many sources since the beginning of sensor development[107] and for different hyper-spectroradiometric sensor types[108]. These sources include the discussion and the general formulation of noise sources (e.g. photon noise, thermal noise, readout noise) and describe the advantages and disadvantages typically for solid-state sensors.

Hence, the complete radiometric sensitivity calculation consists of two parts. The first step is the consideration of the expected TOA radiance (e.g. influenced by solar radiance, Earth reflectance, atmospheric transmission) factors. Thereinafter, the instrumental parameters (such as f-number, lens transmission, efficiency of the grating and quantum efficiency) have to be determined and the SNR analysis can be performed.

[107] Wolfe–1964
[108] Gumbel–1996

3.1.1 Top-of-atmosphere radiance

The top-of-atmosphere (TOA) radiance that is detected by a spaceborne imaging spectrometer is influenced by different parameters such as the atmosphere transmission, the specific geometry between Sun and observer, the albedo of the land and water surface, the scattering and absorption of the water. A simulation of different scenarios have been performed by using an in-house simulation program. Hence, a maximal and a minimal expected TOA radiance for objects with different spectral signatures (water, vegetation, etc.) can be estimated. Moreover, these values were also confirmed by analyzing MOS data obtained in orbit[109]. The resulting TOA radiance is depicted in Figure 15.

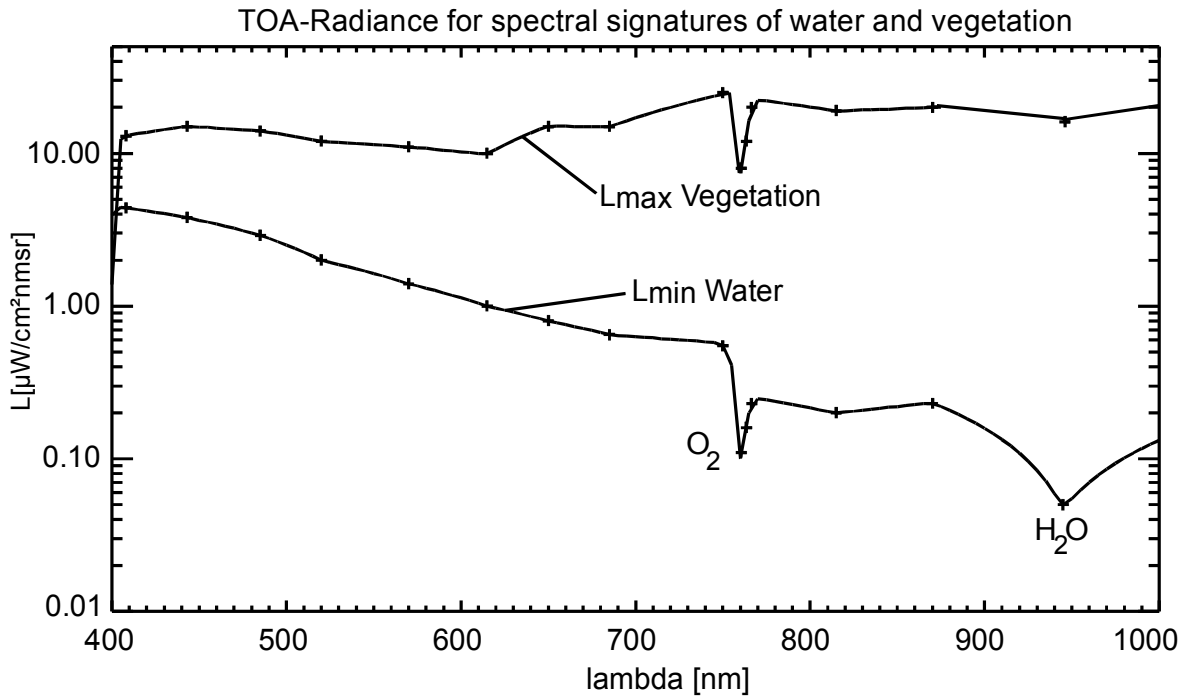

Figure 15: TOA radiances for spectral signatures of water and vegetation (including O_2A and H_2O absorption bands)

3.1.2 Classical signal-to-noise ratio analysis

The SNR outlines the lower limit of light input at which the device can operate and offers the possibility to compare the signal *S*, which will be detected from the sensor, with the noise *N*, i.e. signal level of the sensor in the absence of *S*. The signal *S* consists of a certain number of electrons which are proportional or almost proportional to the number of photons which arrive at the sensor. For an optical grating sensor, the number of electrons can be obtained by applying the following calculation.

[109] Zimmermann–1999

The irradiance at the detector surface can be retrieved from the Abbe sinus relation[110] and determined via

$$E^{\lambda}_{\text{det ector}} = \frac{\pi}{4} L^{\lambda}_{\text{TOA}} T^{\lambda}_{\text{grating}} T^{\lambda}_{\text{objective}} F\#^{2}, \tag{3.–1}$$

where L_{TOA} is the top of atmosphere radiance (see also Figure 15), $T_{grating}$ is the grating efficiency, $T_{objective}$ the transmission of the objective and $F\#$ the inverse f-number.

The calculation of the quantity of electrons and the sensor signal can be achieved with

$$S^{\lambda}_{\text{TOA}} = \frac{E^{\lambda}_{\text{detector}} QE^{\lambda}_{\text{detector}} A_{\text{detector}} T_{\text{int}} d\lambda}{h c / \lambda}, \tag{3.–2}$$

where $A_{detector}$ is the detector sensitive area, QE is the quantum efficiency of the detector, T_{int} is the integration time, $d\lambda$ is the spectral bandwidth, h is the Planck Constant and c is the velocity of light. There is a significant wavelength dependency of the grating efficiency, the transmission of the objective and the quantum efficiency that cannot be neglected.
The measured signal consists of electrons produced by the incoming photons (S_{TOA}) and the dark signal (S_{dark}). The total noise contains the photon noise (N_{photon}), and the noise level related to the sensor (N_{sensor}). The ratio of these readings can be described as

$$\frac{Signal^{\lambda i}_{measured}}{Noise_{total}} = \frac{S^{\lambda i}_{TOA} + S_{dark}}{(N^{\lambda i}_{photon}{}^{2} + N_{sensor}{}^{2})^{1/2}}. \tag{3.–3}$$

For the SNR analysis the measured signal in Eq. 3.–3 has to be reduced to the input radiance S_{TOA}

$$\frac{Signal^{\lambda i}_{TOA}}{Noise} = \frac{S^{\lambda i}_{TOA}}{(N^{\lambda i}_{photon}{}^{2} + N_{sensor}{}^{2})^{1/2}} \tag{3.–4}$$

to receive a SNR which is comparable with the most important instrumental parameter, the noise equivalent radiance NeΔL (see Chapter 1.1.2.2).

[110] Hofmann–1980

This overall noise figure is a combination of different noise sources that all have their specific dependency on the wavelength, temperature and other factors. For a charge coupled device sensor, the noise terms can be reduced to

$$N_{sensor} = (N_{amplifier}^{\ 2} + N_{quantisation}^{\ 2} + N_{readout}^{\ 2} + N_{dark}^{\ 2})^{1/2}, \qquad (3.–5)$$

where N_{sensor} stands for the sum of all sensor contributed-noise sources, $N_{ampifier}$ is the sensor-output-amplifier noise, $N_{quantisation}$ is the analogue digital converter input noise, $N_{readout}$ is the readout noise and N_{dark} is the dark current shot noise. The output-amplifier noise can be split up into thermal noise, 1/f noise and reset noise depending on the mechanisms by which they are generated. The reset noise can be overcome by correlated double sampling, but the thermal noise and the 1/f noise should be taken into account depending on the type of amplifier (buried channel, FET). Some of these noise sources are highly technology related others are unavoidable because of the sensor's operating principle. Details on the technological background of the noise sources can be found in literature[111]. In the following some unavoidable noise sources are described:
The generation of dark current shot noise N_{dark} is a statistical process. Therefore the quantity is proportional to the square root of the mean dark current values. Because of its temperature dependency, a reduction of the dark noise quantity is possible. As example the dark current decreases from 30 000 to 3000 electrons per sec (170 to 50 electrons per sec for the noise) by reducing the operating temperature of the CCD-detector (EEV 25-20) from +25°C to -5°C.
The photon noise

$$N_{photon}^{\lambda i} = \sqrt{S_{TOA}^{\lambda i}} \qquad (3.–6)$$

results from a statistical structure of the incoming photons and is proportional to the square root of the amount of electrons generated by the optical input. The quantity cannot be influenced and dominates at high levels.
Transfer noise (transport efficiency), point defects, column defects, striations and pixel non-uniformities are not discussed in this context, because of the high dependence on the technology quality and the small spectral influence on the total noise budget.

3.1.3 Refined signal-to-noise ratio analysis for 2-d detectors

As discussed in Chapter 2.2.2.3 the frame-transfer CCD is so far the best solution for an imaging spectrometer because of the high fill factor (aperture ratio), the high SNR, and better performance in a space environment. The operating principle of a frame-transfer detector can be described as illustrated in Figure 16. The incoming light of a swath of the Earth scenery is dispersed spectrally and focused in the spectrometer's focal plane. In the focal plane a light-sensitive image zone of a two-dimensional CCD can detect the incoming light. The selection of the required spectrometer parameters (e.g. 512 spectral lines) generally determines the

[111] Theuwissen–1996

horizontal pixel as the spatial resolution (Δx) and the vertical pixel as the spectral resolution ($\Delta\lambda$). These pixels are set into the integrating mode and charges generated by incoming photons are collected in the induced potential wells. At the end of a defined integration time, the CCD shift registers transfer their charged packets to the corresponding CCD lines in the light-insensitive storage zone. During this transfer the imager is not shielded from the incoming light and the generation of electrons continues. This is why this transfer from the image to the storage zone has to be done as quickly as possible to minimise image smear by additional charge generation in the image zone. The electrons generated in the spatial (horizontal) lines are shifted over the λ-columns of the detector. During the slide from the image to the storage zone, each line samples additional information of the λ-columns over which the lines will shift. When the entire information from the image zone has been transferred to the storage zone, the charge packets can be read out. After transferring the horizontal lines to the readout line these lines are finally shifted to the CCD output stage where the charge packets can be converted to an electrical voltage. Thus, processing of the video signal can be started.

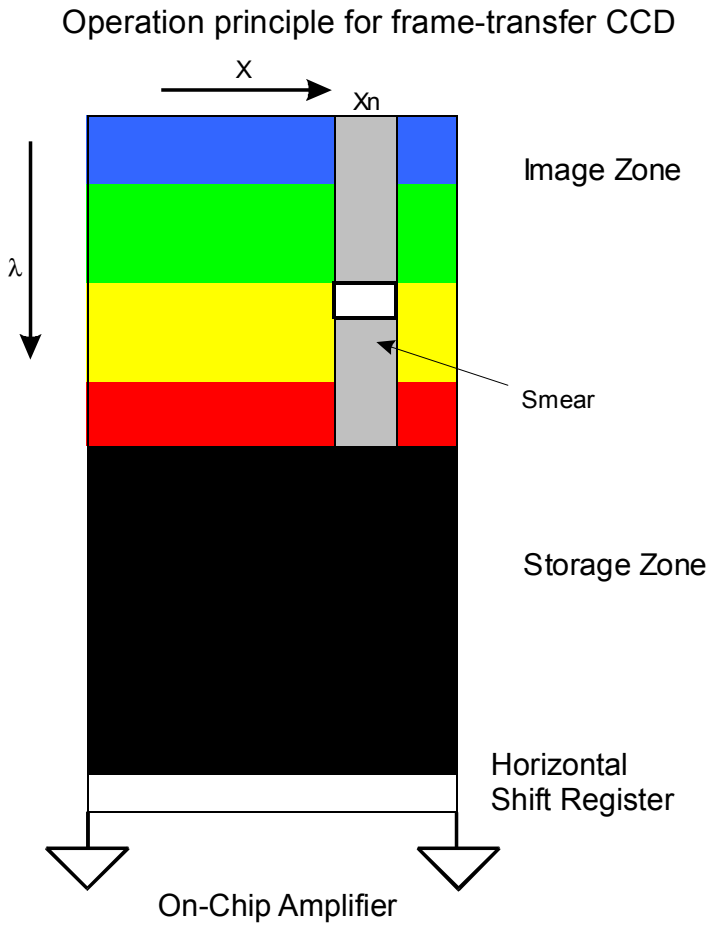

Figure 16: Operation principle for a frame transfer CCD

The shortest vertical transport time T_{trans} of the charge transfer from one line to another line is the reciprocal value of the frame shift frequency F_{trans}. The frame shift frequency is highly technology related and a crucial parameter in the 2-d detector. Because the smear level is proportional to T_{trans} the relation of image smear for a frame transfer CCD is:

$$S_{smear}(i) = \frac{T_{trans}}{T_{int}} \left(\sum_{k=i+1}^{n} S_k + \sum_{k=1}^{i-1} S_k \right), \tag{3.–7}$$

where S_{smear} is the smear level generated by the charged packets during the transport time, n the number of horizontal lines, and k is the spectral line before or after the considered line i. Consequently, the smear level, depending on the spectral signature, is a static amount over the spectrum and is demonstrated in Figure 18 as a horizontal plot line. This signal can be measured by additional smear detection lines which only detect the total smear amount without carrying information of the ground pixel. Presupposing that the amount of electrons generated by image smear is known with high accuracy, a correction algorithm can subtract the additional signal from the measured signal. But it is not possible to compensate for the noise component of the image smear. The signal of the incoming photons as well as the smear signal have a statistical structure. This means that even with the knowledge of the smear signal the smear noise

$$N_{smear}^{\lambda k} = \sqrt{S_{smear}^{\lambda k}}, \tag{3.–8}$$

which is uncorrelated to the other noise sources cannot be neglected in the sensitivity analysis.

Refined SNR

As a result the SNR for two-dimensional pushbroom imagers with frame-transfer CCD arrays has to be refined due to image smear. Hence the measured signal and the noise have to be described as

$$\frac{Signal_{measured}^{\lambda ik}}{Noise_{total}} = \frac{S_{TOA}^{\lambda i} + S_{smear}^{\lambda k} + S_{dark}}{(N_{photon}^{\lambda i\ 2} + N_{sensor}^{\ 2} + N_{smear}^{\lambda k\ 2})^{1/2}} \tag{3.–9}$$

and consequently reduced to the TOA input radiance to

$$\frac{Signal_{TOA}^{\lambda ik}}{Noise} = \frac{S_{TOA}^{\lambda i}}{(N_{photon}^{\lambda i\ 2} + N_{sensor}^{\ 2} + N_{smear}^{\lambda k\ 2})^{1/2}} . \qquad (3.–10)$$

This ratio demonstrates how the smear noise can reduce the real sensor sensitivity. For longer transfer times T_{trans} with respect to the integration time T_{int}, the S_{smear} may reach values of the S_{TOA} and consequently N_{smear} will be in the size of N_{Photon}. The relation T_{tran} / T_{int} determines the ratio of S_{smear} / S_{TOA} and N_{smear} / N_{Photon} for a given ground scene. For an existing spectrometer $T_{tran} / T_{int} = const$ and S_{smear} / S_{TOA} and its noise values are only dependent of the natural scene radiance and the surface. Unfortunately S_{TOA} of water surfaces has a strong spectral gradient (high blue and small NIR values). This means that S_{TOA} (and N_{Photon}) might be small in some spectral regions but the smear noise becomes more and more important because S_{smear} (and N_{smear}) consists of information from all spectral channels. This influence will be explained in the following section by means of an spectrometer example.

3.1.4 Comparison of refined and classical SNR analysis

To illustrate the influence of the smear on the sensitivity analysis a comparison of refined and classical SNR analysis is made using the well-known MERIS sensor[112] as example. For the sensitivity analysis of an imaging spectrometer that utilises a grating and a two-dimensional detector, various instrument related parameters have to be taken into account. Some optical and electronic components parameters are summarised in Table 8.

Table 8: Comparison of sensor parameters

Parameter	**Value**
Pixel size [µm²]	22.5 x 22.5
T_{int} [ms]	40-160
T_{trans} [µs]	3
F#	1 / 2.5
Spectral bandwidth [nm]	1.25

The wavelength dependency of the transmission of the objective ($T_{objective}$) and the efficiency of grating ($T_{grating}$) and detector ($QE_{detector}$) can be retrieved from Figure 17.

[112] Rast–1998

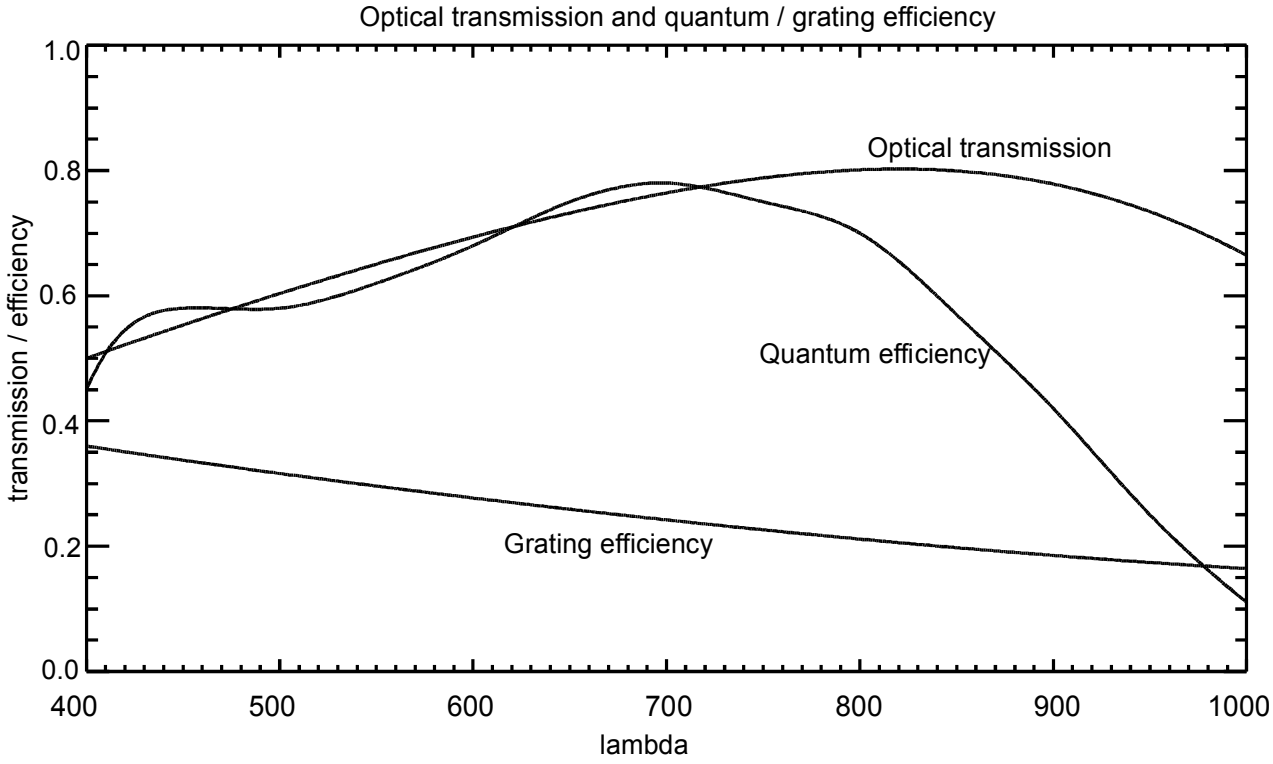

Figure 17: Optical transmission, quantum efficiency, and grating efficiency[113,114]

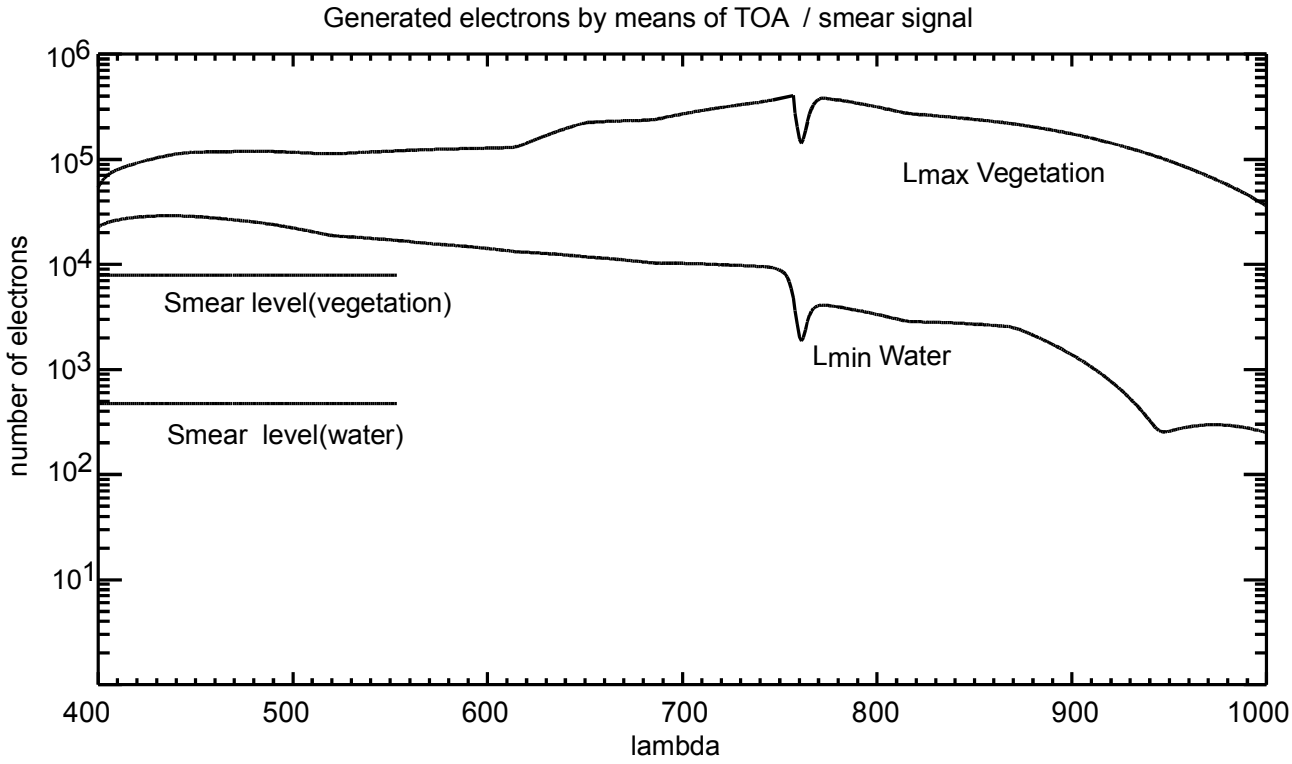

Figure 18: Number of generated electrons (TOA signal, smear level)

[113] Coste–1997
[114] EEV datasheet CCD25-20 EEV–1996

By use of Eq. 3.–1 and 3.–2 the number of electrons, i.e. the TOA signal for vegetation and water, can be plotted versus wavelength (Figure 18). The horizontal line in this plot represents the total smear signal level caused by the water / vegetation spectral signatures. These smear signals are a result of an integration over the entire spectrum and only depend on the spectral signatures for a given spectrometer configuration (T_{tran}, T_{int}, $T_{objective}(\lambda)$, $T_{grating}(\lambda)$, $QE_{detector}(\lambda)$ are constant). It can be seen that the total image smear level can be equal or even greater than the signal level in a NIR channel. This phenomena can occur for minimal water radiance, whereas for the spectral signature of vegetation there is a magnitude of signal-differences between S_{smear} and S_{TOA}.

For the subsequent SNR determination, the entire noise budget of the sensor (N_{sensor}) can be limited with today's ADU technology to 10 noise-electrons[115] for the given integration time. The effect of the smear noise and consequently the reduction of the SNR can be obtained from Figure 19 by applying Eq. 3.–4 for the classical and Eq. 3.–10 for the refined analyse.

For the vegetation signal the reduction is at the ends of the VIS-NIR spectrum only 10% at the ends of the spectrum, whereas the SNR for the water scene decreases by as much as 40%. The limiting factor in the NIR is the result of the instrument's quantum efficiency of silicon detector and the TOA input radiance over water. The other components have a small spectral dependency. Thus, a variation of these factors causes only a constant decrease or increase of S_{TOA} (S_{TOA} in Figure 18) and would not result in a SNR reduction demonstrated in Figure 19.

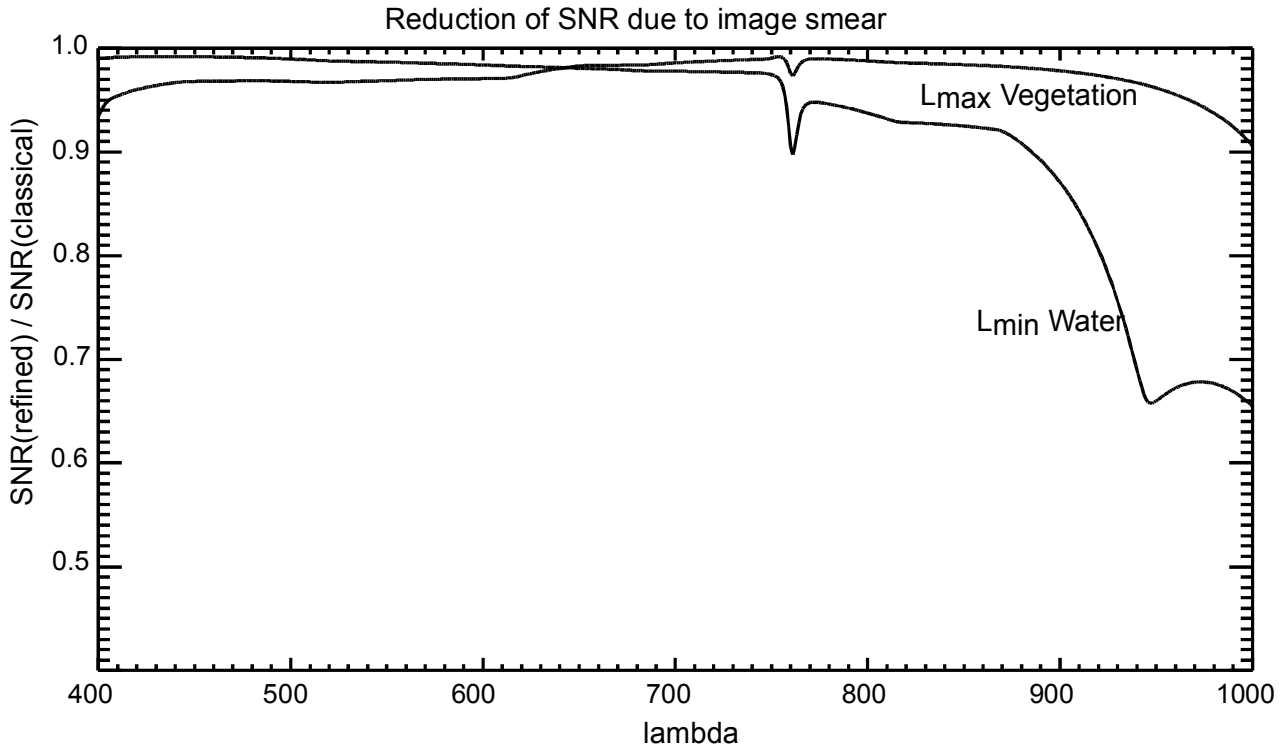

Figure 19: Reduction of the SNR as a result of image smear

[115] Solbrig–1997

Image Smear for other detector types

Smear is a spurious artefact signal which brightens the original signal in the vertical lines of the image (see Figure 16). Depending on the type of imager, image smear is generated in different ways but it takes the same form for most of the detectors:

As explained above the image smear effect for frame-transfer CCDs is generated by photons striking the imaging pixels during the image readout in the storage section. For interline-transfer CCDs, smear is produced by scattered photons entering the vertical CCD shift registers or by stray and scattered electrons collected in the vertical shift registers instead of collecting in the photodiodes[116]. The smear for APS can also be generated by stray electrons and stray photons. But in contrast to interline-transfer CCDs the smear effect will be smaller because of reduced electron transfer length (the amplifier is mostly underneath the pixel). The CIDs are the only type of two-dimensional solid-state detector that are smear-free because the output signal is a displacement current generated in a gate located on top of the silicon and fully isolated from the silicon substrate[117]. However, the main disadvantage of CIDs is the high sensor output-amplifier noise (factor 10) comparing to CCDs.

3.1.5 Conclusion

To fulfill the outlined observation requirements (Chapter 2.2.3) the sensor concept should be able to detect the reflection of various Earth surfaces (clouds, water, and vegetation detection) simultaneously. Further on, high spatial (smaller integration time), spectral (higher number of pixels), and radiometric (higher SNR) resolution is desired. New technology such as pushbroom imaging spectrometers with two-dimensional detectors has shown the potential to serve the needs of the remote-sensing community. For these pushbroom imaging spectrometer the wavelength dependent smear noise was discovered. It originates by application of two-dimensional frame-transfer CCDs in imaging spectrometers where one dimension belongs the spatial and the second the spectral dimension. Consequently the classical SNR analysis has been adapted for two-dimensional detectors, and the noise and offset signal of image smear was analyzed. The use of a refined SNR and the influence of image smear have been demonstrated. For an example spectrometer concept the SNR for clear water scenes (L_{min} water) is dominated by N_{smear}, what makes the near-infrared spectrum data unsuitable for atmospheric correction of these scenes.

Assumed that a very fast frame-transfer CCD ($T_{trans} << 1$ µm) can not be provided, smear suppression possibilities have to be applied: These are mechanical shutters (problem: fixed integration time, mass), electronic shutters (problem: development costs) or using frame-interline CCDs / APS (lowers only the smear level caused by scatted photons and electrons). By applying a smear detection possibility (e.g. readout of additional smear lines which have been shielded from incoming light during integration time) the signal level of smear can be calculated and a simple smear correction algorithm can be realised. For most remote sensing applications (e.g. land, vegetation) the additional photon noise generated by smear (N_{smear})

[116] Ono et al.–1991
[117] Theuwissen–1996

can be neglected. But in the combination of spectral signature (L_{min} water), integration of the image time (high ground resolution), transportation time of the image in the storage section and the number of spectral channels (hyperspectral application), the reduction of the SNR can be crucial.

3.2 The Offner-type imaging spectrometer

On the basis of the scientific tasks for a regional orientated coastal zone mission it has been concluded that the VIS–NIR spectral range is best covered with many narrow spectral channels (see Chapter 1.4). Further on it has been concluded in the optimisation of the system orbit–satellite–sensor, that this VIS–NIR range needs a special sensor type: a pushbroom imaging spectrometer. The pushbroom imaging spectrometer is one of most promising space sensor concepts for remote sensing since it allows the simultaneous acquisition of images in many contiguous, narrow spectral bands with relatively high spatial resolution. Moreover, in particular for coastal zone applications the grating imaging spectrometer might be the best solution when special attention is taken on specific problems, e.g. the straylight and polarisation problem as outlined in Chapter 2.2.2.2.

Recently, some encouraging investigations at DLR, Berlin have been performed to develop a sophisticated pushbroom imaging spectrometer with Offner-layout and special grating design. This Offner-type imaging spectrometer has significant advantages: a low polarisation sensitivity, a low straylight, suppression of the 2nd order spectrum, and a very compact design. In the following this imaging spectrometer will be described, an overview on the performed investigations is given and the results are summarised.

These results were obtained by the following investigations:

- a simulation analysis demonstrating the ability of an Offner-type imaging spectrometer to provide sufficient spectral and spatial image quality,
- a signal-to-noise model-analysis for the overall proof of the entire system (optics, detector, application) and
- an experimental prototype investigations for verifying spectral and geometrical parameters of the simulations.

3.2.1 Ray-tracing and grating simulations

Simulation studies were performed with the goal to find an optimised solution for a coastal zone imaging spectrometer. The analysis started with the definition of the required spectral, radiometric and geometric parameters. Thereinafter, the first simulation analysis (ray-tracing and grating simulation) began which leads to first results for an Offner-type imaging spectrometer. After the selection of a suitable CCD detector for the spectrometer's simulated spot diagrams, the full simulation analysis has been performed for achieving the required geometric and spectral resolution over the entire spectral range (400–1000 nm). The final results are summarised in an internal DLR–BIFO report[118].

[118] List–1997

The resulting spectrometer configuration is able to meet the coastal-water specific radiometric, spectral and geometric requirements and will be described in the following:
The layout of the simulated spectrometer is shown in Figure 20. It is an imaging spectrometer applying the Offner principle[119] in having only one common spherical mirror and a special convex grating with trapezium profile. The incoming light of an object element of the Earth scenery is imaged by the telecentric objective on the entrance slit. This slit acts as field stop masking out all but the desired swath. The radiation coming from the slit is reflected by the spherical mirror onto a holographic convex grating with trapezium profile. This grating disperses the light spectrally and after the second reflection at the spherical mirror the radiation is focused in the spectrometer's focal plane. In the focal plane the selected two-dimensional CCD can detect the incoming light. One detector's picture element in the focal plane represents the rays of one object element at a given wavelength. The spectral information will be detected in the columns and the geometric information in the rows of the CCD, respectively. For the spectrometer the EEV (CCD 47-20) detector was found as a suitable solution in terms of meeting the simulated spot sizes, having a good radiometric performance and being available on the free market. For the detector's pixel size of 13 µm x 13 µm the simulated spectral and spatial spot diagrams show good results. The backside illumination CCD ensures a high quantum efficiency in the blue part of the spectrum. By choosing this CCD detector the required programmability of the spectral channels (binnable pixels) is guarantied, too.

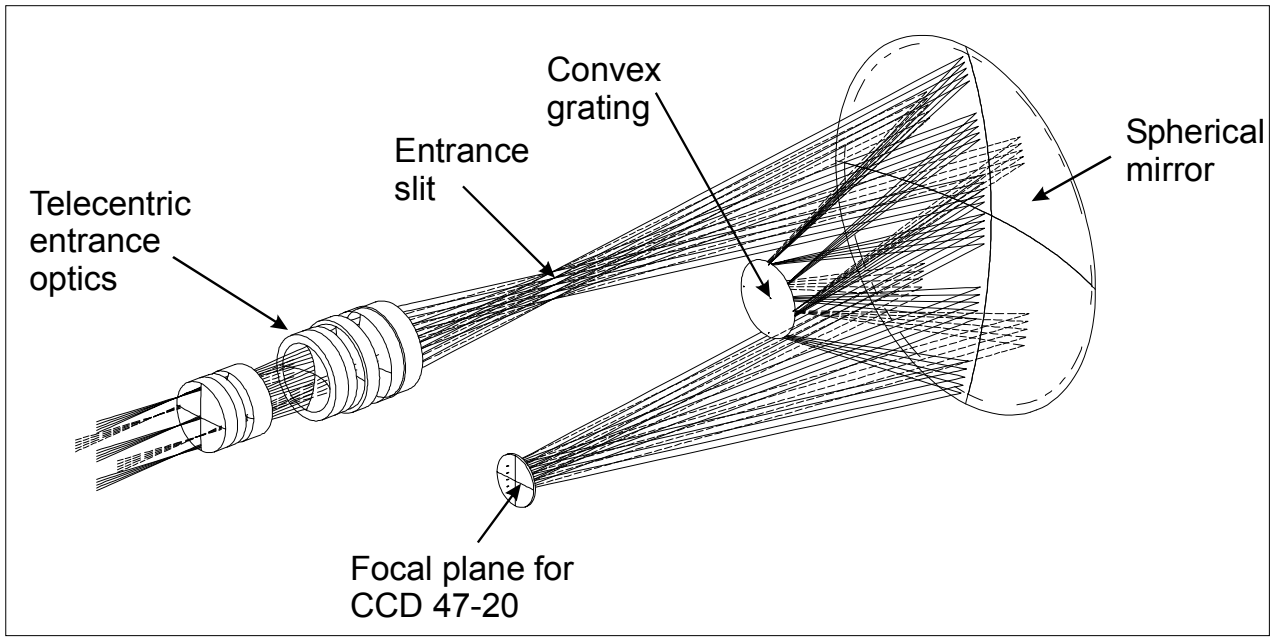

Figure 20: An imaging spectrometer following the Offner principle

[119] Offner–1987

Results

The main results of the simulation analysis are

- the suppression of the second order spectrum and the reduction of the polarisation sensitivity by a holographic convex grating with trapezium profile instead of the classical sine profile,
- no chromatical aberration by using a mirror system,
- a compact design can be achieved by a reduction of the axis angle,
- no coma and distortion because of the symmetrical 1:1-imaging of the entrance slit on the focal plane and,
- an equal focal lengths for the whole spectrum and a spherical correction can be achieved by an optimisation of the telecentric objective for the VIS-NIR spectral range.

Consequently, the design parameters outlined in Table 9 have been selected on basis of the performed simulation analysis.

Table 9: Simulated data for the Offner configuration

Parameters	**Values (for ~800-km orbit)**
Entrance optics	telecentric, 4/100
FOV	7.616 ° = 0.13312 rad = ~103.2 km
IFOV (pixel size)	0.007438 ° = 0.13 mrad = ~100.6 m
Spectral range	400 – 1000 nm
Basic spectral resolution Δλ	1.5 nm (binnable)
Number of selectable channels	512
Polarisation sensitivity	$\leq$ 1 %
Second order spectrum intensity	$\leq$ 0.5 % of first order intensity
Grating efficiency	> 20 %
CCD-detector, 1024 x 512 elements (used)	13.312 mm x 6.656 mm
Element size	13 µm x 13 µm

These results gained in the ray-tracing and grating simulation meet the needed spectral and spatial requirements. Nevertheless spectral and spatial simulation results have to be verified for the experimental prototype.

However, the outlined simulations give no prediction on the radiometric performance of the imaging spectrometer. Therefore a sensitivity analysis has to be performed.

3.2.2 Sensitivity model analysis

The sensitivity analysis evaluates the radiometric performance of a sensor. As analysis tool the signal-to-noise ratio (SNR) calculation is applied. As described in Chapter 3.1 various input parameters are needed for this calculation: the TOA radiance (for various bottom reflectances), the specific spectrometer layout (from the ray-tracing simulation), the efficiencies of the various spectrometer parts (optical and detector transmissions/efficiencies) and the noise budget of the spectrometer. Because in literature the SNR analysis has been described only for one-dimensional detectors, an adaptation for 2-d detectors has been made (see Chapter 3.1). Supposing that special attention is taken on image smear for the envisioned spectrometer (e.g. mechanical or electronic shutters) the SNR for the Offner-type spectrometer was calculated following the classical SNR analysis approach. As a result the wavelength dependence of the SNR for typical spectral signatures have been calculated, however the obtained results need final verification in the experimental prototype experiment.

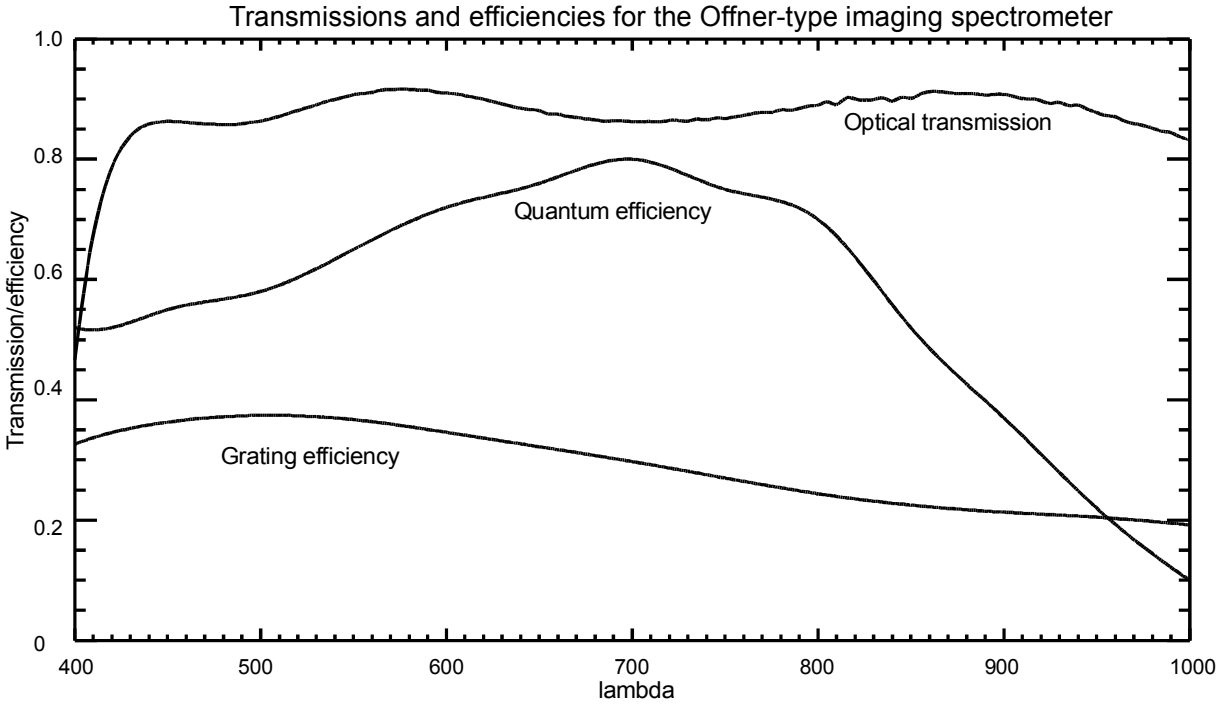

Figure 21: Transmissions and efficiencies for the various parts of the Offner-type imaging spectrometer[120,121]

[120] EEV–1997
[121] Schwarzer–1997

Results

For the SNR analysis the TOA radiance of typical vegetation, coastal (case-2) and ocean (case-1) waters were taken as input parameters. The specific spectrometer lay-out (entrance optics, IFOV, element size, spectral resolution) was determined by the simulation results (see Table 9). The SNR calculation was started after the determination of the grating efficiency, the optical transmission and the detector's quantum efficiency (see Figure 21) and the noise budget of the sensor (N_{Sensor}). N_{Sensor} can be limited to 10 electrons with today's ADU technology[122], and the low noise (N_{Dark}~$1e^{-}$)[123] of the detector at a working temperature of -5°C. After following the calculation steps (eq. 3.–1 and eq. 3.–2), the SNR was determined applying Eq. 3.–4. The result of the calculation is the SNR for the basic spectral resolution of $\Delta\lambda$ = 1.5 nm. Such a high spectral resolution for remote sensing data is mainly necessary in the O_2A-absorption band at ~ 760 nm. Most of the channels in the other VIS–NIR region need a $\Delta\lambda$ of 10-20 nm. By means of the detector's binning capability the future imaging spectrometer's spectral channels are programmable, so that centre wavelength and spectral bandwidths are adaptable. In Figure 22 the resulting SNR plot for $\Delta\lambda$ = 10.5 nm is shown.

The vegetation signature reaches a SNR of over 200 for the entire spectrum with maximum values of about 700. The SNR for the water bottom reflected radiance becomes smaller in the NIR because the typical water signature decreases by means of light absorption (Figure 4). Additional, the sensor performance decrease results from reduced objective transmission and silicon's quantum efficiencies in the NIR (see Figure 21). For typical case-2 waters the SNR reaches maximum values of 300. For longer wavelengths (λ > 900 nm) the SNR values decline below 100. A similar contour has the case-1 waters SNR plot. In contrast to case–2 waters, case-1 waters absorb more light, hence, the TOA radiance is weaker and the resulting SNR plot has smaller values. Consequently, the plot's maximum value is below 200 and the intersection with the SNR=100 line is at 750 nm.

Concluding, for the TOA radiance of vegetation the requirements are reached for all wavelengths. In contrast, the water reflected signals will have small values in the NIR. However, for both water types mainly atmospheric correction measurements are performed in the NIR (as explained in Chapter 1.2.2). These atmospheric correction measurements are realised in NIR atmospheric window channels (compare with MOS channels at 750 nm or 870 nm in Figure 4). For case-1 waters the 750 nm delivers sufficient results because at this wavelength the case–1 waters can be assumed being black. In contrast, atmospheric correction for case-2 waters needs window channels at longer wavelength (e.g. 870 nm) because the NIR water at 750 nm cannot be assumed being black. These measurements (870 nm channel) cause no problem because the SNR of coastal waters is much higher than that of case–1 waters. Thus, the SNR analysis shows that the spectrometer is capable to realise sufficient measurements over the complete VIS–NIR spectral region for different spectral signatures (such as water and vegetation bottom reflectances). Nevertheless, for future applications also the SWIR channels can be used to retrieve additional atmospheric data.

[122] Solbrig–1997
[123] EEV–1997

Consequently, the radiometric performance of the Offner-type imaging spectrometer in combination with the EEV 47–20 detector will deliver adequate measurements to ensure the defined observation requirements.

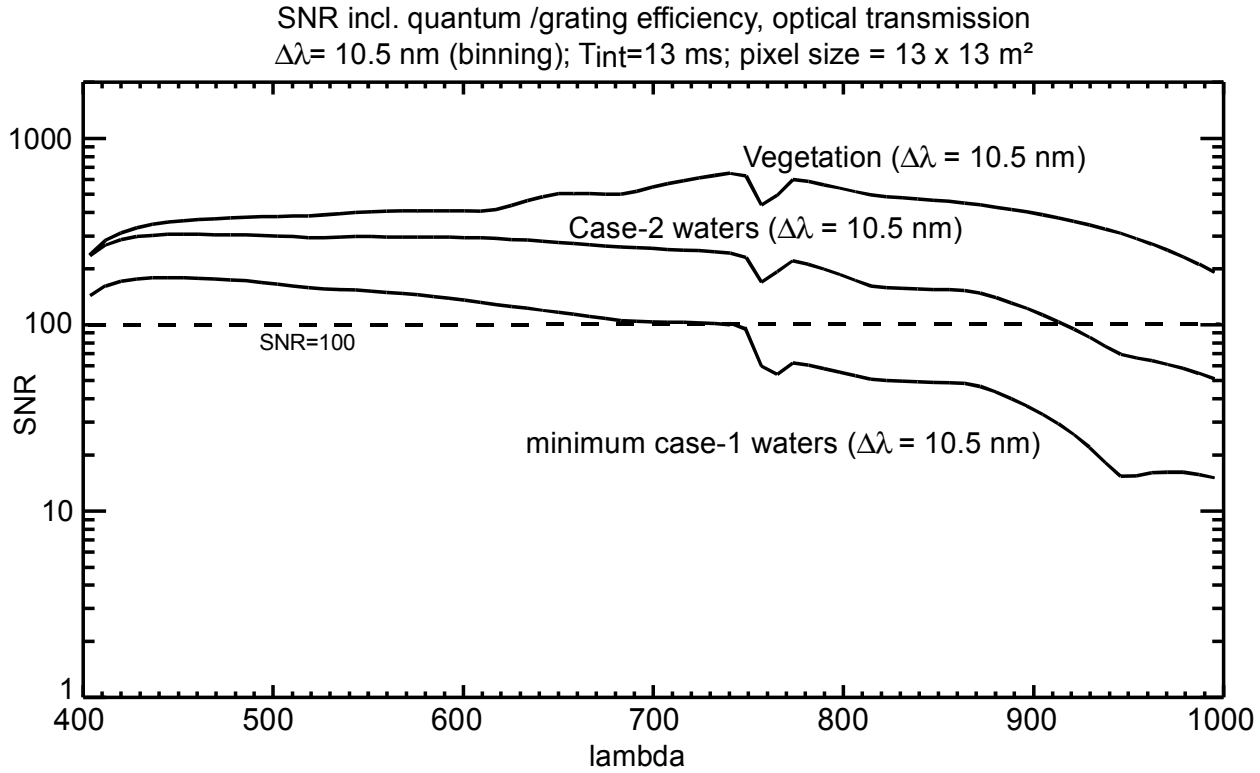

Figure 22: SNR calculation results for various water and vegetation scenes

3.2.3 Experimental prototype study

The goal of an experimental prototype study is to verify the results achieved by the ray-tracing/grating simulation and sensitivity analysis. Such a prototype can be performed when all optical and electrical components are set-up in the laboratory. Because some of these optical parts are still under development (e.g. grating with trapezium profile), components were used having slightly different parameters (e.g. grating with sine profile) than those used for the simulation. Further on the low noise concept for the video channel is currently in an evaluation phase, therefore an engineering model of the control and readout electronic is in use. These modified components are compared in Table 10 with those which will be used in the future imaging spectrometer. Hence, the simulation in Chapter 3.2.1 has been adapted to these modifications in an second ray-tracing simulation. Finally, these components are arranged in the laboratory set-up with the goal to confirm the validity of the adjusted simulation. Figure 23 shows the experimental prototype how it was realised at DLR Berlin including the optical and electrical components and the goniometer head.

Component	**Breadboard**	**Simulation result**
Telecentric objective	4/100	4/100
Slit	13.5 mm x 0.013 mm	13.5 mm x 0.013 mm
Spherical mirror	r = -139.9 mm	r = -234.1 mm
Holographic grating	r = -73.5 mm; g = 224 L/mm; sine profile	r = -116.2 mm; g = 87.0 L/mm; trapezium profile
CCD matrix	CCD 47–20 engineering model, integration time 1.4 s	CCD 47–20 grade one, integration time 13 ms

Table 10: Comparison of the experimental prototype investigation and the simulation

There is no need to realise special spectrometer design in this preliminary breadboard. That is why the grating, the entrance slit and the mirror are positioned with adjustable devices (1–3 degrees of freedom) in the laboratory. A problem results for positioning of the 3-d focal plane assembly. Although there are five dimensions (degrees of freedom), precise (re-) positioning and easy handling had to be ensured. A modified goniometer head with step motors makes possible an easy and exact positioning of the CCD in the focal plane within very narrow error margins (0.4 µm/step, 0.0004°/step) for the imaging spectrometer breadboard studies.

Results

The first results[124] of the experimental prototype analysis verified the adjusted simulation for slightly different electrical and optical components because the measurements in the spectral and spatial domain met the predicted values. The polarisation sensitivity, the exact spectral resolution and the higher spectral order efficiency could not be measured because a sine profile grating was used instead of the trapezium profile grating. The exact radiometric resolution was also not the subject of the investigation because the low noise high dynamic video electronics are still under development. However, this initial prototype study demonstrated that the simulated parameters are attainable, so that the primary simulations (from Chapter 3.2.1) can be achieved in the near future by the advanced prototype. A description of the advanced prototype is given in the following section.

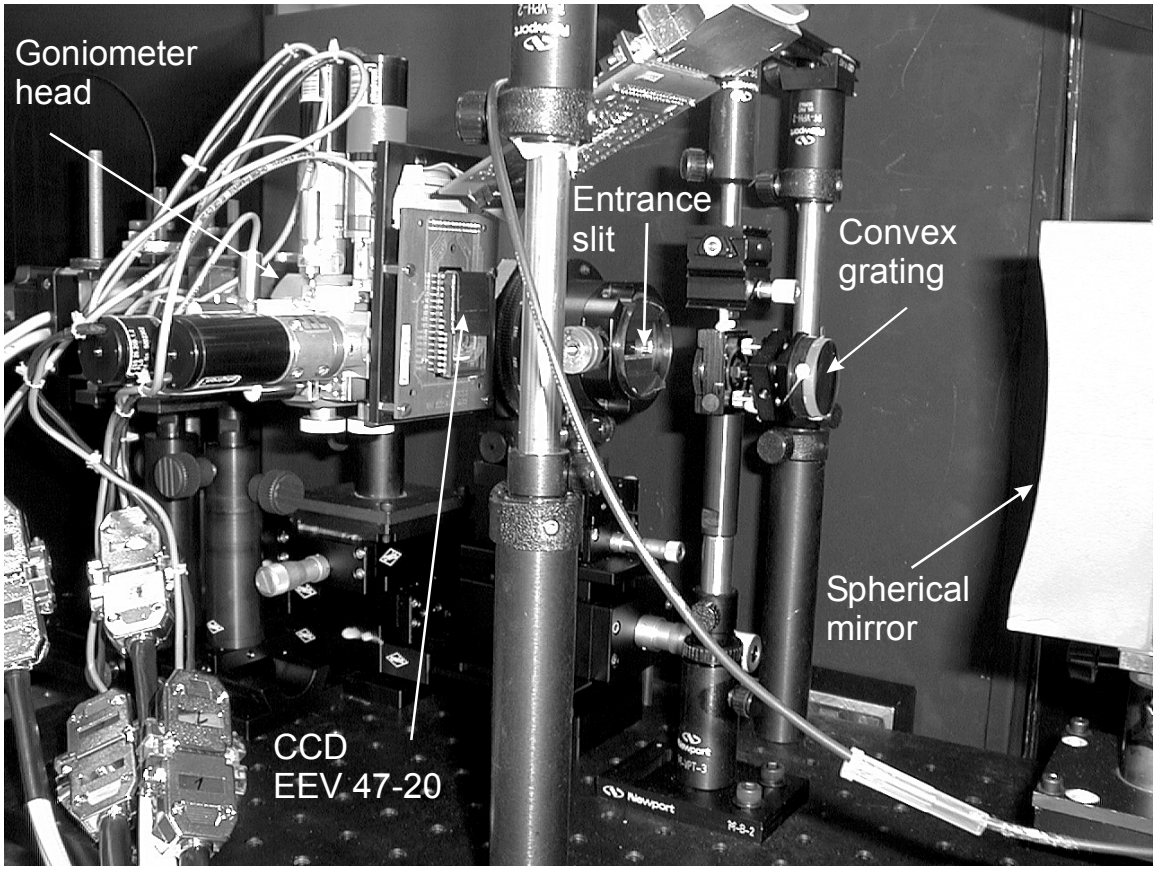

Figure 23: Breadboard with optical and electronic components and goniometer head

[124] Roth–1998

3.2.4 Concluding remarks and outlook

Recently at DLR Berlin encouraging investigations for a new pushbroom imaging spectrometer have been performed. These investigations consist of ray-tracing and grating simulations, sensitivity analysis and an initial experimental prototype study. Hence, the suitability of an Offner-type imaging spectrometer for coastal zone remote sensing purposes has been demonstrated.

The main advantages of this Offner-type imaging spectrometer concept are

- a low polarisation sensitivity and a reduced 2nd order spectrum because of the special holographic convex grating with trapezium profile,
- an improved compactness because of the Offner-type principle and,
- a good radiometric performance because of the low noise concept for the video channel and the backside illuminated CCD.

Moreover, this Offner-type imaging spectrometer has the advantage of relative simple and compact design (mass: ~6 kg; envelop: 480 x 190 x 135 mm³) what makes the spectrometer an excellent candidate for a space mission.

However, the initial breadboard prototype study in the DLR laboratory demonstrated only that the simulated parameters are within reach. Ongoing investigations at DLR cover the low noise video channel and a new prototype set-up. This new breadboard with original optical and electronic components will be finished in near future. The following Figure 24 gives an impression of the compactness of the new prototype.

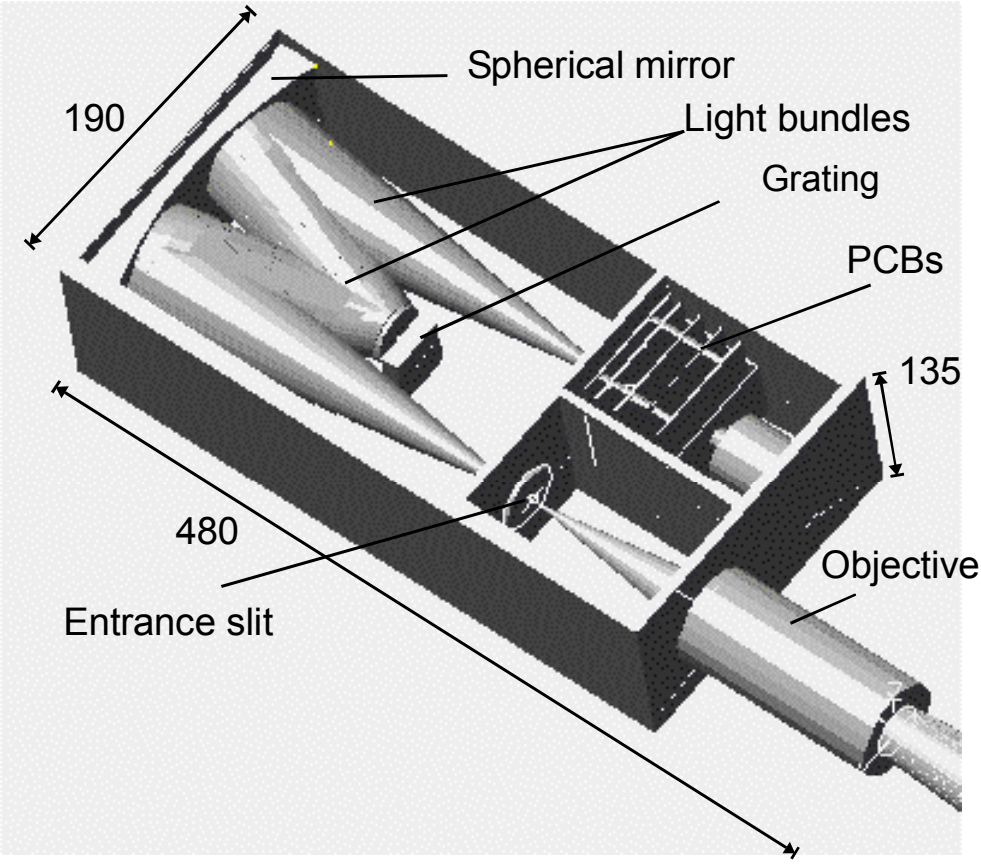

Figure 24: Breadboard experiment with original optical and electronic components

The new prototype of the Offner-type imaging spectrometer (see Figure 24) consists of full spectrometer design which embeds all optical and electronic components. The optical components include the telecentric optic, a spherical mirror and a grating with trapezium profile. The detector is the grade one CCD 47–20 matrix with 1024 x 1024 pixels and a pitch of 13 x 13 m². A low noise concept for the detector will ensure the required low noise budget by in-house developed hybrids for dual-slope integration. All parts of the video channel will be placed on two small PCBs[125] next to the focal plane.

[125] PCB printed circuit board

3.3 Capabilities of LEDs for in-flight calibration

Recent technological developments of semiconductors[126,127] opened LEDs the door for many new applications such as traffic lights, automotive instrument clusters and advertising signs. These technological developments lead to a significant progress in spectral and radiometric performance — in particular of UV, blue and white InGaN diodes.

Because literature did not discuss in-flight calibration with LED so far, it was necessary to investigate the ability of LEDs to serve as tool for spaceborne sensors calibration. Therefore in the following the possibilities of LEDs are analysed to monitor any spectrometer degradation by irradiating as a stable light source passing all optics and to give information on the performance of sun calibration, e.g. degradation of the solar diffuser plate.

The investigation on calibration potentials covers the selection of a set of commercially available LEDs for the specific geometric and spectral requirements of a spaceborne spectrometer measuring land and water signatures of the Earth. This LED set has been characterised regarding temperature and current/voltage dependencies. Finally, space environment simulation has been performed in the DLR facilities[128] KOBE (Komplexe Bestrahlungseinrichtung) and MicroVCM (Micro Vacuum Chamber). After tests completion the main LED problem (temperature dependency of the signal) has been solved by developing a concept for long-term temperature stabilisation. Finally the main results are concluded and a summary of the achievable calibration accuracy with LED calibration is given.

3.3.1 Calibration requirements and LED-set selection

General

In recent years, LEDs have been produced in enormous quantities and in a wide range of different types to meet the very different specifications of a variety of applications. These design variations led to many sizes, colours and materials which have been made use of, e.g. small SMDs[129] or multichip-multicolor LEDs with snap-in panel sockets for easy mounting. For a LED-set selection standardised 5-mm-diameter LEDs have been taken. This ensured inter-LED comparison and has the advantage that this standard size is available by most of the LED manufacturers. The 5-mm-diameter LED consists of a chip, two pins and a capsulating package. The power supply of the chip is guaranteed by an anode and a cathode pin. The chip's band gap is responsible for the wavelength-specific photon emission. Both, chip and parts of the pins are capsulated in an epoxy package.

LED-set selection

Since the development of blue LEDs almost all colours of the VIS/NIR spectrum are available. In general, the LEDs are emitting light at a distinguish wavelength and with a half-width bandwidth of 40 to 80 nm. In contrast, the 'white' LED follows the principle of

[126] Mukai et al.–1999
[127] Evans–1997
[128] Lura et al.–1997
[129] Surface Mounted Devices

luminescence conversion, i.e. the emission of a blue diode is used as primary source for exiting organic or inorganic fluorescent situated in the polymeric epoxy resin[130].
For spectrometer calibration purpose a calibration source should reproduce spectrally and radiometrically the top-of-atmosphere (TOA) radiance spectrum (at minimum bottom reflectance, e.g. water). Such a spectrum cannot be generated by a single LED. This leads to a combination of different colours. Table 11 summarises possible candidates which help to reproduce the TOA spectrum. Samples of each LED type have been gradually disposed by the manufactures[131,132,133].

Table 11: Summery of selected LED performances

Peak wavelength [nm]	**Half width Δλ [nm]**	**FOV [°]**	**E** [μW/cm²nm] **(20mA 21°C)**	**$U_{junc.}$ [V] 21°C**	**Chip material**	**manufacturer / colour**	**type number (5 mm diameter)**
460 / 555	-	20	7.9 / 3.1	3.46	InGaN (YAG)	Nichia / white	NSPW500S, 5mm
465	40	15	31.1	3.43	InGaN	Nichia / blue	NSPB500S, 5mm
525	50	15	10.7	3.43	InGaN	Nichia / green	NSPG500S, 5mm
590	45	15	5.9	1.99	AlGaInP	HP / amber	HLMP-EL15-SV000
605	40	15	15.5	1.90	AlGaInP	HP / orange	HLMP-EJ15-SV000
626	50	15	21.7	1.86	AlGaInP	HP / red	HLMP-EG15-SV000
880	80	22	15.5	1.29	GaAs	Siemens / nir*	SFH486, 5mm
950	55	34	19.1	1.18	GaAs	Siemens / nir*	SFH415, 5mm

*near infrared

Geometrical and spectral requirements for spectrometer calibration

The geometrical requirements of a conceptional spectrometer, which is carried at a Sun-synchronous orbital path satellite, can be retrieved from Figure 25. In the imaging mode the spectrometer receives Earth's TOA radiances from nadir position (without diffuser in the FOV). On the Earth's night side the diffuser panel is turned into spectrometer's FOV. In opposite of the diffuser, lamps or LEDs can be placed for enabling the diffuser illumination by these artificial sources. Subsequently to the LED/lamp calibration, the satellite crosses the terminator and the Sun calibration can be performed: the horizontal incoming sunlight enters through a baffle system and the diffuser is illuminated for the sensor's Sun calibration. The advantages of this calibration procedure is an improved check of possible spectrometer degradations: (1) the light passes all optics (for the TFOV) for recognising possible degradation of spectrometer parts (e.g. optics, electronics). Further on, (2) this method allows to check a possible diffuser degradation. The geometrical distances from diffuser to LED or to

[130] Bogner et al.–1999
[131] Nichia-1998
[132] Hewlett-Packard–1999
[133] Siemens–1997

the spectrometer aperture is ~ 100 mm. The illuminated spot on the diffuser has a diameter of about $D \sim 26$ mm ($FOV_{LED} \geq 15°$).

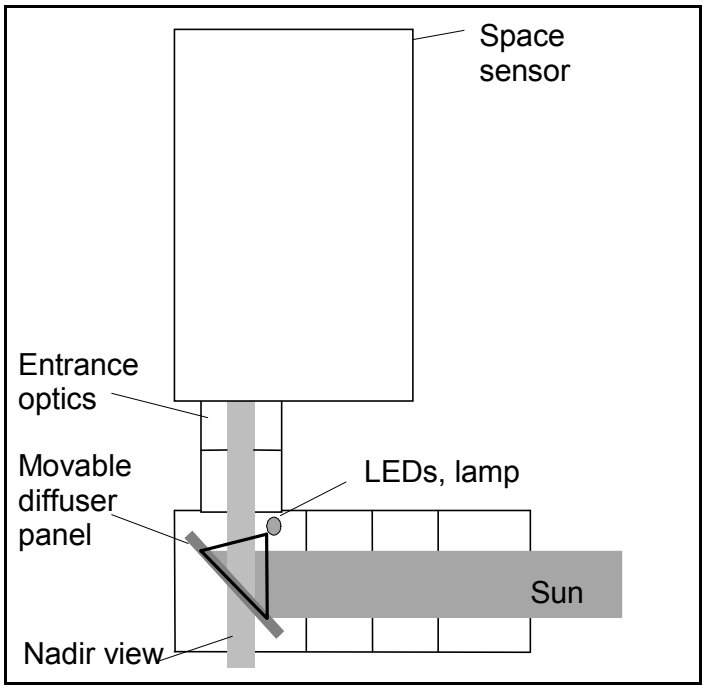

Figure 25: Arrangement for external spectrometer calibration

Taking the design from Figure 25 into account the radiance at the diffuser for different sources can be calculated. Figure 26 shows the results of calculation and laboratory measurements for the diffuser illuminated by LEDs (three samples), by a continuum emitter (tungsten lamp) and by the sun when passing the terminator. The three LED samples are Nichia's white, HP's red and Siemens's NIR950 LEDs. The tungsten lamp is the successful applied calibration lamp[134] from MOS mission but placed for this investigation besides the LEDs for having a direct comparison. The lamp's spectrum shows in contrast to the white LED the main disadvantage, i.e. the low blue signal.

[134] Sümnich–1998

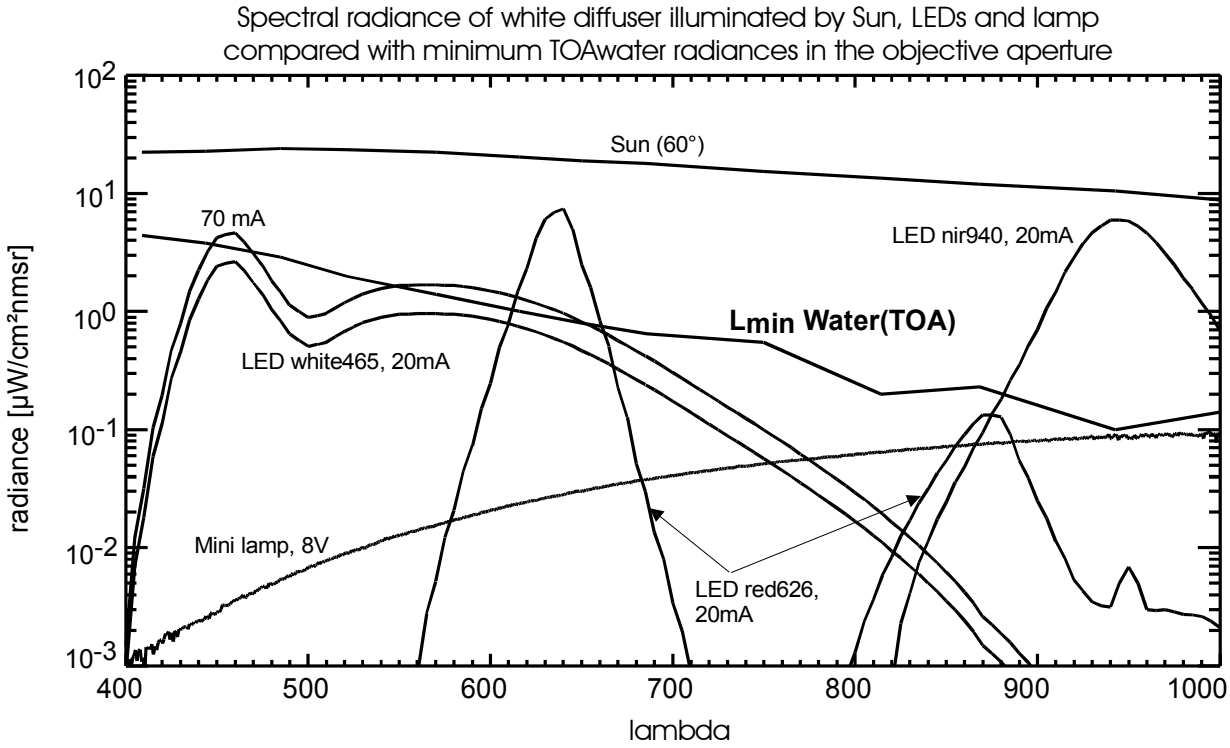

Figure 26: TOA water radiance and sun, lamp and LED radiances via spectral diffuser

The three LED emission spectra in Figure 26 are powered with 20 mA forward current. The signal level can be varied by changing the current with the ratio $\Delta L/I \sim 1.5 \ldots 5\%/mA$. While maximal currents of 70 mA (InGaAs LEDs) or 50 mA (AlGaInP and GaAs LEDs) for long-term application are recommended, there is no minimum minimorum limit for applicable low currents. For comparison of diffuser illumination and nadir signal, Figure 26 shows also the minimum TOA water radiance which can be expected in the spectrometer entrance aperture without diffuser panel.

3.3.2 LED characterisation

Although LED development had found a breakthrough recently, many experts[135,136,137,138] analysed the special behaviour of the new illumination sources. However the possible application of LEDs for spaceborne spectrometer calibration was not the subject of precedent investigations. Therefore the properties of these LEDs (optical, electrical and temperature characterisation) have to be determinated for typical laboratory as well as for space environment conditions. Thereinafter a conclusion on the ability of using the LED for in-flight calibration can be provided.

The classical properties, i.e. the signal and peak wavelength of LEDs with temperature and current/voltage dependencies can be easily characterised with basic laboratory equipment

[135] Commission Internationale de l'Eclairage–1997
[136] Muray–1991
[137] Barton et al.–1998
[138] Osinski et al.–1997

such as climate chamber, spectro-radiometer and high precision power supply. As working region for all (InGaN) LEDs the range from 10 - 50 mA and 5 – 50 °C (70 mA for InGaN LEDs) has been defined. In this region a linear approximation of the temperature and current dependencies can be applied in an initial approach.

At DLR laboratory two different spectro-radiometer served recording the LED emission spectra: MCS UV-NIR from Zeiss with an in-house diffuser device and optical cable development and the Optical Laboratories OL-750 HSD 306 Si/PbS with a 4-inch diameter integrating sphere device. The spectral ranges are 190-1015 nm and 350-2500 nm, respectively. Depending on the demanded accuracy an in-house current stabiliser development, a Keithley 236 or a Toeller (TOE8815) served as current stabilised power supply. A Heraeus-Vötsch CTC-E4 was used as test chamber for temperature control and the transmission measurements were made with a Perkin Elmer Lambda19 (350-2500 nm).

For investigating the behaviour of chip and polymer in space environment (e.g. polymer's ageing effect when introduced to hard radiation), tests in special simulation facilities have been performed:

The space environment parameters have been simulated in KOBE[139]. This facility had been developed in a DLR – FTINT[140] co-operation and it serves for simultaneous irradiation of solar (200 – 2500 nm), ultraviolet (5 – 200 nm), proton and electron (20 – 150 eV) under vacuum conditions. The thermal vacuum test (e.g. 24h, 125°C) has been performed in MircoVCM to determine the outgassing properties of the LED's epoxy following ESA standards[141].

3.3.2.1 Voltage U_F and current I_F dependencies

For analysing the LED's U_F and I_F dependencies these tests have been realised under temperature stabilisation, i.e. constant ambient room temperature and thermal equilibrium of the LED.

The value of U_F depends in principle on the semiconductor material and has at a working point of 20 mA typical values of 1.18 V for near infrared LEDs and 3.46 V for white LEDs (see Table 11). Moreover, U_F depends on I_F and follows as semiconductor diode the well established pattern what gives a first linear approximation of $U_F / I_F \sim 17$ (6 or 4) V/A for white (red or nir950) LEDs in the working region between $I_F > 10$ mA and saturation levels. For a first approximation a linear approach of the dependencies should give sufficient information on a LED performance. Higher precision of the voltage/current characteristics can be retrieved from literature[142] when the diode's differential resistance is taken into account. The current dependencies of the emission (peak) of the selected LED set are summarised in Table 12.

[139] Lura et al.–1997
[140] FTINT physical-technical institute for deep temperatures, Charkow, Ukraine
[141] ESA PSS–01–702, Method A
[142] Commission Internationale de l'Eclairage–1997

Table 12: Current dependencies

peak wave-length [nm]	$\Delta\lambda/I_F$ [nm/mA]	$\Delta L/I_F$ [%/mA]
460/ 555	–0.09	1.7
464	–0.20	3.3
520	–0.30	3.1
589	0.15	3.9
610	0.10	4.2
636	0.13	3.9
879	0.10	4.6
933	0.08	4.4

It is shown that the highest dependency appears for NIR LEDs with $\Delta L/I_F$ ~ 4.5%/mA, whereas InGaN LEDs (white, blue, green) have values of 2-3%/mA. While the wavelength shifts for most LEDs is towards longer wavelength (red shift) with increasing current, InGaN LEDs wavelength have a blue shift which can be explained by the quantum-confined Stark effect resulting from piezoelectric fields[143,144].

3.3.2.2 Temperature dependencies

The analysis of the LED temperature dependencies of signal level and location of the peak wavelength in the spectrum has been performed with a constant current power supply what was either an in-house development, a Keithley 236 or a Toeller (TOE8815). For LED signal measurements the Zeiss spectro-radiometer MCS with global diffuser-plate device has been used. The spectro-radiometer itself has been placed exterior the test chamber in which the temperature has been changed between 5–50°C. The LEDs, located inside the test chamber, were irradiating the global diffuser-plate device. After a 2-min warm-up phase the LEDs reach equilibrium with respect to the temperature in the test chamber and the measurements were realised. The positioning of the LEDs has been performed from exterior by a remotely controlled programmable stepping motor. The LEDs have a noticeable temperatures dependency of signal level and location of the peak wavelength in the spectrum. The temperature coefficients of forward voltage and signal are between $\Delta U/T$ ~ –2.8 ... –1.2 mV/K and $\Delta L/T$ ~ –1.5 ... –0.3%/K, respectively (see Table 13). This depends mainly on the chip material. While InGaN LEDs (460/555, 464 and 520 nm diodes) have small temperature coefficients the other material's coefficients are up to a magnitude higher. The same material related dependency can be retrieved for the wavelength coefficients. Here the dependencies vary from $\Delta\lambda/T$~ 0.04 ... 0.25 nm/K.

[143] Mukai et al.–1999
[144] Im et al.–1999

Table 13: Temperature dependencies

peak wave-length [nm]	$\Delta U/T$ [mV/K]	$\Delta L/T$ [%/K]	$\Delta\lambda$/T [nm/K]
460/ 555	–2.9	–0.5	0.04
464	–2.8	–0.5	0.04
520	–3.0	–0.3	0.05
589	–1.9	–1.4	0.13
610	–1.5	–1.5	0.15
636	–1.3	–1.3	0.16
879	–2.1	–1.1	0.25
933	–1.2	–1.5	0.14

The relation $\Delta(U/I)/T$ is constant in the normal working region (I_F >10mA) and a variability of this relation is caused by imprecise approximation of the U–I relation (see Chapter 3.3.2.1).

New concept for long-term temperature stabilisation

Whereas current stabilisation can be achieved by off-the-shelf technology, temperature stabilisation is still a problem. Therefore a long-term temperature stabilisation has been developed: To maintain a temperature level higher than that at ambient temperature a supplemented heater (see Figure 27) can be used to control the chip temperature. This heating system is thermally connected to the chip via LED pins which have a higher thermal conductivity (λ_{pin} = 350 W/mK >> 0.2 W/mK = λ_{epoxy}) than the chip surrounding epoxy. This heater will level up the chip temperature to $T_{junction} > T_{pin} > T_{ambient}$. The forward voltage $U_{junction}$ of the LED is a function of $T_{junction}$ and can be easily retrieved by measuring the voltage in the power supply circuit. This relationship makes it possible to control the pin temperature and therefore the junction temperature without measuring the chips temperature directly. As power supply of the heating circuit a voltage stabilisation and long-term stability is required. High stability can be achieved by high precision voltage source (such as the ADR 290 from Analogue Device which has a very low and linear temperature drift and a long-term stability of 0.2 ppm (1000hrs at 25°C, U = 15V).

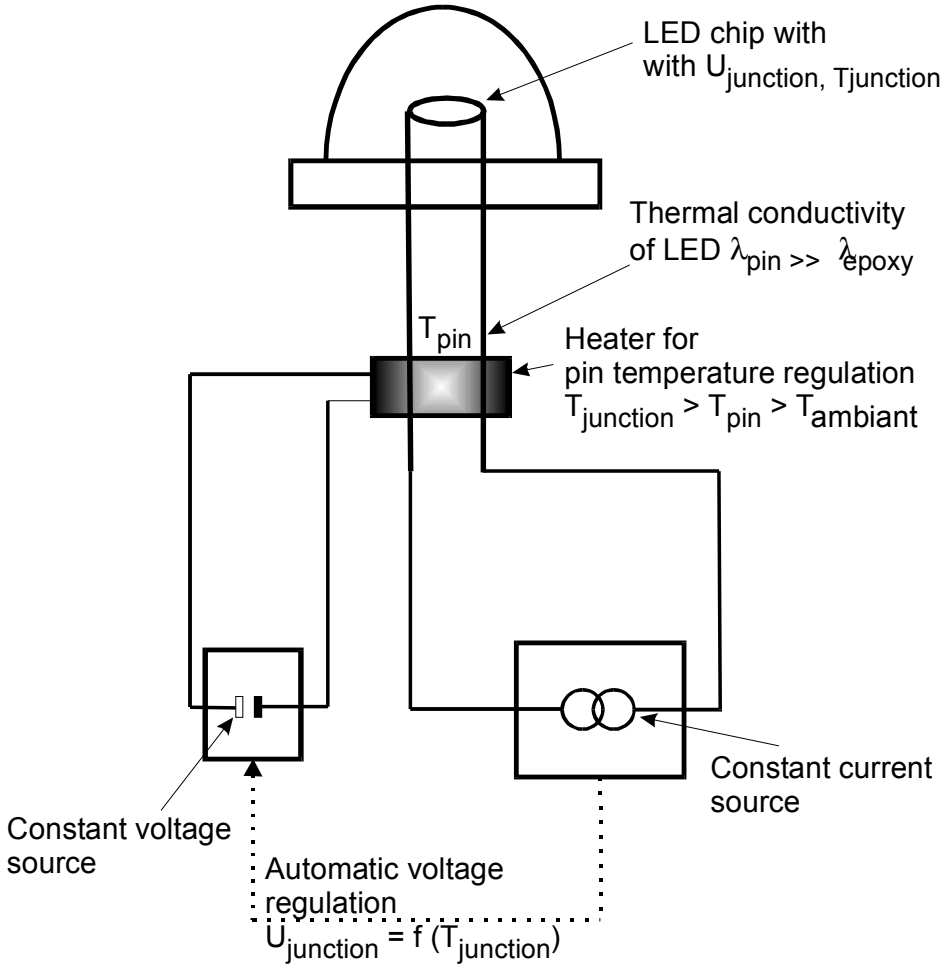

Figure 27: Arrangement of high-precision temperature stabilisation

Space environment tests

Space radiation, i.e. the bombardment with high energetic particles (protons, electrons) and photons (e.g. X-ray) can have a detrimental effect on semiconductor components and other materials used in a spacecraft. The DLR space radiation facility KOBE provides the ability to simulate this environment under vacuum conditions on Earth and enables projects to take this hazard into consideration in a early design phase. Depending on the spacecraft's orbit and mission duration the spectra will differ and have to be reproduced by KOBE individually. The spectrometer concept under investigation will be carried on a polar orbit of about 800 km altitude with inclination above 90°. The location of the LED in the space sensor (see Figure 25) will be shielded in the centre of a solid aluminium housing in opposite of the Spectralon diffuser. Following the European Space Environment Standard[145] the typical annual mission dose behind a 4-mm-aluminium shield is about 1 krad/year. These radiation tests have been performed under vacuum conditions for a envisioned mission duration of 1 to 10 years.

[145] ESA Report–in press

For detecting any effects on the LED semiconductor components or the covering epoxy material three kind of measuring procedures have been performed: epoxy transmission check, LED emission check and epoxy outgassing check. Microscopic surface observation before and after the tests ensured that there was no significant change of the epoxy surface.

Epoxy transmission check

An epoxy-lens-only sample (ELS) has been separated from a Nichia LED for testing the transmission performance independently from the LED chip performance. The radiation doses for ELS were equal to the doses for one, two and seven years (around 1 krad/year). Before and after each radiation simulation the ELS transmission has been measured using a Lambda 19 spectro-radiometer. The results (see Figure 28) normalised at maximal transmission demonstrate that no systematic degradation trend can be detected. The deviations of the transmission measurements result from uncertainties of the Lambda 19 set-up and they are in the magnitude of 2%. The same deviation is reached by repeated measurements of the same samples.

LED emission check

Three LEDs from Table 11 have been selected: White (λ_{peak} ~ 460/555nm), Red (λ_{peak} ~ 626nm) and nir950 (λ_{peak} ~ 940nm). They almost cover the hole range of chip materials and manufactures. These LEDs have been placed in the KOBE for simulating 1, 2, 3, 4, 5 and 10 years of space radiation. Before and after each radiation simulation the LED spectrum has been measured using a OL-750 spectro-radiometer with integrating-sphere device. Figure 29 shows the three different LED spectra over lambda. Like for the transmission measurements no systematic degradation tendency can be determined and the errors are due to uncertainties of the measuring set-up and imprecise temperature normalisation.

Epoxy outgassing check

Additional, a thermal vacuum test has been performed for determining the outgassing properties of the LED's epoxy material. Therefore the MicroVCM experiment has been performed following ESA standard[146]. The result was a total mass loss (TML) of 1.04% what is a bit more than the ESA acceptance limit of 1%. The collected volatile condensable material (CVCM) had a value of 0.00% and the recover mass loss (RML) was under 0.5%. This means that the outgassing material was probably H_2O what is not critical for the envisioned spectrometer concept.

[146] ESA PSS–01–702

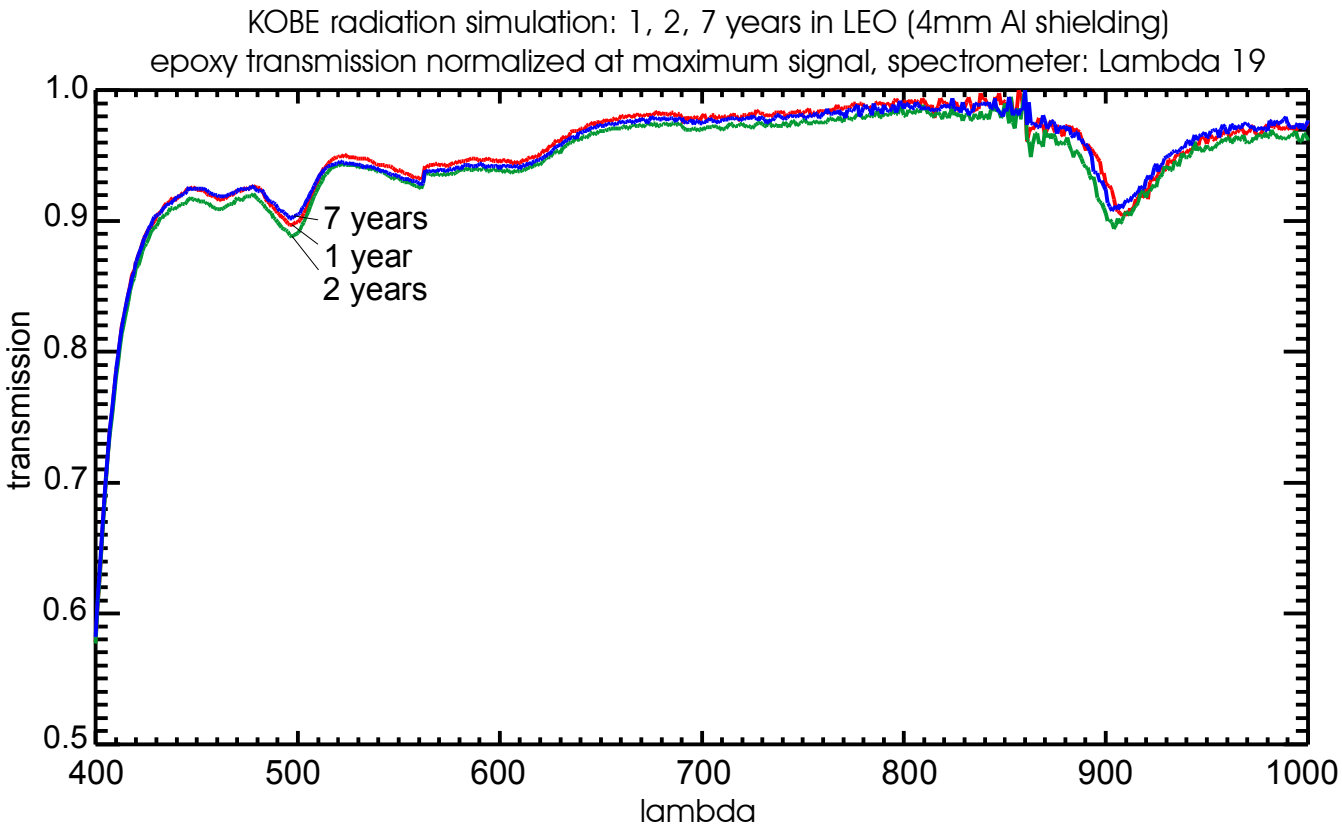

Figure 28: Transmission spectra for epoxy lens (ELS)

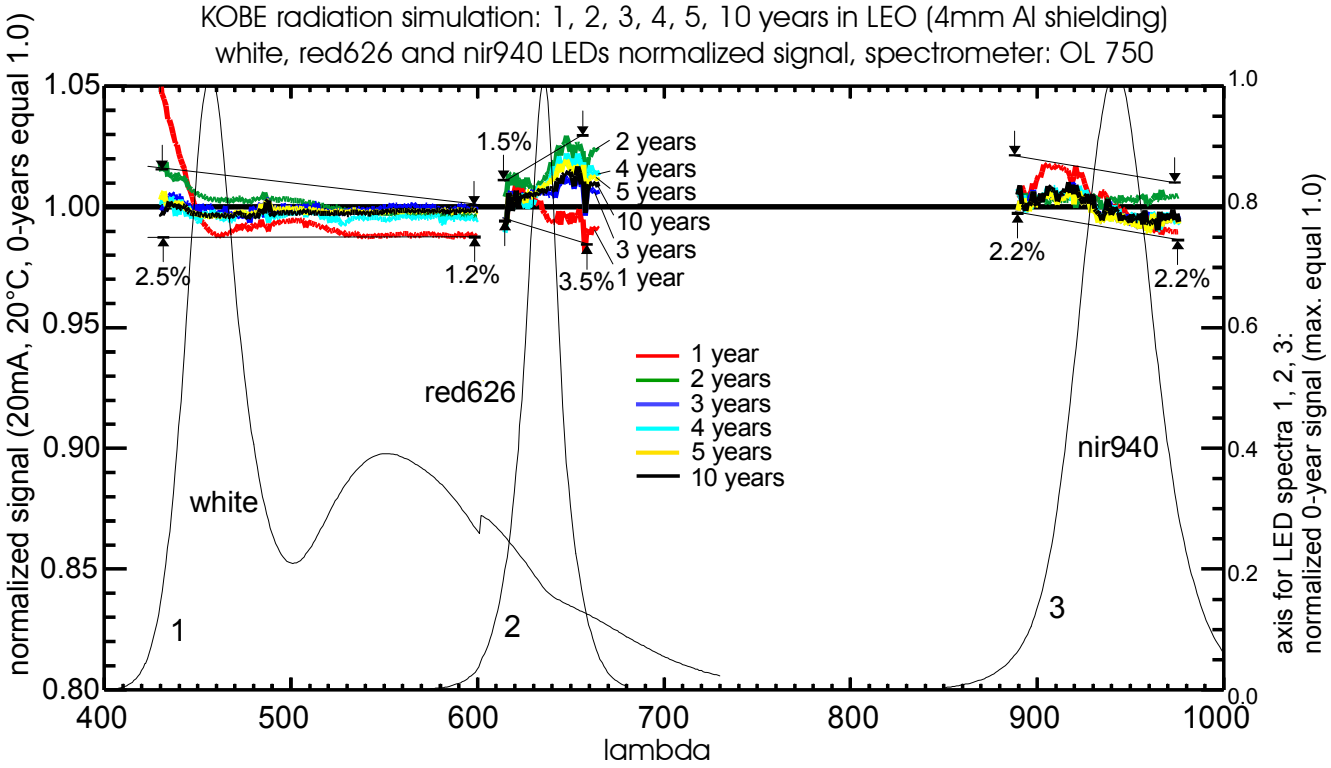

Figure 29: Radiation hardness tests for three LEDs

3.3.3 Conclusion

The objective of this investigation was to analyse the capability of LEDs for monitoring imaging sensor degradation and to help checking possible solar diffuser degradation. Therefore the LED performance under usual laboratory (current and temperature dependencies) and space environment conditions have been investigated. The results are summarised in Table 14.

Table 14: Results of LED characterisation and radiation hardness simulation in space

	instruments, facility	**sample**	**indication of method**	**results**
A	**normal laboratory conditions**			
A 1	climate chamber, spectrometer, high precision power supply	all LEDs from Table 11	current stabilisation	$\Delta U/T$: –3.0 ... –1.2 mV/K $\Delta L/T$: –1.5 ... –0.3 %/K $\Delta\lambda/T$: 0.04 ... 0.25 nm/K
A 2			temperature stabilisation	$\Delta L/I$: 1.7 ... 4.6 %/mA $\Delta\lambda/I$: –0.09 ... 0.15 nm/mA
B	**space environment conditions**			
B 1	2 x 1krad and 1 x 5krad radiation in KOBE, Lambda 19	epoxy material	1, 2, 7 years in orbit	no change of transmission
B 2	5 x 1krad and 1 x 5krad radiation in KOBE, OL 750	white, red626, nir940 LEDs	1, 2, 3, 4, 5, 10 years in orbit	no change of signal output or emitting wavelength
B 3	vacuum test	white	TML, CVCM, RML following: ESA PSS–01–702	TML = 1.04% CVCM = 0.00% RML = 0.46%
	microscopic surface check	before and after each test		no change

Current and temperature coefficients can be retrieved from Table 14 (part A). These coefficients define the requirements for the sensor's LED set-up. If a maximal signal uncertainty of 0.5% and a wavelength stability of 0.1 nm is required the long-term stability for the current should be less than 0.1 mA and less than 0.3 K for the temperature. Whereas an off-the-shelf current stabiliser can reach easily the desired current dependence, temperature stabilisation can not be achieved commercially. This temperature stabilisation can either be realised by keeping the sensor in a small ΔT-regime or by controlling chip temperature using the signal level of the junction voltage. If it is not possible to keep the sensor in the desired ΔT-regime the active temperature control has to be applied.

This control method is maintained by heating the LED pins to a temperature higher than ambient room temperature. As power supply an ADR 290 can provide a long-term stability of 0.2 ppm. Consequently, a higher long-term LED temperature stabilisation than the required 0.1 K can be realised. Taking the temperature coefficients from Table 14 (part A) into account, a long-term signal stability of less than 0.2% for signal and 0.03 nm for wavelength

of the characterised LEDs is achievable. Laboratory investigations showed that the thermal connection of the LED pins to a heat source solves also another problem: the long LED warm-up phase is shortened from ~ 2 min to less than 10 s.
Other LED disadvantages are inhomogeneous spatial radiation distribution and insufficient λ-distribution, i.e. the incapability of a single LED's emission to cover the whole VIS-NIR spectrum. These disadvantages are not avoidable for off-the-shelf technology due to epoxy lens design, semiconductor material and/or consistence of the luminescent material. But these disadvantages are not critical for the quality of in-flight calibration. The inhomogeneous spatial radiation distribution depends on the lens design and it is constant over time. The insufficient λ-distribution in the VIS-NIR can be overcome to a certain extent by providing the emission of various LED at different signal levels.

4 Summary of the regional coastal zone mission

In this chapter the concept for a new mission is summarised which focuses on regional coastal zone observation from a low Earth orbit. This mission will be capable to meet the outlined observation requirements (see Chapter 2.2.3) by applying a sophisticated sensor design and an unique orbit-satellite-payload optimisation. The outlined technical mission concept has been submitted to the ESA call for Earth explorer opportunity mission[147] under the name of ECOMON (A dedicated mission for Regional Ecological Research and Monitoring). It is summarised in the following with small modifications regarding tilt angle and projected life time (design life). During the ESA selection phase other mission objectives achieved higher priorities, however, experimental prototype studies will continue at the DLR Berlin.

In the scope of the thesis a module arrangement analysis was performed to align various sensors on a satellite in a way they meet best the observation requirements. In particular the sensors had to be arranged in a way that they make up a larger FOV to enable the synchronous generation of images over an increased swath width. The boundary conditions for the module arrangement analysis were the S/C allocation constrains, the calibration requirements (e.g. Sun, LED, Lamp calibration) and sensor design conditions.

The proposed S/C[148] is a mini satellite which is able to carry the entire payload (VIS-SWIR-TIR sensors) in a 775 km sun-synchron orbit with a envisioned mission duration of 5 years. Because of low power consumption, reduced mass, small envelop of the payload, and avoidance of large solar array panels (with pantograph mechanisms), the satellite's mass and costs can be reduced significantly to < 300 kg and < 45 M€. With the help of an advanced attitude control subsystem the whole S/C can be tilt to a desired angle (up to ± 30° off-nadir). This tilt angle can be changed for every orbit and has to be chosen before the beginning of recording. The pointing accuracy will be ±0.16° together with a precise attitude knowledge of ±0.003°. More details on the sensors and spacecraft are discussed in the following sections.

4.1 Orbit

Preliminary orbit calculations showed (Chapter 2.3.1) that a 775 km Sun-synchronous (semimajor axis = 7153 km) orbit with 98.5° inclination can fulfil the basic scientific observation requirement of orbit ground track with a repetivity after 3 days.
Because of the S/C tilting capabilities it will be possible to point the whole S/C within ±30° off nadir what would increase the sensor's field of view (FOV) of ~30° to a possible field of regard (*FOR*) of ~87°. This *FOR* would represent a detection possibility within a swath of ~1570 km (for latitudes > 30°) instead of ~400 km. To demonstrate the target detection possibility Figure 30 shows the orbit ground tracks for day 1 and day 2. The swath width results from the calculated possible *FOR* because of tilting the 30° FOV for ±30°. Note, that

[147] Neumann–1998
[148] by OHB for ECOMON

the figure does not include the ground track of day 3 which lays about 930 km eastwards of the day 2 track. The 3rd day's off-nadir tilt would realise a global repetivity after the second day.
Concluding, the off-nadir tilting possibility would ensure consecutively monitoring of catastrophic hazards within 2 days for latitudes > 30° and within 3 days globally.

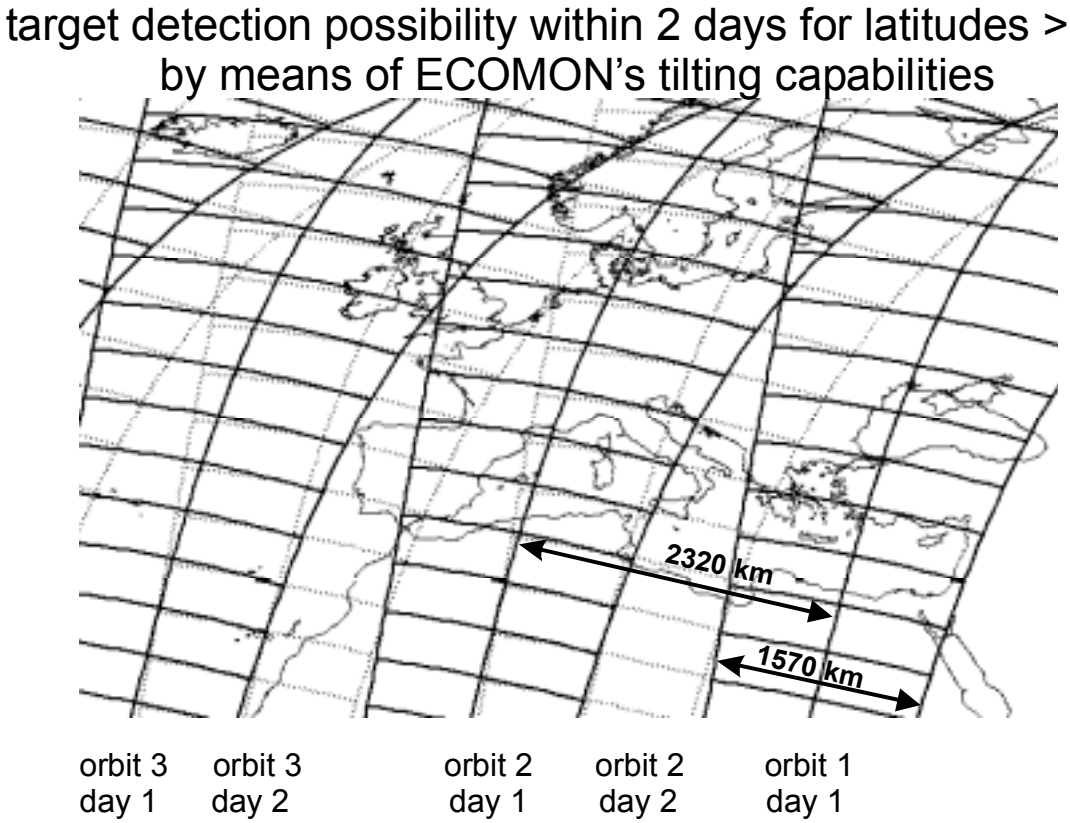

Figure 30: Orbit tracks for 2 days, height = 775 km, inclination = 98.5°, sun-synchronous, descending passes only

4.2 Payload

The proposed ECOMON payload consists of an Offner-type imaging spectrometer, a SWIR camera and a TIR whiskbroom scanner (see Table 15). The arrangement layout of the entire payload is mainly driven by observation requirements (see Chapter 2.3.3), design constrains for the sensor/module, calibration requirements and S/C allocation constrains (e.g. mass, power).

Table 15: Overview of the ECOMON payload

Spectral region	Number of instruments	Type of instruments	Swath [km]	No. of spectral channels
VIS–NIR (0.4 – 1.05µm)	4	Imaging spectrometer	4 x 100	ca. 16, programmable
SWIR (1.2 – 2.4µm)	2	Beam Splitting Camera	2 x 200	4
TIR	1	Whiskbroom scanner	1 x 400	1

In the following these boundary conditions are summarised for the VIS spectrometer and the SWIR camera. These requirements and constrains are not valid for the TIR scanner because of main differences in the optical layout (whiskbroom scanner) and the calibration requirements (no Sun calibration is needed).

Sensor design conditions

- similar sensors (cameras or spectrometers) need identical mechanical, optical and electronic set-ups to reduce fabrication costs,
- each of the sensors have to work autonomously (the failure of one sensor should not have effect on the other instruments),
- the sensors' optical part have to be self-supporting and designed as closed blocks (for the easier realisation of sensor adjustment and obstruction of incoming straylight).

Module design condition

- the spectrometer's swath width is ~100 km, the camera's is ~200 km; a configuration is searched where the conjunction ground tracks are about 400 km,
- posterior to the sensor's optical adjustment all module adjustments have to be performed without any change of the sensor optics (to avoid any optical re-adjustment),
- the optical axis of all sensors of each module must be adjustable to one common reference plate (to enable a geometrical inter-sensor calibration).

Calibration requirements

- Sun calibration must be realised via diffuser to assure Sun radiance measurements during terminator crossing when the Sun illuminates the diffuser (which has a standard orientation to the Earth),
- the diffusers have to be turned into the sensors' FOVs,
- the diffusers should be placed vertical to the flight direction for achieving a uniform illumination of the pixels and spectral channels,
- the Suncal unit's aperture and the baffle system should be symmetrical regarding the seasonable mean angle Sun–flight direction to avoid straylight,
- internal control with LEDs and mini lamps has to be ensured to provide additional calibration measurements,
- the diffusers (or parts of the moving system) should also be used as shutter for enabling dark measurements,
- an illumination of the diffusers by LEDs and/or lamps should provide additional calibration of the sensors and/or diffuser.

S/C allocation constrains (for a mini satellite < 300 kg):

- mass allocation: ≤ 80 kg (sensors); ≤ 25 kg (sensor support)
- power allocation: ≤ 115 W (peak)
- data rate allocation: ≤ 85 Mbit/s

The complexity of the various design conditions and requirements make it necessary to perform a module arrangement analysis to find an optimal solution for the different boundary conditions. By using the 3-d software tool Catia 3.0 a preliminary design was realised. The sensors, the module layout, the sensor control unit (SCU) layout and the calibration concept are described in the following subsections.

ECOMON's sensor and module arrangement

The scientific payload of the proposed mission consists of three different payload modules (PM1, 2 and 3). The similar payload modules PM1 and PM2 will be mounted on the front side of the S/C. Each of the similar PMs consists of two VIS-NIR spectrometer and one SWIR camera. To makes up a TFOV's swath width of 400 km (of 200 km for each module) sensors and modules will be arranged in a fan-shaped form. PM3 is the TIR whiskbroom scanner which will be placed in the bottom part of the S/C behind PM1/2. The overall mass of the TIR scanner will be less than 25 kg[149]; that of PM1/2 less than 45 kg.
The schematic arrangement and the resulting swath are shown in Figure 31.

[149] as proposed by Kayser–Threde GmbH for ECOMON

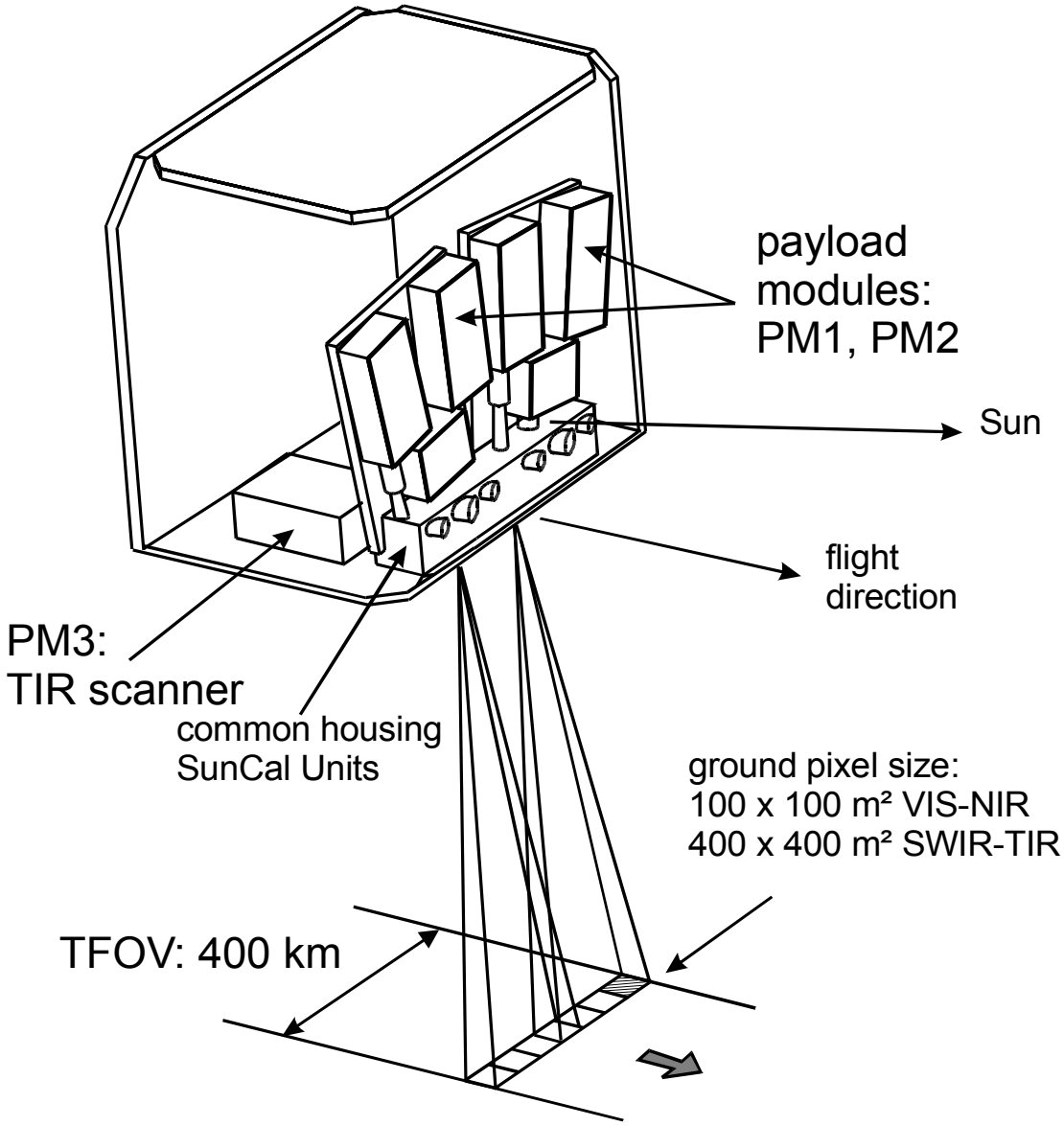

Figure 31: ECOMON S/C with three payload modules

ECOMON's VIS-SWIR payload module

The proposed mounting scheme of the VIS-SWIR payload module is depicted in Figure 32. A base plate serves to support the VIS-SWIR sensors, the SCU (not included in Figure 32) and the SunCal Unit. For each payload module (PM) the VIS/NIR and SWIR instruments and the SCU are mounted on a base plate. Whereas the VIS-NIR is covered by two similar Offner-type imaging spectrometers, the SWIR range is covered by a SWIR-camera which is placed between the spectrometer fore-optics. The three optical blocks of a PM have a common SunCal unit which is placed underneath the VIS-SWIR sensors to ensure the Sun calibration and LED, lamp calibration. The over all dimensions of one VIS–SWIR PM are about 500 x 700 x 150 mm^3; the mass is ~ 22.5 kg.

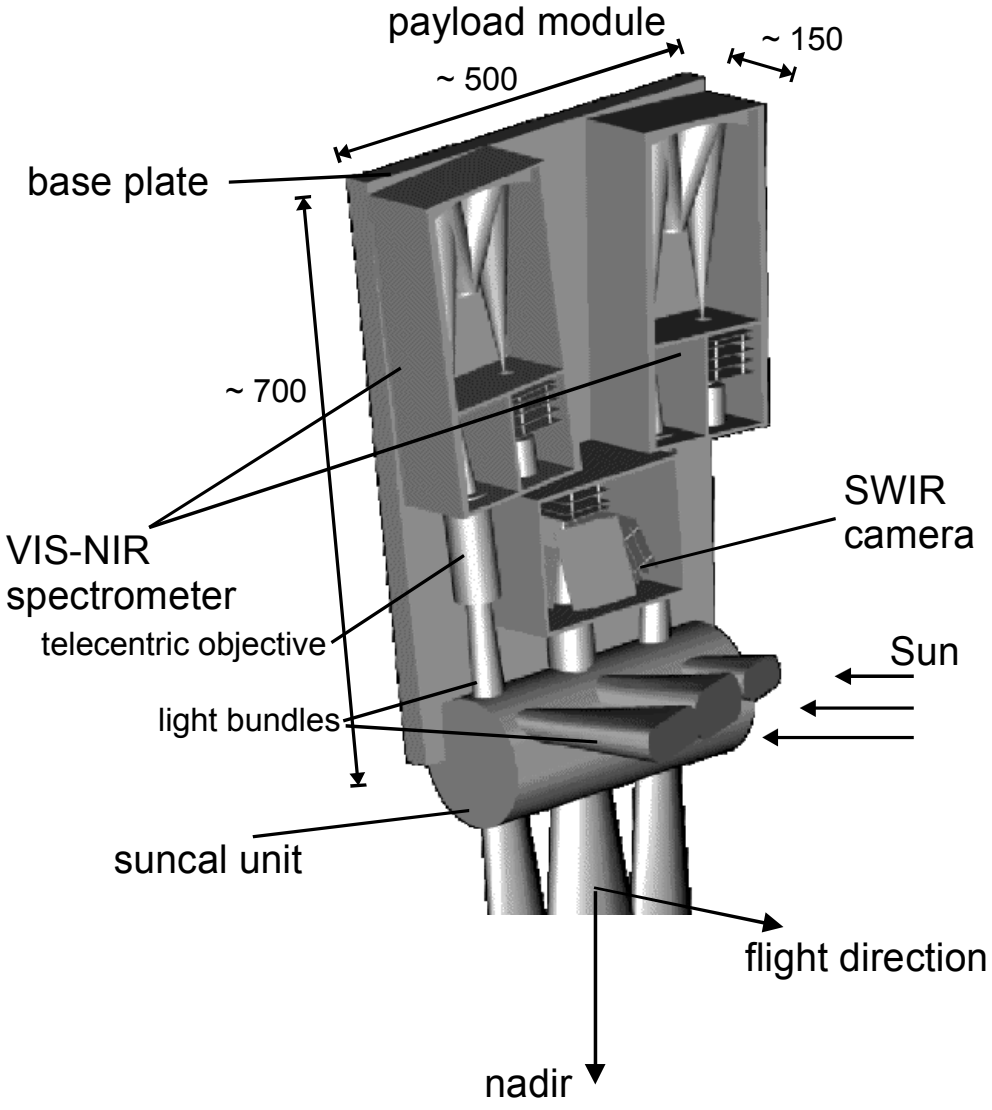

Figure 32: Mounting scheme of the payload module (PM)

4.2.1 Offner-type imaging spectrometer

The VIS-NIR is covered by an Offner-type imaging spectrometer with telecentric fore-optics and trapezium profile grating. The spectrometer prototype is currently under development at DLR Berlin. A description of the ongoing investigation is given in Chapter 3.2. Table 16 gives an overview of the main performance parameters for the proposed mission.

Table 16: Performance data of the Offner-type imaging spectrometer (flight altitude 775 km)

Parameter	Value
Entrance optics	telecentric, 4/100
FOV	7.616 ° = 0.13312 rad = 103.2 km
IFOV (pixel size)	0.007438 ° = 0.13 mrad = 100.6 m
Spectral range	400 – 1000 nm
Basic spectral resolution	1.5 nm
Channel halfwidth	binnable up to 20 nm
Number of selected channels	16 (tbd)
Polarisation sensitivity	$\leq$ 1 %
Second order spectrum	$\leq$ 0.5 %
CCD-detector, 1024 x 512 elements (used)	13.312 mm x 6.656 mm
Dynamic range	16 bit
Element size	13 µm x 13 µm

4.2.2 SWIR camera

The research task in the SWIR range will covered by four spectral channels, i.e. three atmospheric window channels and one water vapour channel. The radiation of the ground pixel is separated spectrally and focussed on four different detectors. The spectral separation is carried out by a beamsplitter assembly. It consists of a set of prisms with dichroic coatings. The spectrally resolved radiance is detected by thermoelectric cooled line detectors. The sensor's dynamic range is between 0.02 – 10 µW/cm²srnm what will cover most of the applications in the SWIR. More instrument details can be retrieved from Table 17.

Table 17: Performance data of the four-channel SWIR camera (flight altitude 775 km)

Parameter	Value
Entrance optic	≈ 4/100
FOV	14.5° (≈ 200 km)
IFOV (pixel size)	< 400 m
Spectral range	1.2 – 2.3 µm
Centre wavelength	1.24, 1.38, 1.63, 2.20 µm
Channel halfwidth	0.01– 0.1 µm
Dynamic range	0.02 – 10 µW/cm²srnm
Radiometric resolution	16 bit
Number of channels	4

4.2.3 TIR scanner

The thermal infrared will be covered by a conventional mechanical whiskbroom scanner[150]. This sensor type has been selected with respect to costs, availability, technical risk and complexity. Via scanner mirror, optics and filter the spectrally separated thermal radiation is focused on a single element CMT (HgCdTe) detector, which will be thermoelectrically cooled: This detector is located in an integrated dewar assembly which has a cold stop to provide effective cold shielding. Calibration blackbodies will be integrated in the unused field angles of the scanner, so that their signals can be referenced at the beginning or ending of every scanned line. More technical details can be found in Table 18.

Table 18: TIR scanner performance data

Parameter	**Value**
Spectral range	10 – 12 μm
Dynamic range	12 bit
Entrance optics	~ 6/ 300
Temp. range	240 K – 340 K
ΔT	< 0.5K
FOV	30°
Ground pixel size	300 m²
Detector	HgCdTe (~ 160 K thermoelectric cooled)
Total mass	< 25Kg
Envelope	320mm x 250mm x 130mm
Power consumption (OPM)	25 W

4.2.4 The Sensor Control Unit (SCU)

The SCU is the interface between the sensors and the S/C for data, control and power. For each module there will be one SCU which will be placed between the Offner-type spectrometer directly on the base plate (not included in the figures).
A DCU has the following interfaces to the three sensors of one payload module and the S/C payload controller:

Interfaces (IF) within the payload module

- Data interfaces for the two Offner and one SWIR camera (DI1, DI2, DI3)
- Control interface for SunCal unit (SI)
- Power interfaces for the two Offner and one SWIR camera (PI1, PI2, PI3)
- Power interfaces to cooling system of the two Offner and one SWIR camera (CI1, CI2, CI3)

[150] as proposed by Kayser–Threde GmbH for ECOMON

Interfaces to S/C

- Command IF from S/C for the hole module (Cmd-IF)
- Telemetry IF to the S/C (TM-IF)
- Power interface (P-IF)
- house keeping data telemetry channel (HKD-IF)

The SCU consists of

- Data interfaces for Offner1 & Offner2, SWIR
- Control unit for calibration unit
- Processing Unit (µP)
- Power Supply
- Command interface
- Telemetry interface
- HKD telemetry channel

The bi-directional serial data interface of the SCU consists of an up-link channel which is necessary to change software parameters for the payload control and a down-link channel for receiving the pixel data flow from the spectrometers and the camera. This data interface is realised as galvanic isolated interface for minimising ground bounce and prevent ground loops. For synchronisation and to prevent the influence of time skews the pixel data write in a buffer (FIFO-memory or swing buffer memory). The buffer size will be dimensioned for one full readout of the sensor and the input buffer control is realised by a FPGA[151].
The command interface receives all commands from the S/C and transfers it to the corresponding payload controls. As command interface a standard type (e.g. MIL-STD[152] 1553 bus or serial interface) can be used.
The main task for the processing unit is to initialise input controller (data interface), output controller (telemetry interface), to control the calibration timing, to check the performance of other parts (self tests), to observe the command interface, to observe the status of payload and to generate house keeping data (HKD). This does not include any data processing. The HKD will be transmitted to the output controller of telemetry interface where the hole data stream will be forwarded to the S/C. For minimising costs a standard interface type (e.g. MIL-STD 1355 or serial IF) can be utilised. The minimal channel capacity has at least 40 MBit/sec. Within the telemetry interface a FPGA controls the readout of several input buffers and completes this data stream with the suitable HKD.
The task of the calibration control interface is to control the timing of the LEDs, the miniature lamps and the shutter of the external calibration unit.
The power supplies generate all necessary voltages for the SCU from the S/C raw voltage. The power supplies for the spectrometers and the camera only pass through the SCU block.

[151] Field-programmable gate arrays
[152] Military standard

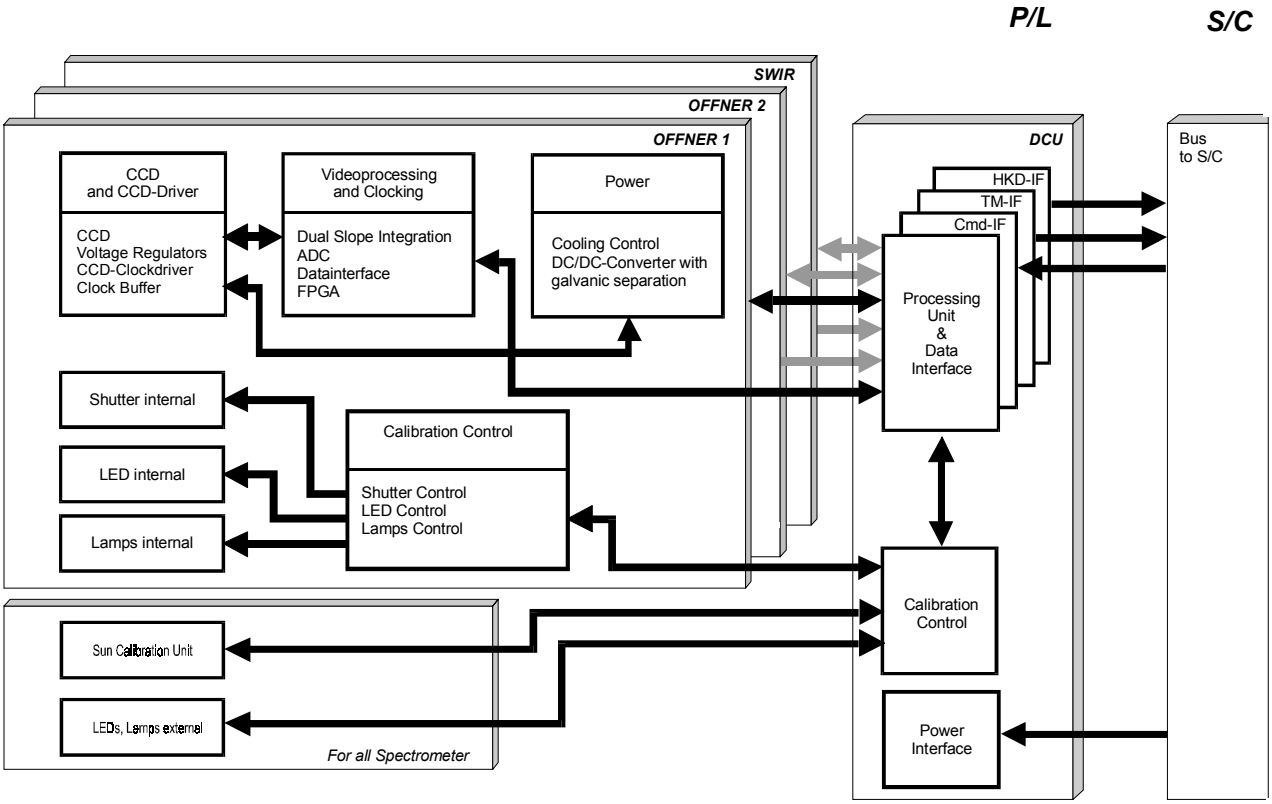

Figure 33: Payload module electronics

4.2.5 In-flight Calibration

In-flight calibration guaranties the re-calibration of selected instrument parameters during the flight mission in providing a reference to extraterrestrial Sun irradiance or other radiance sources (e.g. lamps, blackbodies). The TIR scanner will be re-calibrated by two blackbodies of different temperatures. In contrast, the SWIR cameras and the spectrometers perform in-flight calibration by an advanced procedure: The technical realisation of this calibration approach encloses internal sources and an external calibration unit (SunCal unit). Additional shutters will guarantee to perform the calibration with internal sources and/or dark signal measurements (see Figure 34).

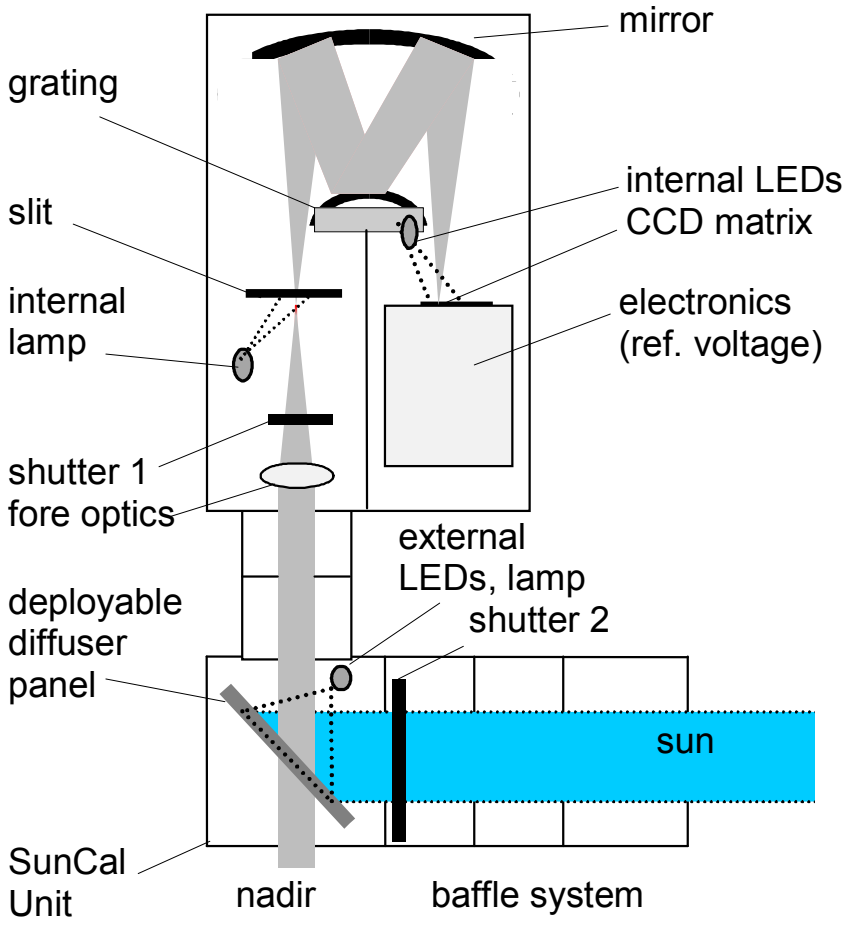

Figure 34: In-flight calibration tools for the Offner-type imaging spectrometer

Internal calibration

The internal calibration components consist of reference voltages, LEDs, mini lamps and a shutter for darkening. When shutter 1 closes the instrument, the internal calibration can be performed: after dark measurements, the check of the electronic data is ensured by reference voltage in the electronics. The CCD performance (e.g. on-chip amplifier linearity check, conversion factor determination and trap correction) is checked when the CCD is illuminated with LEDs and a characterisation of the spectrometer's spectral and geometric parameters is provided by the internal lamp.

External calibration (SunCal Unit)

The calibration cylinder of the SunCal Unit guarantees the correct alignment of the diffuser for the calibration (diffuser towards the sun during terminator crossing), for dark signal measurements, and for nadir measurements (free FOV). The calibration procedures consist of Sun, mini lamp and LED calibration.

The Sun calibration is realised during terminator crossing by turning a diffuser into the FOV. The spectral radiance of the Sun illuminated diffuser depends on its BRDF, and therefore it can be used as an absolute calibration source. During lamp and LED calibration the diffuser is illuminated by the mini lamps and the LEDs, but neither the Sun light nor Earth reflectance are able to enter the SunCal unit (shutter 1 open, shutter 2 closed). The measurements of this calibration procedure allow to check (1) a possible spectrometer degradation (because light passes all optics before detected), and (2) a possible diffuser degradation (in comparison with Sun calibration).

4.3 Spacecraft Platform

The proposed S/C[153] belongs to the category of minisats having an envelope of 1 x 1 x 1.2 m³ and a mass budget of ca. 300 kg. Because of the low power allocation of the payload (ca. 230 W in operation mode) the satellite will work with a three small panel solar generator (GaAs semiconductors). One panel is attached to one S/C side and the other two are de-folded in orbit after the launch phase. During the launch phase they are attached to the S/C sides. The GaAs generator will charge the batteries during the pole flyover and outside the ground station visibility, when no imaging takes place.

The main features of the S/C comprise advanced ACS technology allowing tilting manoeuvres of up to ± 30° along or cross track, and an instrument support subsystem to provide the capability of storing 85 MBit/s sensor output into a data storage of 25.6 GBit minimum storage capability, including the appropriate X-band downlink (100 MBit/s for real-time transmission).

Preliminary subsystem accommodation of the S/C is depicted in Figure 35. A summary of the proposed S/C is shown in Table 19.

Table 19: Summary of the ECOMON S/C

Spacecraft Summary					
Name	**ECOMON**		**Power Subsystem**		
Life Time	5	years	total Power	253	W
Orbit			P/L Energy	222	Wh
Altitude	775	km	total Energy	423	Wh
Inclination	98,5	°	Power Bus	28	V
ECT	TBD	A.M.	**Solar Generator**		
P/L DH			Type	GaAs	
Sensor Data Rate	85	Mbit/s	Eta	20%	
Memory	33	Gbit	Panel Area	3,5	m²
Science Data	26	Gbit	Power EOL	755	W
Downlink	100	Mbit/s	Gen. Power	570	Wh
			Mass	27	kg
P/L High Rate Downlink			**Batteries**		
Frequency	8200	MHz	Type	NiH2	
Data Rate	100	Mbps	Capacity	644	Wh
EIRP	32,0	dBW	Mass	20	kg
Margin	7,5	dB	**TMTC Link**		
S/C total			Frequency	2000	MHz
P/L +Supp. Mass	105	kg	Data Rate	10	kbps
total Mass	300	kg	EIRP	-13,0	dBW
Volume	1000	mm	Margin	9,8	dB
	500	mm			
(height)	1200	mm			

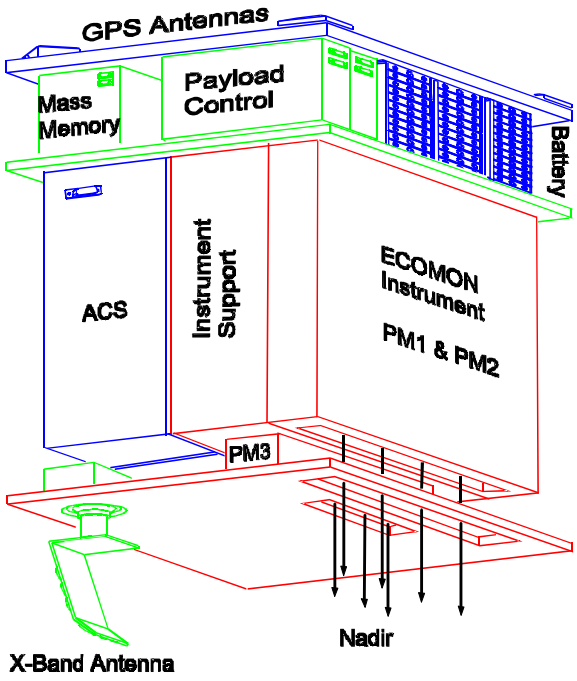

Figure 35: S/C's instrument accommodation (after OHB System)

[153] as proposed by OHB–System for ECOMON

Attitude and Orbit Control Subsystem

The S/C has to ensure a precise attitude knowledge. Therefore, the 3-axis stabilised S/C will use an ACS subsystem, which consists of star sensor, Sun sensor, gyros and wheels (see Figure 36). This system will enable a high pointing accuracy of ± 0,03° together with a precise attitude knowledge of ±0.003°. In order to enhance the Earth coverage, the sensor swath will be capable of being shifted to the maximum useful off-nadir angle of about ± 30°. This can be performed by using the satellite control system to rotate the whole satellite accurately to the desired angle before recording of the remote sensing data begins.

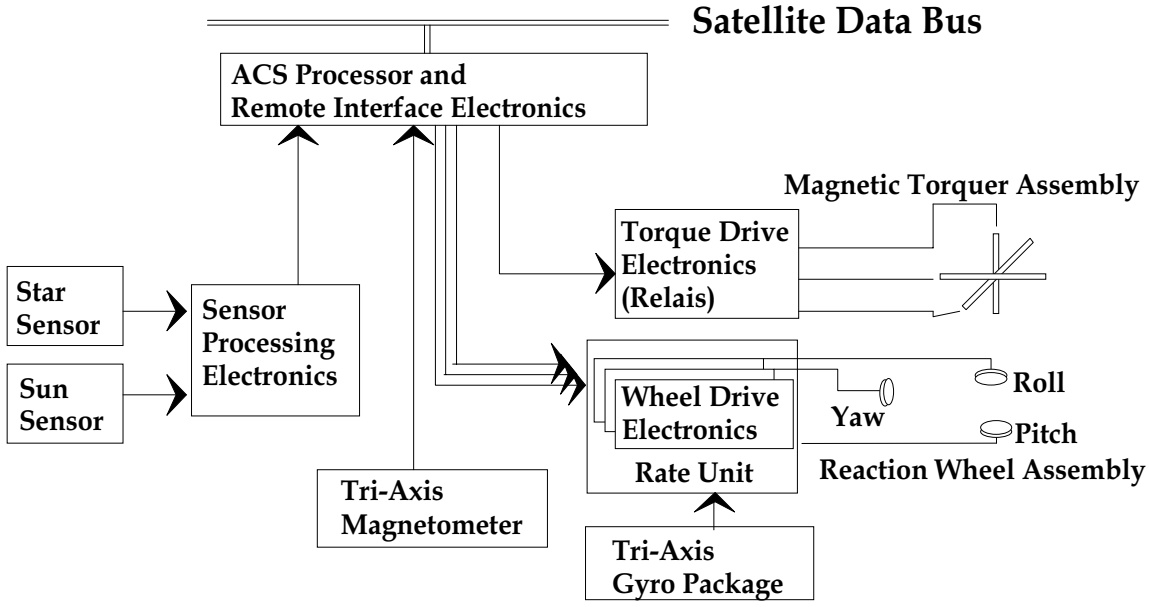

Figure 36:Technical concept of the ECOMON ACS

More details on the S/C's operation modes, the mass and power budgets are outlined in Appendix B.

5 General Conclusion

Motivation

In recent times, the coastal zone science community (e.g. International Ocean-Colour Coordinating Group) expressed the opinion to improve the observation of coastal zones for receiving a better knowledge about the space-time quantification and distribution of ecological parameters such as water constituents[154]. This knowledge can be used to obtain important assumption about the stability and the grade of pollution of the ecosystem coastal zone in a regional point of view. Out of this results the demand for a regional orientated coastal zone mission. In contrast to local or global orientated sensors (as COIS or MODIS, MERIS, SeaWiFS), a regional mission has to be capable to retrieve information on rapid changes of the coastal ecosystem (e.g. pollution on river estuaries, flooding in contaminated regions, critical algal blooms).

Background

The first and so far most successful ocean colour remote sensing mission, was the CZCS on NIMBUS 7 in the years from 1978 and 1986. Grace to this experimental mission important knowledge on the development of global ocean colour remote sensing methods and algorithm development have been made. Since March 1996, a new experimental mission — the pushbroom imaging spectrometer MOS-IRS — delivers important data for the progress of remote sensing methods. Launched on the Indian satellite IRS-P3, it samples data of the coastal zone and open ocean with 18 spectral channels (17 VIS-NIR and 1 SWIR). This sensor represent both, a proof-of-concept instrument and it helps to develop new algorithms for a better understanding of the coastal-zone environment. Because of the extensive experiences at the DLR institute in Berlin in terms of instrument and algorithm development first investigations for a MOS successor development started. As a result a technical-realistic mission concept[155] has been proposed to ESA (Call for Earth Explorer Opportunity Missions); however, other mission objectives received higher preferences.

Goals of the thesis

The goal of the thesis was to develop in several investigations and in the framework of the mission study a detailed technique-realistic mission concept which is able to meet the requirements of the coastal zone community for a regional coastal zone mission.

[154] IOCCG–2000
[155] Neumann et al.–1998

Thesis's results

For the development of a mission concept different theoretical and experimental investigations have been performed, which are summarised in the following:

0. Systematisation of Earth observation sensors

In a first step a systematisation of existing and future Earth observation sensors gives basic directions for future in-house developments, i.e. the systematisation offers an overview on various concepts and provides the basis for prospective mission concept developments.

1. Development of a detailed sensor and calibration concept

A ray-tracing and grating simulation study[156] showed the ability of an imaging Offner-type spectrometer with convex trapezium-profile grating to provide a sufficient spectral and spatial image quality. This spectrometer has a low polarisation sensitivity (< 1%), low straylight by suppression of the 2nd order spectrum (≤ 0.5%) and is very compact. In the frame of the thesis the signal-to-noise ratio has been calculated by using the simulation results and the CCD performance parameters (spectral and spatial resolution, efficiencies of optic and detector etc.). In the signal-to-noise ratio simulation the radiometric properties of the system optics-grating-detector were determined. This analysis explains the effect of image smear and shows that the smear's photon noise is inevitable for frame-transfer CCDs in conjunction of small input signal, small integration time and many spectral channels. Possibilities of corrections are mechanical or electronic shutters. An experimental prototype study[157] showed that the spectral and geometrical parameters of the simulation can be verified: The spectrometer under investigation would have a ground resolution of 100 m and a swath width of 100 km in a 800-km orbit. The spectral range is covered from 400 to 1050 nm with a spectral resolution of $\Delta\lambda$ < 1.5 nm. In the frame of the thesis the laboratory set-up has been improved. The focal plane is adjustable with a step motor control with high positioning accuracy (0.4 µm/step; 0.0004°/step) for laboratory measurements and for the optimisation of the spectrometer's parameters.

Another experimental investigation shows the possibility of luminescence diodes (LEDs) to be used for in-orbit calibration. In the scope of this investigation the characteristics (e.g. dependencies of signal level and location of the emission maximum in the temperature region from 5°–50°, utilisation of LEDs in space environment conditions). Hence, it was demonstrated that LEDs can be used in space when the LED environment temperature is stabilised. Therefore, a method was developed which guarantees a long-term stabilisation of the LEDs independently of the ambient temperature.

[156] List–1997
[157] Roth–1998

2. Definition of a mission scenario with emphasis on regional coastal zone remote sensing

The pushbroom imaging spectrometer which has been developed at DLR Berlin is an excellent tool for remote sensing of coastal zones in the VIS–NIR. For the regional coastal zone mission scenario this spectrometer can be integrated as VIS–NIR component. The compactness of the instrument enables an arrangement of several similar spectrometers in a fan-shaped form to extent the total swath width to overcome the pushbroom imaging spectrometer related narrow swath widths (Field of view < 8°). An integration of further sensors concept realises the coverage of the SWIR/TIR spectral range of the remote sensing mission.

In a module arrangement analysis a sensor arrangement have been selected which enables the mounting of various sensors (e.g. fan-shaped) on a mini satellite (~ 300 kg) in a way that scientific requirements, satellite integration conditions and calibration requirements can be met. Because of this module arrangement the proposed mission covers the spectral range from VIS to TIR with 21 (partly programmable) channels. The swath width is 400 km and the spatial resolution 100 m, respectively. The field-of-regard (*FOR*) is 87° which is ensured by the satellite's tilting capability (± 30° off nadir). In conjunction with suitable orbit parameters (Sun-synchron orbit, 775-km average orbit height) every location (latitude > 30°) can be detected within two days; a global repetition is ensured for the 3rd day.

Consequently, the proposed mission is an excellent technique-realistic concept for investigating the ecosystem coastal zone with high cost-efficiency by means of developed technologies and presented results.

Outlook

The polarisation sensitivity was stated in a grating simulation to be smaller 1%. This has to be verified by the experimental prototype. Further on, the exact radiometric, spectral and geometrical resolutions have to be determined using both, the final version of the trapezium grating and the new low-noise high dynamic range video electronics.

The image smear can be reduced by applying APS detectors or frame-transfer CCDs with electronic shutters. These detectors are currently not available with adequate performance parameters (military or custom design). These conditions can change in near future what would solve the image smear problem. However, for the utilisation of APS detectors the individual calibration characteristics of each detector should be taken into account.

The precise focal plane positioning of the experimental prototype is ensured by step motors of a goniometer head. Dimensions and mass of this positioning system are to large to be integrated in the flight model. A version of the flight model has the following procedure: Instead of integration of a positioning system, the focal plane can be adhered in its end position to the inner spectrometer wall for reducing additional constructive efforts and mass. However, the disadvantages of an adhesive bonding have to be considered (e.g. the size of displacement from the focal plane's end position during the bonding procedure etc.).

6 References

Abreau, V.; Lidar from orbit; Optical Engineering; Vol. 19; pp. 489–493 (1980)

Barbe, D.F.; State of the art in visible solid-state imagers; SPIE; Vol. 1987; pp. 20–34 (1987)

Barnes, R.A., A.W. Holmes, W.L. Barnes, W.E. Esaias, C.R. McClain, T. Svitek; SeaWiFS Prelaunch radiometric calibration and spectral characterization; NASA Tech. Memo. 104566; Vol. 23; pp. 55 (1994)

Barnes, W.L. et al.; Prelaunch characteristics of the MODIS on EOS-AM1; IEEE, Trans. Geoscience and Remote Sensing; Vol. 6, No. 4 (1998)

Barton, D.L., M. Osinski, P. Perlin, C.J. Helms, N.H. Berg; Life tests and failure mechanisms of GaN/AlGaN/InGaN Light Emitting Diodes; SPIE; Vol. 3279; pp. 17–27 (1998)

Bischoff, K., et al.; First results of the Intercosmos Satellite IK 21; Acta Astronautica; Vol. 10, No. 1; pp. 31–35 (1983)

Blechinger, F., B. Harnisch, B. Kunkel; Optical concepts for high resolution imaging spectrometers; SPIE; Vol. 2480; pp. 165 – 179 (1995)

Bogner, G., A. Debray, G. Heidel, K. Höhn, U. Müller, P. Schlotter; White LED; SPIE; Vol. 3002; pp. 143 – 150 (1999)

Braam, B.; personal communication; fax reply, the 12th March 1997 (1997)

Braam, B., J. Okkonen, M. Aikio, K. Mäkisara, J. Bolton; Design and first test results of the Finnish airborne imaging spectrometer for different applications (AISA); SPIE; Vol. 1937; pp. 142 – 151 (1993)

Cauruso, P., J. Hrastar; Technology infusion plan for the MTPE program, Feb. 1996; NASA GSFC, Greenbelt, Maryland (1996)

CEOS, Committee on Earth Observation Satellites; Resources in Earth observation – 1997; CD-ROM produced by CNES (1997)

Cerutti-Maori, G. and J.P. Durpaire; Un radiomètre optique multispectral pour l'etude des oceans; ESA Journal; Vol. 6; pp. 163–183 (1982)

Chu, W.P., M.P. McCormick J.M. Zawodny, L.E. Mauldin; Stratospheric aerosol and gas experiment III (SAGE III); SPIE; Vol. 3117; pp. 11–18 (1997)

Claybaugh, W.; Commercial space transportation study # Remote sensing; NASA HQ, Office of Space Access and Technology, Phase 1 study composed by NASA and six major United States Aerospace Corporation (1997)

Commission Internationale de l'Eclairage (CIE); Measurements of LEDs; ISBN 3 900 734 84 4; Publication CIE 127 (1997)

Coste, G.; private communication; fax reply, the 25th Nov. 1997 (1997)

Digenis, C., D.E. Lencioni, W.E. Bicknell; New millennium EO-1 Advanced Land Imager; SPIE; Vol. 3439 (1998)

Dinguirard, M. and P. N. Slater; Calibration of space-multispectral imaging sensors: a review; Remote Sensing of Environment; Vol. 68; pp. 194–205 (1999)

Dinguirard, M., X. Briottet, P. Henry, A. Meygret, P.N. Slater, R. Santer, J.L. Deuze; Calibration of the SPOT HRV Cameras; submitted to Remote Sens. Environ (1998)

EEV; Back illuminated CCD25-20 datasheet; EEV Ltd (1996)

EEV; Back illuminated CCD47-20 datasheet; EEV Ltd (1997)

EG&G Judson datasheet; Multiplexed InGaAs photodiode arrays J18–28P–W500U: 512E; EG&G Judson (1998)

Endemann, M., H. Fischer, Envisat's high-resolution limb sounder: MIPAS; European Space Agency Bulletin; Vol. 76; pp. 47–52 (1994)

ESA PSS–01–702 Method 'A'; Issue 1, March 1983; pp. 1–21 (1983)

ESA Report; European Space Environment Standard; ECSS E-10-04; pp. 9–30 (in press)

ESA Report; Final report on the High Resolution Imaging Spectrometer HRIS; ESA Doc. Ref. HS–DAS– FR–01, May 1994 (1994)

Evans, D.L.; High Luminance LEDs replace incandescent lamps in new applications; SPIE; Vol. 3002; pp. 142–153 (1997)

Evans, R.H and H.R. Gordon; Coastal Zone Colour Scanner 'system calibration': a retrospective examination; Journal of Geophysical Research; Vol. 99, No. C4; pp. 7293–7307 (1994)

Flügge, S.; Handbuch der Physik; Optische Instrumente; Springer-Verlag Berlin, Heidelberg, New York; Band XXIX; pp. 597 (1967)

Fossum, E.R.; Assessment of image sensor technology for future NASA missions; SPIE; Vol. 2172; pp. 38–53 (1994)

Fujisada, H.; Overview of ASTER instrument on EOS–AM1 platform; SPIE; Vol. 2268; pp. 14–36 (1994)

Goetz, A.F.H., L.C. Rowan, M.J. Kingston; Mineral identification from orbit: Initial results from the Shuttle Multispectral Infrared Radiometer; Science; Vol. 228; p. 1147 (1982)

Goetz, A.F.H. et al.; High resolution imaging spectrometer: Science opportunities for the 1990s; Instrument Panel Report, Earth Observation System, NASA, Washington, DC; Vol. IIc; pp. 1 – 73 (1987)

Goetz, A.F.H.; Hyperspectral imaging: advances in a spectrum of applications; Proc. Fifth Australasian Remote Sensing Conference, Perth, Australia, October 8-12 (1990)

Gordon, H.R. and A.Y. Morel; Remote assessment of ocean color for interpretation of satellite visible imagery; Springer-Verlag New York; pp. 1–114 (1983)

Gordon, H.R., D.K. Clark, J.W. Brown, O.B. Brown, R.H. Evans, W.W. Broenkow; Phytoplankton pigment concentrations in the Middle Atlantic Bight: Comparison of ship determinations and satellite estimations; Applied Optics; Vol. 22, No. 20 (1983)

Gordon, H.R., R. Smith, J.R. Zanfeld; Introduction to ocean optics; SPIE; Vol. 489 (1984)

Gordon, H.R.; Ocean color remote sensing systems: radiometric requirements; SPIE; Vol. 924; pp. 151 – 167 (1988)

Guenther, B., W. Barnes, E. Knight, J. Barder, J. Harnden, R. Weber, M. Roberto, G. Godden, H. Montgomery, P. Abel; MODIS calibration: a brief review of the strategy for at-launch calibration approach; Journal of Atmos. Ocean. Technol.; 13; pp. 274 – 285 (1996)

Gumble, H.; System considerations for hyper/ultra spectroradiometric sensors; SPIE; Vol. 2821 (1996)

Hamamatsu datasheet; InGaAs linear image sensors G6890, G6891, G6893 series; Hamamatsu Photonics K.K (1997)

Harger, R.O.; Synthetic aperture radar systems; Academic Press, New York (1970)

Hewlett-Packard Company; Precision optical performance AlInGaP LED lamps HLMP-Exxx; Palo Alto (1999)

Hofmann, C.; Die optische Abbildung; Akademische Verlagsgesellschaft Geest & Portig K. G., Leipzig, Chap. 3; p. 113. (1980)

Im, J.S., H. Kollmer, O. Gfrörer, J. Off, F. Scholz, A. Hangleiter; Piezoelectric fields effects on optical properties of Ga/N/GaInN/AlGaN quantum wells; MRS Internet J. Nitride Semicond. Res. 4S1, G6.20 (1999)

Intercosmos; Scientific report on the results of the satellite experiments Intercosmos–20 and Intercosmos–21 (1979–1982) (in Russian); Editor: Sowjet Intercosmos; Moskau; pp. 1–149 (1984)

IOCCG; Minimum requirements for the operational, ocean-colour sensor for the open ocean; Report No. 1 of the International Ocean-Colour Coordinating Group (IOCCG); pp. 1–43 (1998)

IOCCG; Status and plans for ocean-colour missions: considerations for complementary missions; Report No. 2 of the International Ocean-Colour Coordinating Group (IOCCG); pp. 1–43 (1999)

IOCCG; Remote sensing of case-2 waters; Report No. 3 of the International Ocean-Colour Coordinating Group (IOCCG); in preparation (2000)

Jerominek et al.; Micromaschined, uncooled VO_2–based IR bolometer arrays; SPIE; Vol. 2746; pp. 60–71 (1996)

Jouan, J., J.F. Reulet, G. Costes; SPOT HRVIR: a significant improvement of high resolution visible SPOT camera to IR wavelength; IAF–89 (1989)

Kempainen, S.; CMOS image sensors: eclipsing CCDs in visual information?; EDN, October 1997; pp. 101–119 (1997)

Kramer, H.; Observation of the Earth and its environment – survey of missions and sensors; Third Enlarged Edition, Springer Verlag; pp. 1–960 (1996)

Krawczyk, H., A. Neumann, T. Walzel; Interpretation potential of marine environments multispectral imagery; Third Thematic Conference on Remote Sensing for Marine and Coastal Environments; Sept. 1995, Seattle/Washington, USA; pp. II-57 – 68 (1995)

Kunkel, B., W. Posselt, E. Schmidt, U.D. Bello, B. Harnisch, R. Meynart; Hyperspectral imager survey and developments for scientific and operational land processes monitoring applications; EUROPTO European Symposium on Environmental Sensing III (1997)

Kwo, D., M. Chrisp; Design of a grating spectrometer from a 1:1 Offner mirror system; SPIE; Vol. 818; pp. 275–279 (1987)

Lansing, J.C., R.W. Cline; The four and five band multispectral scanners for Landsat; Optical Engineering; Vol. 15, No. 4; pp. 312–322 (1975)

List, E.; Komplexe Durchrechnung eines spekrographischen Systems; Interne Studie von BIFO and DLR, Berliner Institut für Optik (1997)

Lockyer, E.M.; Applications hold the key to imager choice; Photonics Spectra, March 1997; pp. 80–90 (1997)

Lucey, P.G., K. Horton, T. Williams, K. Hinck, C. Budney; SMIFTS: A cryogenically-cooled spatially-modulated imaging infrared interferometer spectrometer; SPIE; Vol. 1937; pp. 130–141 (1993)

Lura, F., D. Hagelschuer, V.V. Abraimov; KOBE – the simultaneous simulation of space environment effects for the investigation of spaceborne material properties; Proceedings of the 3rd International Symposium on Environmental Testing for Space Programmes, ESA–ESTEC, Noordwjik, The Netherlands (1997)

Markham, B.L., J.L. Barker, E. Kaita, I. Gorin; LANDSAT–7 Enhanced Thematic Mapper Plus: radiometric calibration and pre-launch performance; SPIE; Vol. 3221; pp. 170–178 (1997)

McClain C.R., R.S. Fraser, J.T. McLean, M. Darzi, J.K. Firestone, F.S. Patt, B. D. Schieber, R.H. Woodward, E. Yeh, S. Mattoo, S.F. Biggar, P.N. Slater, K.J. Thome, A.W. Holmes, R.A. Barnes and K.J. Voss; Case studies for SeaWiFS calibration and validation, Part 2; NASA Technical Memorandum 104566; Vol. 19 (1994)

Mukai, T., M. Yamada, S. Nakamura; InGaN-based uv/blue/green/amber/red LEDs; SPIE; Vol. 3002; pp. 2–13 (1999)

Muray, K.; Photometry of diode emitters. Light emitting diodes and infrared emitting diodes; Applied Optics; Vol. 30, No. 16 (1991)

Myers, W.A., R.D. Smith, J.L. Stuart, M. Griggs, D. Utley; NEMO satellite sensor imaging payload; SPIE; Vol. 3439 (1998)

Nakajima, T.Y, T. Nakajima, M. Nakajima, H. Fukushima, M. Kuji, A. Uchiyama, M. Kishino; Optimization of the Advanced Earth Observing Satellite (ADEOS) II Global Imager (GLI) channels by use of radiative transfer calculations; Applied Optics; Vol. 37, No. 15; pp. 3149–3163 (1998)

Neckel, H. and D. Labs; The solar radiation between 3300 and 12500 Å; Solar Physics; Vol. 90; pp. 205 – 258 (1984)

Neumann, A., G. Zimmermann, N. Hoepffner, A. Perdigao, T. Pyhälahti, J. Gower, T. Platt, G. Coste, A. Ginati, S. Hofer; ECOMON – A dedicated mission for regional ecological research and monitoring; Mission proposal for ESA call for Earth explorer opportunity mission as internal DLR report, Berlin; pp. 1– 65 (1998)

Nichia Chemical Industries, LTD; Specifications on Nichia white, blue, green LED NSPx; Tokyo (1998)

Nieke, J., M. Solbrig, K.H. Sümnich, G. Zimmermann, Röser; Spaceborne Spectrometer Calibration with LEDs; presented at the SPIE Conference on Earth Observing Systems V, 2000 in San Diego, USA; SPIE Vol. 4135 (2000)

Nieke, J., M. Solbrig, A. Neumann; Noise Contribution for Imaging Spectrometer; Applied Optics, Vol. 38, No. 24; pp. 5191–5194 (1999)

Nieke, J., H. Schwarzer, A. Neumann, G. Zimmermann; Imaging spaceborne and airborne sensor systems in the beginning of the next century; SPIE; 3221 (1997)

Oaku, H., M. Shimada, Y. Mitomi, Y. Miyachi, R. Green; Calibration of OCTS; SPIE; Vol. 3221; pp. 101–109 (1997)

Offner, A.; Annular field systems and the future of optical microlithography; Optical Engineering; Vol. 26, No. 4; pp. 294–299 (1987)

Olij, C., J.G. Schaarsberg, H. Werij, E. Zoutman, G. Baudin, B. Chommeloux, J.L. Bézy, G. Gourmelon; Spectralon diffuser calibration for MERIS; SPIE; Vol. 3221; pp. 63–74 (1997)

Ono, H., T. Ozaki, H. Tanaka, Y. Kawamoto; Analysis of smear noise in interline-CCD image sensor with gate-free isolation structure; Japanese Journal of Applied Physics; Vol. 30 (1991)

Osinski, M., P. Perlin, P. Eliseev, J. Furioli; Current transport and emission mechanisms in high-brightness green InGaN/AlGaN/GaN single-quantum-well light-emitting diodes; SPIE; Vol. 3002; pp. 15–25 (1997)

Pagano, T.S. and R.M. Durham; Moderate resolution imaging spectrometer (MODIS); SPIE; 1939 (1993)

Palmer, J.M. and P.N. Slater; A rationing radiometer for use with a solar diffuser; SPIE; Vol. 1493; pp. 106 – 117 (1991)

Palmer, J.M.; Calibration of satellite sensor in the thermal infrared; SPIE; Vol. 1762 (1992)

Persky, M.J.; A review of spaceborne infrared Fourier transform spectrometers for remote sensing; Rev. Sci. Instrum. 66, 10; pp. 4763–4797 (1995)

Pflug, B.; private communication (1999)

Posselt, W.; In-flight characterisation approach and hardware trades; PRISM Pre-Phase A, Doc.No.: PRI-DSS-TN-013; pp. 1 – 31 (1997)

Prabhakara, C., G. Dalu, V.G. Kunde; Estimation of sea surface temperature from remote sensing in the 11- to 13 μm window region; Journal of Geophysical Research, 79; pp. 5039-5044 (1974)

Puschell, J.J. and P. Tompkins; Imaging spectrometers for future earth observing systems; SPIE; Vol. 3117; pp. 36–48 (1997)

Rast, M.; ESA MERIS: a review of its mission, system and data products; In: Proceedings of the 2nd International Workshop on MOS-IRS and Ocean Color, Berlin, 10-12 June 1998; pp 205–210 (1998)

Rast, M.; Imaging spectroscopy and its application in spaceborne systems; ESA SP–1144; pp. 1–144 (1991)

Readings, C. et al.; Report of the Earth observation user consultation meeting; ESA SP-1143; pp. 1–290 (1991)

Roberts, E., L. Pfitzner, M. Petkovic, T. Stapinski; Infrared focal plane for the Advanced Along-Track Scanning Radiometer; SPIE Vol. 2552; pp. 88–97 (1995)

Röser, H.P. and M. Schönermark; Comparison of remote sensing experiments from airborne and space platforms; Acta Astronautica; Vol. 39, Nos. 9–12; pp. 855–862 (1996)

Roth, J.; Untersuchungen zur Charakterisierung eines Konzeptes für ein abbildendes Spektrometer; Diplomarbeit für die Fachhochschule Lübeck (1998)

Saint, G.; Vegetation onboard SPOT 4 mission specification; Joint Research Centre Report: VGT/PS/940518/1; pp. 1–32 (1994)

Scherz, J.P. and A.R. Stevens; An introduction to remote sensing for environmental monitoring; Madison (The University of Wisconsin) pp. 1–80 (1970)

Schroeder, M., P. Reinhartz, R. Mueller; Radiometric calibration of the MOMS-2P camera; ISPRS Proceedings; Vol. 32; pp. 14–19 (1998)

Schwalb, A.; The TIROS–N / NOAA A–G Satellite Series; NOAA Technical Memorandum NESS 95; pp. 1–75 (1979)

Schwarzer, H.; private communication (1997)

Shimada, M., H. Oaku, H. Oguma, Y. Miyachi, R. Green; Calibration of AVNIR; SPIE; Vol. 3221; pp. 86–92 (1997)

Siemens AG; GaAs-IR Lumineszenzdioden SF 4xx; Munich (1997)

Solbrig, M..; private communication (1997)

Sümnich, K.H and H. Schwarzer; In-flight calibration of Modular Optoelectronic Scanner (MOS); Int. Journal of Remote Sensing; Vol. 19, No. 17; pp. 3237–3259 (1998)

Theuwissen, A.; Solid-state imaging with charge-coupled devices; Kluwer Academic Publisher Dordecht (1996)

Thyagarajan, K., A. Neumann, G. Zimmermann; The IRS-P3 remote sensing mission, Acta Astronautica; Vol. 39, Nos. 9 – 12 (1996)

Twomey, S.; Table of the Planck function for terrestrial temperatures; Infrared Physics; Vol. 3; pp. 9–26 (1963)

UNEP / Information Unit for Conventions; Climate change information kit; UNEP/IUC, Geneva Executive Center, C.P. 356, 1219 Châtelaine, Switzerland; pp. 1–64 (1998)

Vane, G., A.F.H. Goetz, J.B. Wellman; Airborne imaging spectrometer: a new tool for remote sensing; Proceedings of the Int. Geosci. Remote Sensing; 6.1–6.5 (1983)

Warren, S.G.; Optical properties of snow; Rev. Geophys. Space Phys.; Vol. 20, No. 67 (1982)

Willoughby, C.T., J. Marmo, M.A. Folkman; Hyperspectral imaging payload for the NASA small Satellite Technology Initiative Program; IEEE Aerospace Applications Conference, Cat. No. 96-CH-35904; pp. 67–79 (1996)

Wolfe, W.; Handbook of military infrared technology; Infrared Information and Analyse Center, Environmental Research Institute of Michigan (1965 and 1978)

Zarnowski, J., E. Eid, F. Arnold, M. Pace, J. Carbone, B. Williams; Performance of a large-format charge injection device; SPIE; Vol. 1900; pp. 110–120 (1993)

Zimmermann, G., W. Badaev, M.S. Malkevich, B. Piesik; The MKS-M remote sensing experiment for determination of ocean and atmospheric parameters from SALYUT-7; Acta Astronautica; Vol. 12, No. 7/8; pp. 475–483 (1985)

Zimmermann, G.; Fernerkundung des Ozeans; Akademie Verlag Berlin; pp. 1–420 (1991)

Zimmermann, G., A. Neumann, K.H. Sümnich, H. Schwarzer; MOS/PRIRODA - An imaging spectrometer for ocean remote sensing; SPIE; Vol. 1937; pp. 201-206 (1993)

Zimmermann, G. and A. Neumann; Imaging spectrometer for ocean remote sensing; International Symposium of the International Academy of Astronautics (IAA), Berlin, Nov 4–8 1996; pp. 113–122 (1996)

Zimmermann, G.; private communication (1999)

Zimmermann, G. and A. Neumann; The imaging spectrometer MOS on IRS-P3 — three years of experience; Journal of Spacecraft Technology; Vol. 10, No. 1; pp. 1–9 (2000)

Appendix A: Systematisation of sensors

This appendix gives a brief profile of over 80 high resolution spaceborne and airborne Earth observation sensor systems (H < 800 km) planned to be operating in the year 2000 and beyond. This systematisation covers multi- and hyperspectral civil, land and ocean nadir viewing observation sensors in the spectral range from the ultraviolet to the thermal infrared. A summary of the performance of each system, from image parameters (spectral and ground resolution) to the image generating procedure (spectral selection mode, image acquisition mode) is presented. The sensor data is taken from a sensor overview[158] as long as no update reached the authors.

A.1 Spaceborne sensors

For this systematisation the space sensors are divided into four application orientated groups:

High global coverage

Within 2-5 days the Earth will be covered by these sensors by means of a wide swath of more than 800 km. A few sensors of this group have a relatively high spectral resolution ($\Delta\lambda$ > 20 nm) which improves the possibility of vegetation and ocean mapping. For these sensors the ground resolution is more than 250 m. Sensor examples are MERIS, MODIS, SeaWiFS and GLI.

Frequent global coverage

This group follows Landsat's Thematic Mapper footsteps. For this group the global coverage will be around 16 days for nadir-only viewing sensors (with a swath width of 100–200 km). Further sensors are included having a reduced swath width but provide tilting capability for increasing the repetivity rate. Other characteristics of this sensor group are a relative high ground resolution (around 10-50 m) and broad spectral bands (60–90 nm) for classical land and vegetation remote sensing (e.g. NDVI, land classification). Sensor examples are HRVIR on SPOT and ETM+ on Landsat-7.

High spatial resolution (1 m-Commercials)

These sensors are a spin-off from reconnaissance technology and marked by very high ground-resolution (1-5 m) and a small area coverage. Without tilting capability the global coverage could takes years. This group consists of sensors like Ikonos or OrbView-3.

Scientific and military hyperspectral application tests

The last group consists of technical demonstrators and test orientated missions. Sensors like ALI on EO-1 and COIS on NEMO are a new millennium testbed for hyperspectral grating spectrometers. Other approaches are new wedge filter sensors or Fourier Transform spectrometers.

[158] Nieke–1997

Sensor	Country	Mission	Launch	Sensor types	No. of bands @ ground resolution								Tilting capability	Swath [km]	dλ [nm]	Image acquisition mode	Spectral selection	Sensor mass [kg]
					PAN	VNIR [m]				SWIR		M/TIR						
					[m]	1	2	3	4	5	6	7						
High global coverage (swath > 800 km)																		
SeaWiFS	U.S.	SeaStar	Aug 97	M		8 bands @ 1100							20° a	2800	20-40	whiskbroom	filter	45
WIFS	India	IRS-1 D	Sep 97	M				188	188				-	800	60/90	pushbroom	filter	50
HIRS/3	U.S.	NOAA-K	May 98	M		1 bands @ 20km						19 @ 20 km	-	2160	N/A	whiskbroom	filter	N/A
AVHRR/3	U.S.	NOAA-K	May 98	M		2 bands @ 1100				1 @ 1100		3 @ 1100	-	2900	100-1000	whiskbroom	filter	27
OCM	India	IRS-P4	May 99	M		8 bands @ 360m							+/- 20° a	1400	20-40	pushbroom	filter	150
VGT	EC, Fr, Be, S, I	SPOT 4	Mar 98	M		4 bands @ 1000				1000			-	2200	40-170	pushbroom	filter	150
WFI	China-Brazil	CBERS-1	Oct 99	M				258	258				-	900	60/120	pushbroom	filter	N/A
MODIS	U.S.	EOS AM-1	Dec 99	H		16 bands @ 250/500/1000				4 bands		16 bands	-	2330	10-500	whiskbroom	filter	250
MERIS	ESA	ENVISAT	4 Q 01	M		15 bands @ 300/1200							-	1150	2.5-30	pushbroom	grating	205
GLI	Japan	ADEOS-2	Dec 01	H		23 bands @ 250/1000				6 bands		7 bands	+/- 18.5° a	1600	8-1000	whiskbroom	filter	475
POLDER	France	ADEOS-2	Dec 01	M		15 bands @ 6000							-	2400	20-40	staring	filter	N/A
WIFS	India	IRS-2A	2000	M				125	125				-	800	60/90	pushbroom	filter	50
MODIS	U.S.	EOS-PM1	May 01	H		16 bands @ 250/500/1000				4 bands		16 bands	-	2330	10-500	whiskbroom	filter	250
Oceansat	India	IRS-P7	>2000	M		N/A							N/A	N/A	N/A	N/A	N/A	N/A
S-GLI	Japan	ADEOS-3	2005	H		23 bands @ 250/1000				6 bands		7 bands	+/- 20°c,45°a	1500	8-1000	whiskbroom	filter	N/A
AMODIS	U.S.	EOS-PM2	2006	H		N/A							N/A	N/A	N/A	N/A	N/A	N/A
AMODIS	U.S.	EOS-AM2	2004	H		N/A							N/A	N/A	N/A	N/A	N/A	N/A
AVHRR / HRIS	U.S.	NOAA-L-N	2000-07	M		N/A							N/A	N/A	N/A	N/A	N/A	N/A
Frequent global coverage (global coverage around 16 days)																		
LISS-3	India	IRS-1 D	Sep 97	M			23	23	23	70			-	140	60-150	pushbroom	filter	170
HRVIR (2)	Fr (Be, S)	SPOT 4	Mar 98	M&P	10		20	20	20	20			+/-27°c	(120) 60	90-170	pushbroom	filter	N/A
IRMSS	China-Brazil	CBERS-1	Oct 99	M&P	80					80	80	160		120	70-2500	whiskbroom	filter	N/A
HRCC	China-Brazil	CBERS-1	Oct 99	M&P	20	20	20	20	20				+/- 32°c	120	70-120	pushbroom	filter	N/A
ASTER	Japan	EOS AM-1	Dec 99	M			15	15	15	6 @ 30		5 @ 90	+/-24°a, 8°c	60	80-1700	whisk-/pushbr.	filter	421
ETM+	U.S.	Landsat 7	Apr 99	M&P	15	30	30	30	30	30	30	60	-	185	70-2100	whiskbroom	filter	407
HRCC/IRMSS	China-Brazil	CBERS-2	2000	M		N/A							N/A	N/A	N/A	N/A	N/A	N/A
LISS-3	India	IRS-2A	2000	M			23	23	23	23			-	140	70-150	pushbroom	filter	170
M10	U.S.	R21-A, B, C, D	2000	M		10	10	10	10	20			40°c, 30° a	205*	70-300	pushbroom	filter	4 smallsats
GEROS	U.S.	GEROS I - VI	2000	M		10	10	10	10	10			N/A	N/A	N/A	N/A	N/A	6 smallsats
ARIES	Australia	ARIES-1, 2, 3	2000	H&P	10	32 bands @ 30				64 ba. @ 30			+/-30°c	15	30	pushbroom	N/A	Minisat
PRISM	ESA	LSPM	>2000	H		60(190)bands @ 50				140 bands		2 ba.	+/- 30°c	50	(3)10-1000	pushbroom	N/A	206
HRG	Fr (Be, S)	SPOT 5A	2002	M&P	5		10	10	10	20			+/-19°a,27°c	60	90-170	pushbroom	filter	N/A
AVNIR-2	Japan	ALOS	2003	M		10	10	10	10				+/- 44°c	70	80-130	pushbroom	filter	210
XSTAR	France	XSTAR-A,B	2002	M		10 bands @ 20m							N/A	320	N/A	N/A	N/A	2 smallsats
HRG	Fr (Be, S)	SPOT 5B	2007	M&P	5		10	10	10	20			+/-19°a,27°c	60	90-170	pushbroom	filter	N/A

N/A not available
H hyperspectral
M multispectral
P panchromatic

dλ spectral resolution in nm
a along track
c cross track

* for 4 Smallsats

Table-A.1a: Spaceborne sensors, part A

Sensor	Country	Mission	Launch	Sensor types	No. of bands @ ground resolution								Tilting capability	Swath [km]	dλ [nm]	Image acquisition mode	Spectral selection	Sensor mass [kg]
					PAN	VNIR [m]				SWIR		M/TIR						
					[m]	1	2	3	4	5	6	7						
High spatial resolution (1 - 5 m)																		
PAN	India	IRS-1 D	Sep 97	P	6								+/- 26° a,c	70	250	pushbroom	filter	150
Ikonos	U.S.	SpaceImaging	Sep 99	M&P	1	4	4	4	4				30° a,c	11	70-140	N/A	filter	150
EROS-A, B	Israel / USA	West Ind. Space	2 Q 00	P&M	1.5 / 1								N/A	14 / 20	N/A	staring (TDI)	filter	7 Minisats
PAN	India	IRS-P5 Cartosat	2001	P	2.5								a stereo	30	250	pushbroom	filter	N/A
Quick Bird 1,2	U.S.	EarthWatch	2 Q 00	M&P	1	4	4	4	4				30° a,c	22	70-130	staring (TDI)	filter	N/A
OrbView-3	U.S.	OrbImage	2 Q 00	M&P	1 / 2	8	8	8	8				N/A	4 / 8	50-140	N/A	filter	N/A
LISS-4	India	IRS-2A	2000	M			5	5	5				+/- 26° c	23	60-90	N/A	filter	150
LISS-4	India	IRS-P6	>2000	M		N/A							N/A	N/A	N/A	N/A	N/A	N/A
RapidEye	Germany	RapidEye	2002	M		4-6 bands @ 5-7 m							N/A	200	N/A	N/A	N/A	4 Minisats
PRISM	Japan	ALOS	2003	P	2.5								stereo	35 (70)	250	pushbroom	filter	600
Scientific, military, hyperspectral application tests																		
MOS	Germany	IRS-P3	Mar 96	M		18 bands @ 520 (1000)							-	200	1.4-100	pushbroom	grating	35
SPIMs 1-5	U.S.	MSX	May 96	H		272 bands @ 770							-	15	0,5-2,9	pushbroom	grating	N/A
UVIS imager	U.S.	MSX	May 96	M		10 bands @ 80							-	141	10-170	pushbroom	filter	N/A
VIRS	U.S.	TRMM	Nov 97	M		1 bands @ 2100				1 @ 2100		3 @ 2100	-	720	80-1000	whiskbroom	filter	48.6
MISR	U.S.	EOS AM-1	Jun 98	M		250	250	250	250				stereo	378	20-60	pushbroom	filter	157
OCI	Taiwan	ROCSAT-1	Jan 99	M		6 bands @ 800							-	690	20-40	N/A	N/A	Minisat
SUNSAT	South Africa	SUNSAT	Apr 99	M		15	15	15					+/- 22° a,c	52	N/A	pushbroom	filter	Minisat
SHC/ 2x MSC	GB	UOSAT-12	Apr 99	M	10	35	35	35	35				-	60	N/A	staring	filter	6.6/ 2x3
DLR Tub-sat	Germany	DLR Tub-sat	May 99	M	6	3 bands @ 120m							-		< 70	staring	filter	
FTHSI	U.S.	Mighty Sat II	2000	H		256 bands @ >50							-	15	2-6	pushbroom	interferometer	Minisat
PROBA	B, GB, ESA	CHRIS	Jul 00	H		19 bands @ 25 m							-	19	1.3-11	pushbroom	grating	15
ALI	U.S.	NMP / EO-1	Nov 00	M&H	10	128 bands @ 30				233 @ 30			-	10	20-80	pushbroom	grating/wedge	74
Hyperion	U.S.	NMP / EO-1	Nov 00	H		220 bands @ 30 m							-	7.5	10	pushbroom	grating	23
AC	U.S.	NMP / EO-1	Nov 00	H						200@300			-	77	4-10	staring	wedge-filter	9.1
MMRS	Argentina	SAC-C	Nov 00	M		175	175	175	175	175			-	360	10-150	pushbroom	filter	20
OSMI	Korea	KOMPSAT	Jul 99	M		6 bands @ 850							-	800	20-40	N/A	N/A	Minisat
WAOS-B	Germany	Bird	2000	M		2 bands @ 150					2 ba.	@ 300		430	50-1000	pushbroom	filter	24
Orbview	U.S.	Orbview-4	March 01	H		280 bands 0.4 to 5µm @ 8 m							+/- 45° a,c	8	9-25	pushbroom	N/A	260
AATSR	ESA	ENVISAT	4 Q 01	M		3 bands @ 1000				2 bands	2 bands		-	500	N/A	whiskbroom	filter	100
COIS / PIC	U.S.	NEMO	2000	H	5	210 bands, 0.4 to 2.5µm @ 30							-	30	10	pushbroom	grating	61
CIS	China	N/A	2000	H		64 bands @ N/A				24 bands		3 ba.	-	N/A	20-500	whiskbroom	N/A	N/A

N/A not available
H hyperspectral
M multispectral
P panchromatic

dλ spectral resolution in nm
a along track
c cross track

Table-A.1b: Spaceborne sensors, part B

A.2 Airborne sensor

The airborne sensors can be used more flexibly because of the variation of height (flight level) and the forward scan velocity (aircraft, drone, zeppelin). Therefore spatial resolution and swath width can be adapted more easily and the systematisation of the spaceborne sensors is not transferable to the airborne sensors.
Table–A.2 gives a list of the airborne sensors which have more than three spectral channels.

The environmental research application group

This group is identified by large area covering, e.g. wide field of view (FOV > 70°). A broad spectral coverage is necessary to cover most of the environmental applications.

Scientific, simulating, pre-space and military application tests

Having mostly a low Field Of View (FOV < 70°) and a very low In Field Of View (IFOV) this group applies a broad palette of applications: testbeds for new spaceborne systems, sensors with very high spectral resolution for scientific research and military use.

Sensor	Availibility since	Spectr. bands @ IFOV [mrad] VNIR 1	2	3	4	SWIR 5	6	M/TIR 7	Channels	Tilting mirror	FOV [°]	dλ [nm]	Image acquisition mode	Spectral selection	Sensor mass [kg]	Company
Environmental research application group (FOV > 70°)																
AMSS-GLI	95	37 bands @ 2x3				4 bands		5 ba.	46	-	80	10-1000	whiskbroom	grating, filter	164	NASDA, GLI-Program
AMSS-Mk II	89	32 bands @ 2x3				8 bands		8 ba.	48	-	92	20-530	whiskbroom	grating, filter	N/A	Geoscan PTY LTD, Perth Western Australia
AOCI (SAS)	88	9 bands @ 2.5						1 ba.	10	-	86	20-4000	whiskbroom	grating, filter	N/A	NASA Ames,Daedalus Enterprises
CIS	93	64 bands @ 1.2				24 bands		3 ba.	91	-	80	10-1000	whiskbroom	grating/filter	N/A	Shanghai Institute of Technical Physics, Shanghai 200083, China
DAIS-16115	94	76 bands @ 3				64 ba.		20 ba.	160	yes	78	8-333	whiskbroom	grating	N/A	Geophysical Environmental Research (GER) Corporation; New York 12
DAIS-2815 /AAS	91	1 band @ 1-5				23 bands @ 1-5			24	-	82	300-700	whiskbroom	grating	N/A	Geophysical Environmental Research (GER)
DAIS-3715	94	33 bands @ 5				2 bands		2 ba.	37	-	90	20-4000	whiskbroom	grating	N/A	Geophysical Environmental Research (GER)
DAIS-7915	94	32 bands @ 3.3				40 bands		7 ba.	79	-	78	10-2000	whiskbroom	grating, filter	300	GER/DLR/JRC
GER 63 / AIS	86	24 bands @ 2/3/4				39 bands			63	-	90	16-120	whiskbroom	grating, filter	N/A	Geophysical Environmental Research (GER)
MAIS	91	32 bands @ 3				32 @ 4.5		7 ba.	71	-	90	20-800	whiskbroom	grating	N/A	Shanghai Institute of Technical Physics, Chinise Academy of Sciences,
MAMS	94	7 bands @ 5						4 ba.	11	-	85	70-1800	whiskbroom	grating, filter	N/A	NASA MSFC, Daedalus Enterprises
MAS / AHS	91	9 bands @ 2.5				16 ba.		25 ba.	50	-	86	20-1500	whiskbroom	grating, filter	96	NASA GSFC, Daedalus Enterprises
MASTER	97	11 bands @ 2.5				14 ba.		25 ba.	50	-	86	40-700	whiskbroom	grating, filter	100	NASA JPL,Daedalus Enterprises, Inc.
MISI	96	61 bands @ 1				2 bands		7 ba.	70	-	90	10-2000	whiskbroom	grating, filter	N/A	Rochester Institute of Technology
MIVIS	93	20 bands @ 2				72 @ 2		10 @ 2	102	-	72	8-500	whiskbroom	grating, filter	200	Daedalus Enterprises, Inc.
POLDER	90	9 bands @ 7							15	-	86	20-40	staring	filter	N/A	CNES
TIMS	81					6 bands @ 2.5			6	-	76	400-1000	whiskbroom	grating	N/A	NASA JPL,Daedalus Enterprises, Inc.
Scientific, simulating, pre-space and military application tests (FOV < 70°)																
AAHIS-1	94	36 or 72 bands @ 1							36/72	-	11	11	pushbroom	N/A	N/A	SETS Technology, Inc.(HI)
ADS	00	3 pan & 3 spectral bands							4	stereo	62.5	50	pushbroom	filter	N/A	DLR
AHI	97					32ba. @ 0.5			32	-	7	125(31)	pushbroom	grating	150	DARPA
AISA	93	286 bands @ 1							286	-	21	1.6-9.4	pushbroom	grism	15	Specim Spectral Imaging Ltd. Oulu, Fi
AMS	90	16 bands @ N/A							16	-	N/A	N/A	wiskbroom	N/A	N/A	Shanghai Institute of Technical Physics, Shanghai 200083, China
APEX	02	200 bands @ N/A				200 ba. @ N/A			200 prog.	-	28	<15	pushbroom	prism	135	ESA
ASAS	92	62 bands @ 0.8							62	+70/-55	19.3	11	pushbroom	grating	N/A	http://asas.gsfc.nasa.gov
ATMX /TMS	92	8 bands @ 2.5				2 ba.		2 ba.	12	-	43	30-5500	whiskbroom	prism, filter	127	NASA Ames,Daedalus Enterprises, Inc.
AVIRIS	89		224 bands @ 1						224	-	30	32-192	whiskbroom	grating	270	Jet Propulsion Laboratory
CASI	88	288 bands @ 1.2							39 prog.	-	35	3	pushbroom	grating	55	ITRES Research, Calgary, CA
HRIS	99	65 /120 ba. @ 0.05				140 bands			205 / 260	+/- 30	2.2	9-12	pushbroom	grating	N/A	ESA / DSS
HRSC-A	97	9 bands @ 0.04							5	stereo	36	40-180	pushbroom	filter	32	DLR
HYDICE	95		206 bands @ 0.5						206	-	9	7-15	pushbroom	prism	176	Hughes Danbury Optical Systems, Inc.
ISM	91	64 bands @ 3x11				64 bands			128	-	40	12 / 25	whiskbroom	N/A	N/A	DES Dept. d'Etude Spatiale, IAS Institute d'Astrophysique, OPS Observ
MEIS	83	8 bands @ 0.7							8	+/- 35	40	2.5	pushbroom	N/A	N/A	McDonnell Dettwiler and Associates, Canada
PHI	97	244 @ 1.5							8-128	-	21	Sep 99	pushbroom	grating	21	Shanghai Senstron Institute of Information Technology
PHILLS	94	372/1024 @ 0.08/3							372/1024	-	3-72	0.5-1	pushbroom	grating	4	Naval Research Laboratory
Probe-1	97	N/A @ 2				N/A @ 2		yes	N/A	-	60	12-16	whiskbroom	N/A	75	ESSI Earth Search Sciences Incorporated
ROSIS	92	105 bands @ 0.5							81 prog.	+/- 20	16	7.2	pushbroom	grating	25	DLR, GKSS, DSS
SciTec	95					256 @ 0.25			256	-	3.7x8	8-96	N/A	wedge/grating	N/A	SciTec/TRW
SFSI	95					115 ba.@ 0.3			115	-	9.4	10	pushbroom	grating	100	CCRS of Ottawa
SMIFTS	93					110 bands @ 0.6			110	-	6	5-50	pushbroom	interferometer	N/A	University of Hawaii
SWIR-Scan	95					12 ban. @ 6			12	-	N/A	20-800	whiskbroom	filter	N/A	Shanghai Institute of Technical Physics, Chinise Academy of Sciences,
TRW-II	92					80 ba.@ 0.5 / 1			80	-	7/14	12	pushbroom	grating	N/A	TRW
TRW-III	95	128 bands @ 0.9				256 bands @ 0.9			384	-	13	5-6	pushbroom	grating	N/A	TRW
TRWIS-A	90	128 bands @ 1							128	-	14	3.3	pushbroom	grating	N/A	TRW
TRWIS-B	91	90 bands @ 1							90	-	14	5	pushbroom	grating	N/A	TRW
VIFIS	94	60 bands @ 1							60	-	31.5	10-18	N/A	filters	N/A	University of Dundee
WIS-VNIR/SWIR	96	432 bands @ 0.66				190 @ 0.66			622 (812)	yes	12-19	5-27	staring	wedge	20	Hughes Santa Barbara Remote Sensing

Table-A.2: Airborne sensors

A.3 Sensors and mission acronyms

In the following are listed the acronyms and abbreviations used in Tables A.1a, A.1b and A.2:

AAHIS-1	Advanced Airborne Hyperspectral Imaging System
AATSR	Advanced Along Track Scanning Radiometer
AC	Atmospheric Corrector
ADEOS	Advanced Earth Observation Satellite
ADS	Airborne Digital Sensor
AHI	Airborne Hyperspectral Imager
AISA	Airborne Imaging Spectrometer for different Applications
ALI	Advanced Land Imager
ALOS	Advanced Land Observation Satellite
AMODIS	Advan. Moderate-Resolution Imaging Spectroradiometer
AMS	Airborne Multispectral Scanner Daedalus)
AMSS-GLI	Advanced Multi-Spectral Scanner (GLI-NASDA)
AMSS-Marc II	Airborne Multispectral Scanner (GEOSCAN)
AOCI (SAS)	Airborne Ocean Color Imager Spectrometer
APEX	Airborne Prism Experiment
ARIES	Australian Resource Information and Environment Satellite
ASAS	Advanced Solid-State Array Spectroradiometer
ASTER	Advanced Spaceborne Thermal Emission and Radiation Radiometer
ATMX /TMS	Airborne Thermic Mapper - extended
AVHRR	Advanced Very High Resolution Radiometer
AVIRIS	Airborne Visible-Infrared Imaging Spectrometer
AVNIR-2	Advanced Visible and Near-Infrared Radiometer
Bird	Bispectral Infrared Detector
CASI	Compact Airborne Spectrographic Imager
CBERS	China-Brasil Earth Remote Sensing Satellite
CIS	Chinese Imaging Spectrometer
CHRIS	Compact High-Resolution Imaging Spectrometer
DAIS	Digital Airborne Spectrometer
ENVISAT	Environmental Satellite
EOS	Earth Observing System
EROS-A, B	Earth Resources Observation Satellite
ETM+	Enhanced Thematic Mapper Plus
FTHSI	Fourier Transform Hyperspectral Imager
GER 63 / AIS	Geophysical and Environmental Research Corp.
GLI	Global Imager
HIRS	High Resolution Infrared Sounder
HRCC	High Resolution CCD Camera
HRG	High Resolution Geometry
HRIS	High Resolution Imaging Spectrometer
HRSC	High Resolution High Resolution Stereo Camera – Airborne
HRVIR (2)	High Resolution Visible and Infrared sensor
HSI	Hyperspectral Spaceborne Imager
hybrid VIFIS	Variable Interference Filter Imaging Spectrometer
HYDICE	Hyperspectral Digital Imagery Collection Experiment
IRMSS	Infrared Multispectral Scanner
IRS	Indian Remote Sensing Satellite
ISM	Infrared Imaging Spectrometer
LEISA	Linear Etalon Imaging Spectrometer Array
LEWIS-SSTI	Small Spacecraft Technology Initiative Lewis
LISS	Linear Self-Scanning Sensor
M10	Multispectral 10m resolution
MAIS	Modular Airborne Imaging Spectrometer
MAMS	Multispectral Atmospheric Mapping Sensor
MAS / AHS	MODIS Airborne Simulator

MASTER	Modis Aster Airborne Simulator
MEIS	Multi-detector Electro-optical Imaging Sensor
MERIS	Medium Resolution Imaging Spectrometer
MISI	Modular Imaging Spectrometer
MISR	Multi-Angle Imaging SectroRadiometer
MIVIS	Multispectral Infrared and Visible Spectrometer
MODIS	Moderate-Resolution Imaging Spectroradiometer
MOS	Modular Optpelectronic Scanner
MSX	Midcourse Space Experiment
NMP	New Millennium Program
NOAA	National Oceanic and Atmospheric Administration
OCI	Ocean Color Imager
OCM	Ocean Colour Monitor
PHILLS	Portable Hyperspectral Imager for Low Light Spectroscopy
POLDER	Polarisation and Directionality of the Earth's Reflectance (airborne)
PRISM	Process Research by an Imaging Space Mission
PROBA	Project for On-Board Autonomy
R21-A,B,C,D	Resource 21
ROCSAT-1	Republic of China Satellite
ROSIS	Reflective Optics System Imaging Spectrometer
SeaWiFS	Sea-viewing Wide Field Sensor
SFSI	SWIR Full Spectrographic Imager
SMIFTS	Spatially Modulated Imaging Fourier Transform Spectrometer
SPIMs 1-5	Spectrographic Imager
SPOT	Système Pour l'Observation de la Terre
SROM	Spectroradiometer for Ocean Monitoring
TIMS	Thermal Infrared Multispectral Scanner
TRMM	Tropical Rainfall Measuring Mission
TRW	Thompson Ramo and Wooldrige Inc.
UVIS imager	Ultraviolet / Visible Imaging and Spectrographic Imaging
VGT	Vegetation
VIRS	Visible Infrared Scanner
WAOS-B	Wide Angle Optoelectronic Stereo Scanner
WFI	Wide Field Imager
WIFS	Wide Field Sensor

Appendix B: ECOMON S/C details

The appendix outlines the power profile in different operation modes for the proposed ECOMON mission[159]. Further on, the mass and power budget is summarised.

The ECOMON mission will use a electrical power system (EPS), which is specifically designed concerning the power profile of the payload during the nominal modes (cooling, satellite acquisition and imaging). The design of the electrical power system is sufficient to provide all the required power within the complete mission lifetime. The different operation modes of the ECOMON S/C are presented in Table-B.1.

Table-B.1: Operation modes for ECOMON

Operation Modes							
	ECM	**BCM**	**CCM**	**ACM**	**OPM**		
Duty Cycle (min)	**35,0**	**25,3**	**20,0**	**5,0**	**15,0**		min
Duty Cycle	35%	25%	20%	5%	15%		% per orb
Battery required	**x**			**x**	**x**		yes/no
Time for charging		**x**	**x**				yes/no
Solar gen. efficiency		**x**	**x**				yes/no
						total	
Discharge Time	35,0			5,0	15,0	55,0	min
Charge Time		25,3	20,0			**45,3**	**min**
					total	**100,3**	**min**

ECM : Eclipse Mode
BCM : Battery Charge Mode
CCM : Cooling Mode
ACM : Acquisition Mode
OPM : Operation Mode (Imaging)

[159] as proposed by OHB–System for ECOMON

Mass and the power budget

The predicted mass and the power budget for the ECOMON S/C — including the main subsystems — is given in Table-B.2 and Table-B.3.

Table-B.2: Mass budget for ECOMON S/C

Mass Budget					
	Subsystem	**Element**	**No.**	**Elem. Mass [kg]**	***Subsys. Mass [%]***
S/C Bus					
	OBDH			**10**	*3%*
	Electrical Power			**58**	*19%*
	Navigation			**5**	*2%*
	Structure			**26**	*9%*
	Thermal Control			**10**	*3%*
	TM / TC			**10**	*3%*
	ACS			**40**	*13%*
	OCS			**0**	*0%*
sub total				***159***	***53%***
Payload	Sensor			**80**	*27%*
		PM1 PM2 PM3	1	25 25 30	
	Sensor Support			**25**	*8%*
		PDP + Mass Mem. TCS HDTx	1	5 10 10	
sub total				***105***	***35%***
Margin				***36***	*12%*
Dry Weight [kg]				***300***	***100%***
Total Weight [kg]				***300***	***100%***

ACS: Attitude control subsystem
DHS: Data handling subsystem
EPS: Electrical power subsystem
IFU: Interface unit
OBHH: On board data handling
OCS: Output control subsystem
PM1-3: Payload module 1-3
TCS: Thermal control subsystem
TM/TC: Telemetry /telecommand

Table-B.3: Power budget for ECOMON S/C

Power Budget						
Mode	**Operation Modes**					
	ECM	**BCM**	**CCM**	**ACM**	**OPM**	
Duty Cycle (min)	**35,0**	**25,3**	**20,0**	**5,0**	**15,0**	min
Duty Cycle	35%	25%	20%	5%	15%	% per orb
Battery required	**x**			**x**	**x**	yes/no
Time for charging		**x**	**x**			yes/no
Solar gen. efficiency		**x**	**x**			yes/no
DHS	**20**	**20**	**20**	**20**	**20**	**W**
ACS	**30**	**40**	**40**	**60**	**40**	**W**
EPS	**20**	**20**	**20**	**20**	**20**	**W**
TM/TC	**20**	**20**	**20**	**20**	**20**	**W**
req. P/L Power	**95**	**95**	**175**	**125**	**230**	**W**
req. P/L Energy	**55**	**40**	**58**	**10**	**58**	**Wh**
req. Instrument Power	**10**	**10**	**80**	**30**	**115**	**W**
PM1	0	0	25	10	45	W
PM2	0	0	25	10	45	W
PM3	10	10	30	10	25	W
req. Instr. Support Power	**85**	**85**	**95**	**95**	**115**	**W**
PDP	10	10	20	20	10	W
IFU	40	40	40	40	40	W
TCS	35	35	35	35	35	W
HDTx	0	0	0	0	30	W
margin	**10%**	**10%**	**10%**	**10%**	**10%**	
total (required)	**204**	**215**	**303**	**270**	**363**	**W**
(without EPS efficiency)	119	91	101	22	91	**Wh**

System total power consumption	
total peak power	**363 W**
avg. power per orbit	**253 W**
energy per orbit	**423 Wh**

Danksagung

Ganz herzlich möchte ich mich bei meinen Gutachtern, Betreuern und Kollegen für deren großzügig gewährleistete Unterstützung bedanken.
Hier sind insbesondere Prof. Dr. H.-P. Röser, Direktor des DLR Institutes für Weltraumsensorik und Planetare Erkundung nennen, der mich offen in sein Institut aufgenommen hat und mir für Fragen und Diskussionen jederzeit zur Verfügung stand.
Besonders herzlich möchte ich mich ebenfalls bei Prof. Dr. G. Zimmermann und Dr. A. Neumann bedanken, die mich in ihr tolles Team integrierten. Sie ließen mir große Freiheit und Verantwortung für den Fortgang meiner Dissertation — ohne dass ich mich aber jemals alleine fühlte.
Auch bei den Abteilungsleitern Dr. K.H. Sümnich (Kalibration und Validation) und Dr. F. Lura (System Konditionierung), die mir Laborraum und Geräte zur Verfügung stellten oder wichtige Bestrahlungstests durchführen ließen bedanke ich mich recht herzlich. Speziell seien auch R. Preusker, A. Lauterbach, A. Woitkoviak, K. Bachmann und K.H. Degen erwähnt, die für mich all die kleinen Dinge arrangierten, die sehr zum Gelingen der Arbeit beitrugen.
Sensorkonzeptentwicklung für die Fernerkundung umfasst die Teilgebiete Elektronik, Optik und Anwendung. Für ein besseres Verständnis dieser Gebieten halfen mir unter anderem die Diskussionen mit Drs. M. Solbrig, H. Schwarzer und B. Piesik bei denen ich mich hier bedanken möchte.
Herzlichen Dank auch an Prof. Dr. J. Albertz für die Betreuung in der Funktion als zweiter Gutachter und an Prof. Dr. W. Nitsche für die Übernahme des Promotionsausschusses.
Hinzukommen der besondere Dank an die ständig motivierende Dr. B. Nieke und an J. Schwarz und B. Ak für die Durchsicht des Manuskriptes.